RE-EVALUATION OF KOMBAT-STYLE MINERALIZATION AND IMPLICATIONS FOR EXPLORATION IN THE OTAVI MOUNTAINLAND, NAMIBIA.

A MINI-THESIS SUBMITTED IN PARTIAL FULFILMENT

OF THE REQUIREMENTS FOR THE DEGREE OF

MASTER OF SCIENCE (APPLIED GEOLOGY)

OF

THE UNIVERSITY OF NAMIBIA

BY

Abner Nghoongoloka

200513532

September 2020

SUPERVISOR: Prof. A.F. Kamona (University of Namibia)

CO-SUPERVISOR: Prof. R. Bowell (Queens University, Kingston, Ontario, Canada)

ABSTRACT

This study re-evaluates the Cu-Pb and Fe-Mn ore mineralization of the Kombat Mine (ML-16, ML-73B) and Gross Otavi Mine (ML-73C), situated between 19°41' 30" S, 19° 39' 00" S and 17°40' 00" E, 17°35' 00" E (WGS84) based on the field geology, fluid inclusions, petrology, mineralogy and geochemistry. This was to determine the genetic relationship between Fe-Mn and Cu-Pb mineralization. The study has established that the Cu-Pb ore at the Kombat Mine can be classified as an MVT-type deposit, whereas, the Fe-Mn ore can be classified as a stratiform-syn-sedimentary deposit. The formation of the MVT-type deposit is associated with a hydrothermal fluid system with a mean temperature of 183°C and mean salinity of 12.85 NaCl wt. % equivalent, as determined by fluid inclusion studies. Upward brine migration enabled leaching of metals from underlying sediments and precipitation of Cu-Pb ore at upper levels in the carbonate host rocks due to structural traps and chemical interaction. The syn-sedimentary Fe-Mn ore, which is largely associated with calc-silicate lithologies, consists mainly of magnetite and hematite with minor pyrite, hausmannite and jacobsite, was deposited by diagenetic and hydrogenetic processes under changing oxic and anoxic conditions within the sedimentary basin. Acceptable geochemical exploration indicators of the existing mineralization include anomalous values of 0.5% Cu, 0.2% S, 0.05% Pb, 0.03% As; 0.01% Zn; V, W, Mo and Ag is 0.002% each based on portable XRF sample analysis. Mineralogical indicators based on field observations, optical and XRD prospecting include major ore minerals such as chalcopyrite, bornite, covellite, and galena with minor chalcocite, sphalerite, and pyrobelonite, for the Cu-Pb MVT-type ores. For the Fe-Mn ores, hausmannite, hematite with minor, manganite may be are considered.

TABLE OF CONTENTS

LIST OF TABLES

LIST OF FIGURES

LIST OF ABBREVIATIONS

Ag →Silver

Alb → Albite

Amp → Amphiboles

Cal → Calcite

Cc → Chalcocite

Cp → Chalcopyrite

Cu → Copper

Fe → Iron

FIS → Fluid Inclusion Study

Gl → Galena

GPS → Geographic Positioning system

GSN → Geological Survey of Namibia

Ma → Million years of age

Mn → Manganese

ML → Mining License

Ml →Malachite

MVT → Mississippi Valley-type deposits

Jb → Jacobsite

O → Oxygen

OMEG → Otavi Minen-und Eisenbahn Gesellschaft

OML → Otavi Mountainland

Pb → Lead

Py → Pyrite

SEDEX → Sedimentary Exhalative deposit

SHMS → Sediment-Hosted Massive Sulfides

Sr → Strontium

TCL →Tsumeb Corporation Ltd

VMS → Volcanic Massive Sulfides deposit

XRD → X-Ray Diffractometer

XRF → X-ray fluorescence

VMS → Volcanic Massive Sulfides deposit

ºC → Degree Celsius

ACKNOWLEDGEMENTS

I would like to express my appreciation and gratitude to the following people and institutions which rendered help in the course of the study: Prof. Fredrick Kamona, University of Namibia as the main supervisor of this thesis, for the academic guidance and supervision throughout the work. Robert Bowell, Queens University (Canada) and SRK Consulting (UK), coo-supervised this study and contributed with XRD and fluid inclusion analyses. He also kept on guiding the layout of the write-ups as well as cross checking progress. Thanks are due also to Trigon Metals (Limited) Namibia for their cooperation in allowing access to the Kombat Mine site and offering the assistance of a handyman during field work; Christopher Brought (UK) for reviewing the first two chapters of the initial draft. To my colleagues at the Geological Survey of Namibia, Dr. Ute Schreiber, Ms. Helke Mocke, Ms. Ester Kapuka and Ms. Tolene Kruger for their comments on the draft version of this thesis as well as Mr. Dennis Hiskia who assisted with image modification.

DEDICATION

This thesis is dedicated to my mother Victoria Kamati, for being an outstanding woman who strived and succeeded in raising me and my siblings up on her own. Thus, her tribulation episodes of life during my toddler to early teenage edified my differentiation of trivial matters from gruesome life challenges. Her sweats and pains experienced during striving to save and guide us shall be inverted.

Also, dedicated to my aunt Frieda Namupolo and uncle Festus Matheus who have been my guardians through my Junior Secondary education until to date. In the same vein, dedicated to Rosanne and Michael Hodin family and their family friend Mark Fletcher, who supported me during my BSc studies.

Finally, dedicated to my elder brothers Abed Nghoongoloka and the late Abel Nghoongoloka (may his soul rest in peace) who played a fatherly role to ensure my wellbeing throughout my secondary and tertiary education.

DECLARATIONS

I, Abner Nghoongoloka, hereby declare that this study is my own work and is a true reflection of my research, and that this work, or any part thereof has not been submitted for a degree at any other institution.

Abner Nghoongoloka	……	21.09.2020
Name of Student	**Signature**	**Date**

1. INTRODUCTION

1.1. Background of the study

The re-evaluation of the Kombat-style mineralization project presented an opportunity to study mineralogy and geochemical relationship between iron-manganese (Fe-Mn) and copper (Cu) mineralization at the Kombat Mine in the Otavi Mountainland (OML). The study area is located in the Grootfontein District, Otjozondjupa region, along the B8 highway, midway between the towns of Otavi (42 km to the west) and Grootfontein (49 km to the east; Figure 1.1.1). The area is dominated by carbonate rocks, phyllite and minor sandstone hosting the past-producing Kombat Mine ore (mining licences: ML-9, ML-16, and ML-73B). It covers an area from the geographic (WGS84) latitude 19°41' 30" S to 19°43' 00" S and longitude 17°40' 00" E to 17°44' 30" E; Gross Otavi (ML-73C) is located between latitude 19°40' 30" S to 19° 39' 00" S and longitude 17°35' 00" E to 17°37' 00" E. Kombat Mine is currently under care and maintains status by Trigon metals with a plan to set up an open-pit targeting the historically ignored shallow Cu-Pb (Ag) mineralization which is associated with Fe-Mn mineralization. Mineral exploration can make use of direct field observations or if mineralized rocks are covered by non-mineralized material can use structural relationships, geophysical or geochemical methods to "see" below the cover and attempt to locate potential mineralization. Although different exploration techniques can be applied for the exploration of Kombat-style mineralization, exploration techniques are based on the genesis of the deposit. Historic activities of Kombat Mine were based on "Fracture Zone model" proposed by Tsumeb Corporation Ltd (TCL; 1940 – 1998) and Otavi Minen- und Eisenbahn

Gesellschaft (OMEG; 1906 – 1940) geologists (Kotze, 2019). But, later a "Roof Pendants (Ore Lenses) Hanging on Rollover Structures model" (Deane, 1995) was most adopted. Hence the genetic relationship between Fe-Mn ore and Cu-Pb (Ag) ore at the Kombat deposit remains arguable. Thus, the current study focused on establishment of the genesis of Kombat polymetallic deposit and provide hides for further exploration.

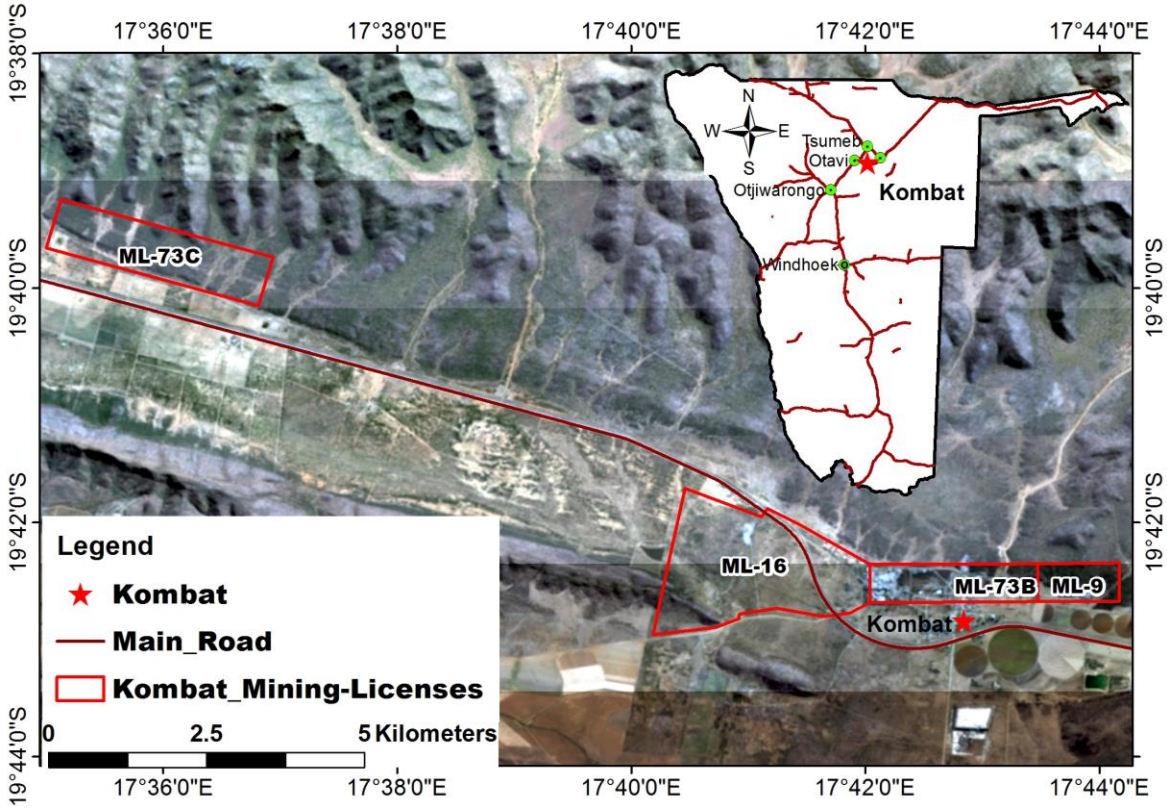

Figure 1.1.1: Geographic location of the Kombat Mine mining licenses (ML) study area (Image source: Google Earth pan-sharpened Landsat 8).

1.2. Statement of the problem

The relationship between Fe-Mn ore and Cu-Pb ore at the Kombat Mine is not understood, therefore the Kombat style mineralization indicators and implications for

exploration remains challenging. There is currently no integrated exploration model for the Fe-Mn ore and Cu-Pb (Ag) ore at Kombat Mine.

1.3. Objectives of the study

a) To establish suitable mineralogical and geochemical indicators which can be used in exploration for Kombat-style polymetallic base metal Fe–Mn and Cu-Pb (Ag) carbonate replacement deposits in the Otavi Mountainland.

b) To re-evaluate the genetic model of the Kombat polymetallic deposit.

c) To develop an integrated exploration model for Kombat-style mineralization based on the association between Fe-Mn and Cu-Pb (Ag) ore at the Kombat mine.

1.4. Significance of the study

This study will contribute to the exploration activities being conducted in the Kombat Mine area by providing the geochemical indictors which can be used in exploration in order to increase the mineral resource at the mine. In addition, other exploration companies could also benefit from the use of the exploration model elsewhere in the OML or elsewhere in searching for similar deposits.

1.5. Limitation of the study

The mine is currently under care and maintenance and hence, there was a requirement for access permit application to gain the restricted access. In addition, the underground mine shafts are flooded and pose a safety risk during entry. Instead, samples were collected from the open pits at the mine site.

1.6. Delimitation of the study

The study was restricted to the Kombat Mine area, where access was granted (Appendix 3) through the office of the Executive Director (ED), Ministry of Mines and Energy, Windhoek.

2. LITERATURE REVIEW

2.1. Exploration and Production History

Kombat-style mineralization was first reported by Sir Francis Galton in 1851 ("European Discovery", 2015). From 1909 and 1911, the historic Gross Otavi and the Kombat Mine respectively, were mined by Otavi Minen- und Eisenbahn- Gesellschaft (OMEG) until 1941 (Cairncross, 1997). The operations included limited surface production and underground mining at both Kombat and Gross Otavi. The operations restarted in 1962 until 2008, when the underground Kombat Mine was shut down due to a flooding incident (Routledge et al., 2014). The historic production totals some 12 million tonnes at 2.5% to 3.0% copper grade with lead and silver as by-products (Routledge et al., 2014). In addition, Van Heerden et al. (2018) calculated that the existing resources at the Kombat Mine were still substantial (open pit and underground) with an indicated mineral resource estimate of 1.529 million tonnes at a grade of 1.14% copper, 0.72% lead and 2.88 g/t silver, and a further 5.511 million tonnes of inferred mineral resources at a grade of 3.05% copper, 1.25% lead and 22.93 g/t silver.

In addition, exploration activities started post-WWII - 1950s, when Tsumeb Corporation Ltd (TCL) purchased assets from OMEG and carried out soil geochemical, and ground magnetic, (induced polarization and seismic) surveys in the vicinity of the Kombat Mine

from the 1960s to 1990s, however, documentation and results are not available for all surveys (Routledge et al., 2014). Routledge et al.'s (2014) technical report on the Kombat Copper Project outlined that in 1986 TCL carried out surface diamond drilling covering 1,600 m of strike length from No. 1 shaft towards the Asis Far West shaft (Figure 2.1.1). Also, the technical report revealed that TCL was liquidated in 1999 and ownership passed to Ongopolo Mining Limited who sunk an 800 m shaft at Asis Far West with a loan guarantee from the Namibian government in 2005. Weatherly Mining Namibia Limited purchased Ongopolo Mining Limited in 2006 and carried out over 1,200 drill holes including diamond core (10 holes), reverse circulation (258 holes: 27,750 m) and percussion (16,500 m) with positive results in 2007 (Routledge et al., 2014). The drilling tested a potential for near-surface copper mineralization over the three km west from the Asis Ost orebody to the No. 1 Shaft at the Kombat Mine (Figure 2.1.1).

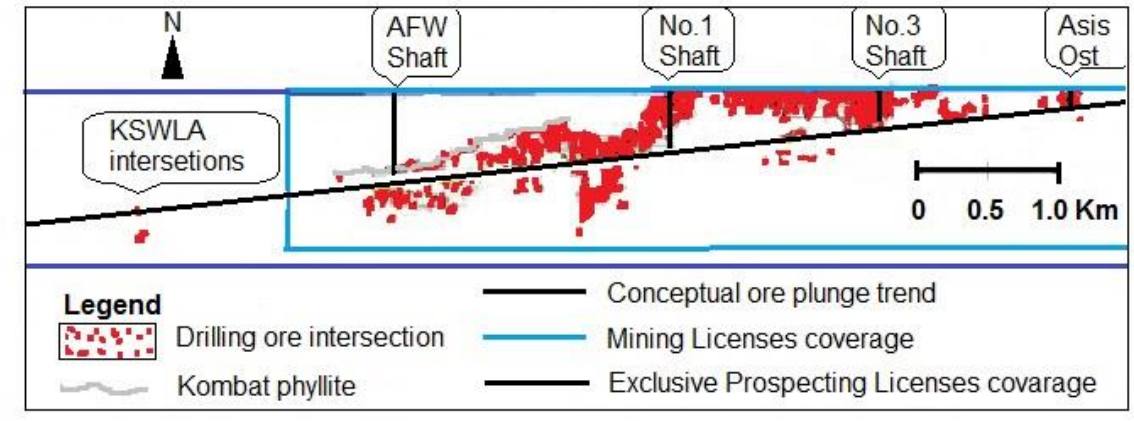

Figure 2.1.1: Exploration drilling intersections for the Kombat style mineralization (Kotzé, 2019).

2.2. Geology of the Kombat Mine, Otavi Mountainland (OML)

The Kombat Mine area is situated on the northern limb of the Otavi Valley Syncline (Figure 2.2.1) (Deane, (1995); Innes and Chaplin (as cited in Minz, 2008)). The basement rocks of the OML comprise felsic (alkaline/calc-alkaline granites and granodiorites) and mafic rocks (anorthosites, gabbros and amphibolites) of the Grootfontein Mafic Boy (GMB) and the Grootfontein Matamorphic Complex (GMC) aftern refered to as Grootfontein Inlier ((Miller, 2008; Laukamp, 2006). Paleoproterozoic age of the Grootfontein Inlier is constrained at 2 022 ± 15 Ma (Hoal et al., 2000), and poorly constrained at 1.946 +299/-333 Ma (Armstrong (as cited in Miller, 2008; Laukamp, 2006)). Overlying the Grootfontein Inlier are the metasedimentary rocks of the Neoproterozoic Damara Supergroup deposited during the Gondwana supercontinent aggregation from 900 to 600 Ma, involving intracratonic rifting followed by basin closure at 520 Ma (Trompette, 1997). These rocks underwent various stages of deformation and metamorphism during the Damara Orogen.Within the Damara Orogen distinct tectonostratigraphic zones can be distinguished based on metamorphic grade, degree of deformation and stratigraphy; within and around the OML these are the Northern Platform (NP), the Khorixas Zone (KZ) and the Northern Zone (NZ) (Figure 2.2.2).

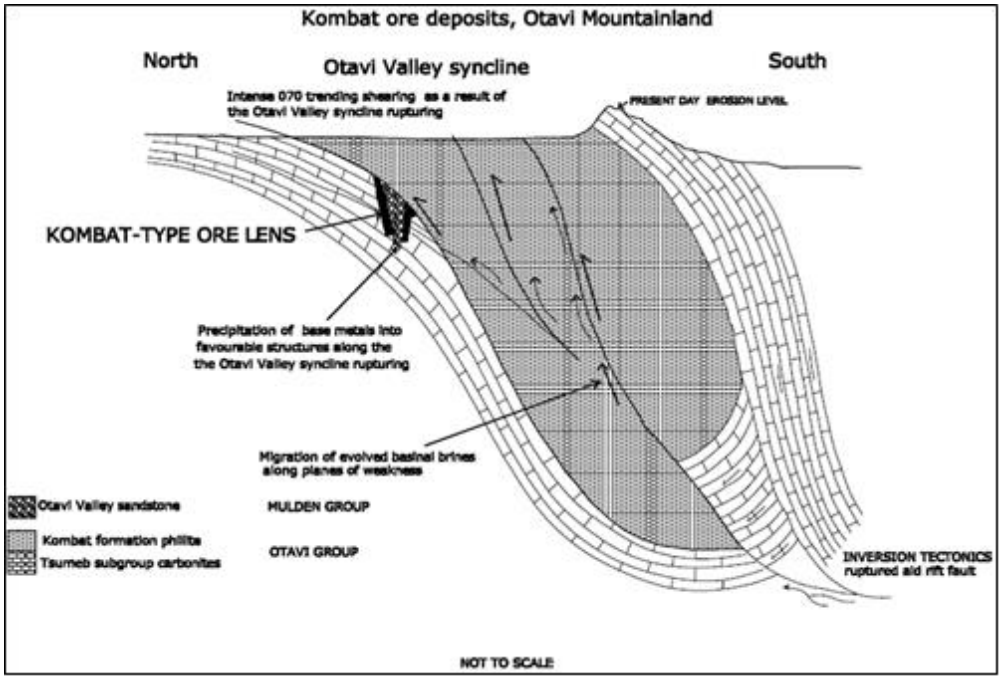

Figure 2.2.1: Tectonic setting of the Kombat mineralization (after Deane, 1995).

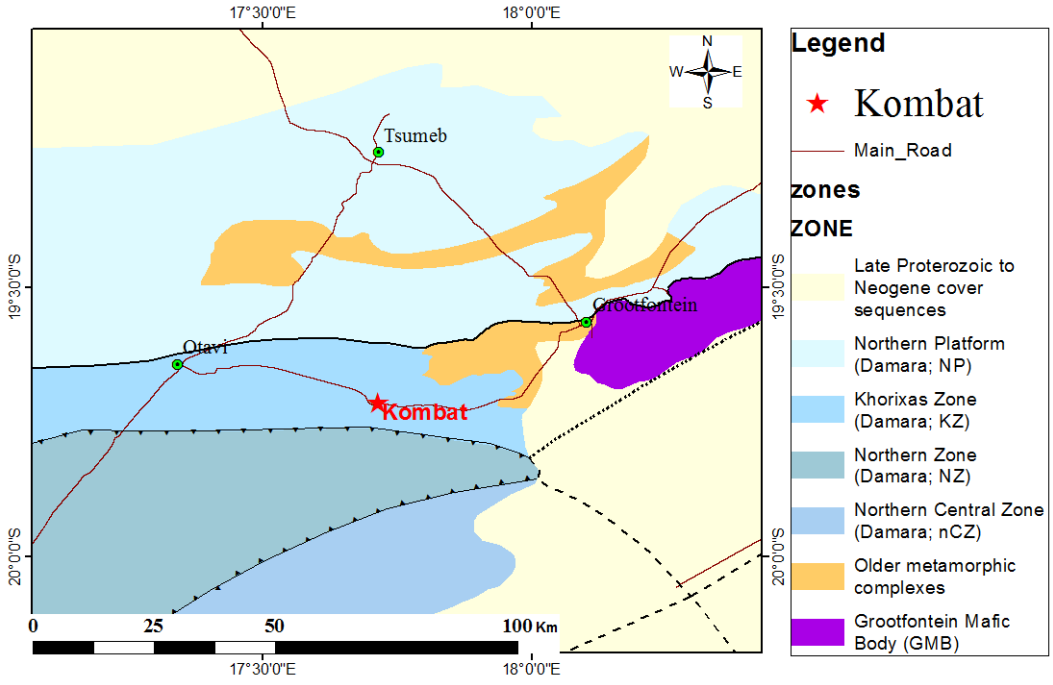

Figure 2.2.2: Tectonostratigraphic zones of the Damara Belt, showing position of Kombat Mine (red star), (source of data: Geological Survey of Namibia).

The geological succession of the Khorixas Zone (KZ), which is part of the Northern Platform (NP) where the Kombat Mine-sites are situated (Figure 2.2.3), consists of the basal Nosib Group followed by the Otavi Group carbonates and glacial deposits, and finally the Mulden Group clastic sediments. The 780-740 Ma Nosib Group represents horst-graben deposits (Melcher et al., 2004) laid down during the break-up of the Mesoproterozoic Rodinia Supercontinent. It is made up of arkose, quartzite, shale, phyllite and local conglomerate (Nabis Formation) and the predominantly volcanogenic Askevold Formation (epidote, agglomerate, chlorite schist and dolostone). The clastic Nosib sequence is followed by the Otavi Group carbonates, which are subdivided into the Ombombo, Abenab and Tsumeb Subgroups by two global glaciation events namely the 720 Ma Chuos Formation and the 635 Ma Ghaub Formation. The two formations consist of characteristic glacial diamictites and are followed by cap carbonates represented by a thick succession of carbonate platform deposits (Kamona and Günzel, 2007; Laukamp, 2007; Minz, 2008). These carbonates were laid down during deglaciation and renewed sea level rise (Hoffman *et al*., 1998). The syntectonic Mulden Group deposited between the first (D1) and second (D2) phases of Damaran deformation on the Northern Platform and comprises of the erosional debris of the developing orogen. It consists of the lower Tschudi (sandstone, shale, siltstone, conglomerate) and the upper Kombat Formation (phyllite, shale) deposited at approximately ~575 Ma (Goscombe *et al*., 2005).

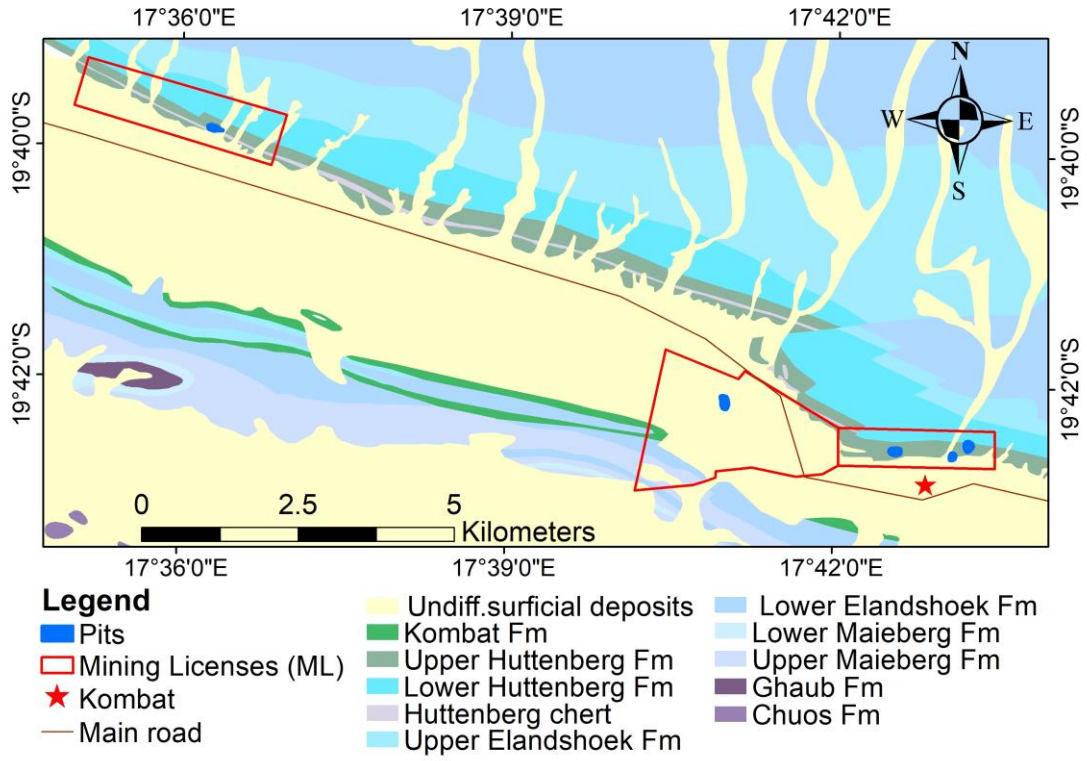

Figure 2.2.3: Geological map of the Kombat Mine area along the northern limb of the Otavi Valley Syncline, Otavi Mountainland (source of data: Geological Survey of Namibia).

2.3. Stratigraphic position of the deposit

The regional stratigraphic setting of the Kombat mineralization, (Figure 2.3.1) was discussed by various authors such as Deane (1995), Kamona and Günzel (2007) and Laukamp (2007). It is hosted by the Hüttenberg Formation of the Otavi Group, up to the contact with the overlying Kombat Formation (Mulden Group). The Kombat Mine deposit is similar to other deposits in the Otavi Mountainland, for example the Tsumeb and Berg Aukas deposits (Turner *et al*., 2012). In addition, there are over 600 known,

but uneconomic, mineral showings in the area, which are considered Mississippi Valley-type mineralization (Deane, 1995).

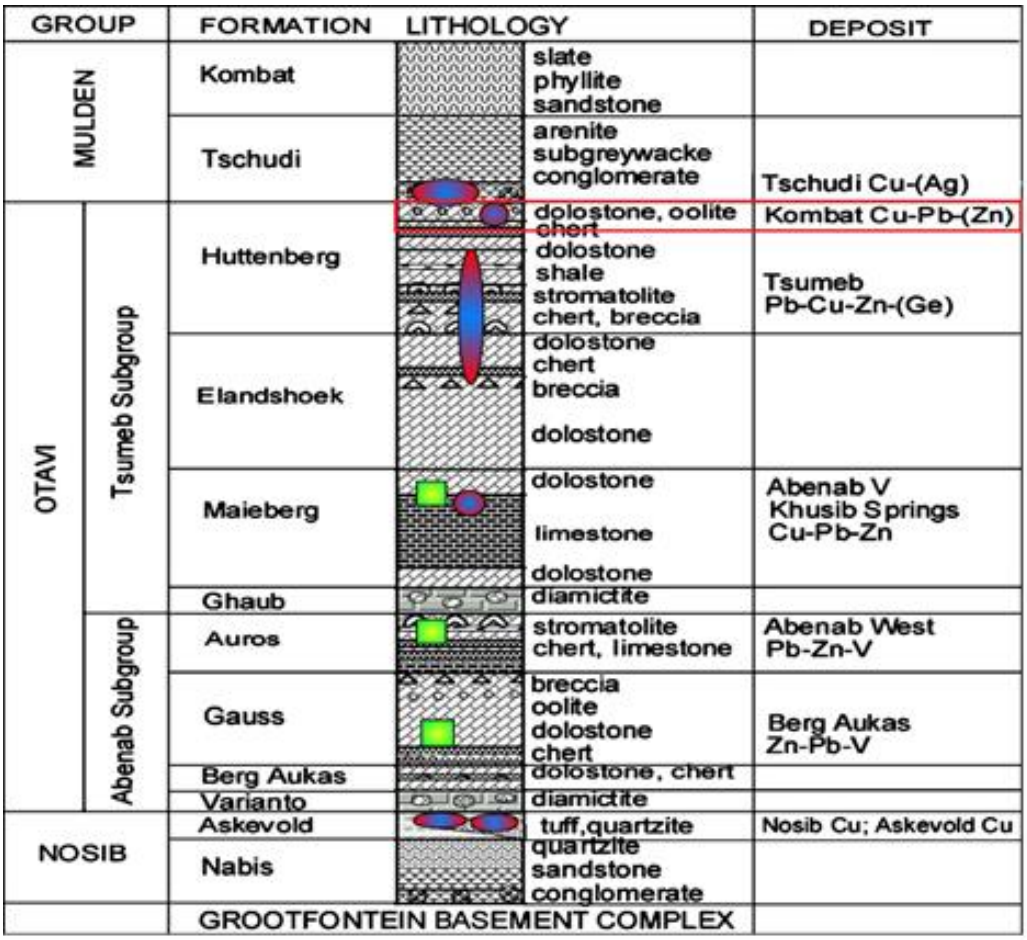

Figure 2.3.1: Stratigraphic position of Kombat-style mineralization (Kamona and Günzel, 2007)

2.4. Kombat-style mineralization model

Currently there is no satisfactory Kombat-style mineralization genetic model (Minz, 2008); and sub vertical tectonically controlled ore zones indicated through drilling and mining data analysis (Kotze, 2019) are comparable to the basic features (such as, discrete vertical ore bodies, limited to structures) of the MVT deposit (Leach et al.,

2010; Paradis et al., 2007). Generally, average thermodynamic parameters based on fluid inclusions studies for MVT deposits include the temperature range of 50°C to 250°C, and salinity of 10 to 30 wt. percent NaCl equivalent (Leach and Sangster, 1993; Giordano and Barnes, 1981). However, two models have been proposed for Kombat-style mineralization:

1) Fracture Zone model proposed by Tsumeb Corporation Ltd (TCL; 1940 – 1998) and Otavi Minen- und Eisenbahn Gesellschaft (OMEG; 1906 – 1940) geologists (Kotze, 2019).
2) The "Roof Pendants (Ore Lenses) Hanging on Roll Structures" model (Deane, 1995), which was adopted by various authors.

2.4.1. Fracture Zone model

This model is supported by the Regional Structural Monoclinal Trend (RSMT) mapped by Deane (1995) and is based upon observations from underground mining and extensive exploration data (Kotzé, 2019). It comprises up to five depositional phases illustrated in Figure 2.4.1.

Phase 01

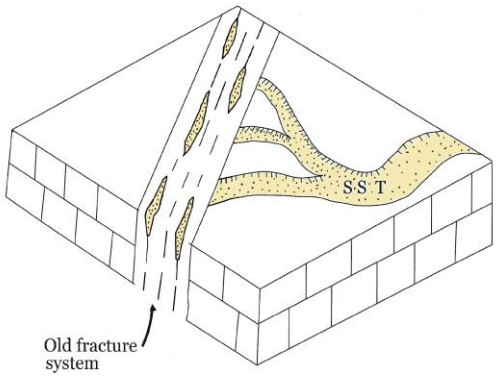

Phase 02

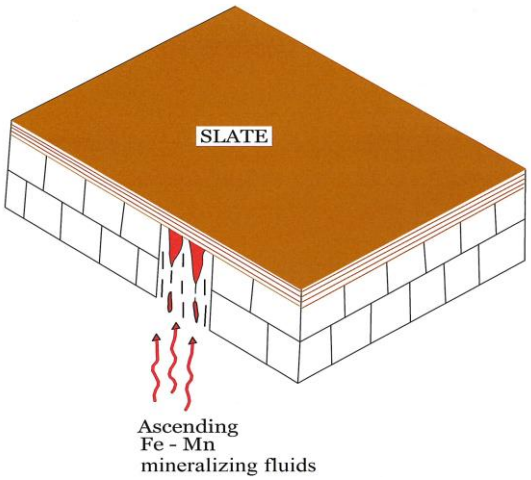

Phase 03

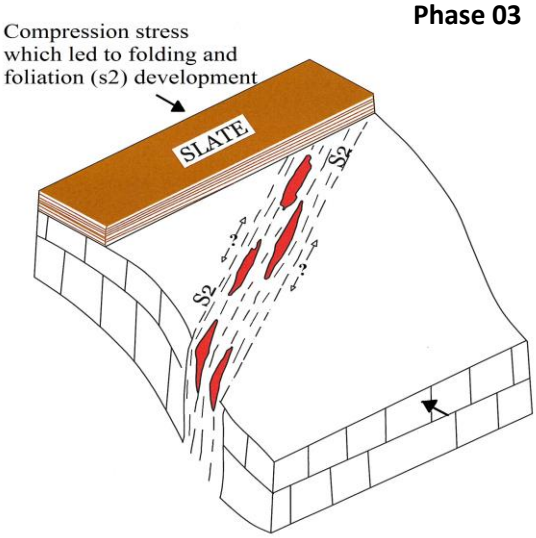

Phase 04

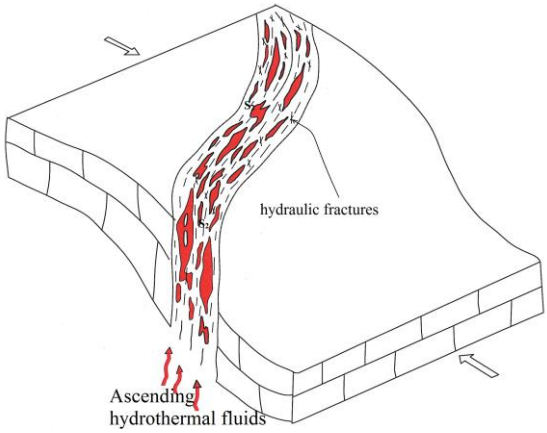

Phase 05

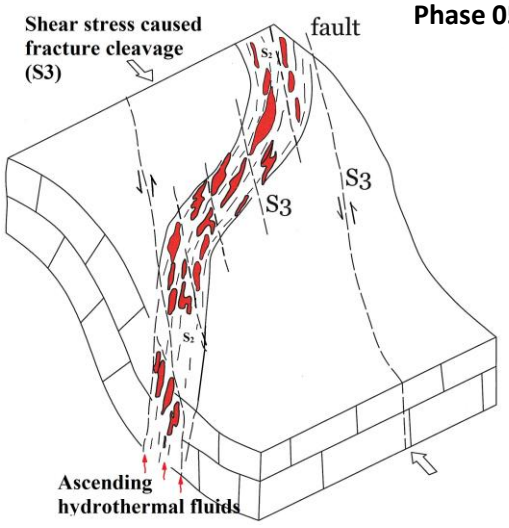

Figure 2.4.1: Block models showing five phases of depositional development of the Kombat-style mineralization. Phase 01: The old fracture system infilled with fluvial sandstones; Phase 02: Deposition of less permeable shale trapped the hydrothermal fluids; Phase 03: Start of deformation which developed foliation (S2); Phase 04: Continuous deformation reactivated old penetrative fractures conduits for ascending hydrothermal fluids rich in Cu and Pb; Phase 05: Continued deformation leads to localized brittle fracture cleavage (S3) confined to fault and shear zones with Cu-Pb (Ag) ore (modified after Kotzé, 2019).

Phase 01: The old fracture system developed cutting through the carbonate (limestone) sedimentary rocks associated with karsts. Subsequently, carbonate karst holes and fractures were infilled with fluvial sandstones which were deposited by the overlying stream system.

Phase 02: Deposition of less permeable shale (now slate) provided a trap for hydrothermal fluids channeled through deep penetrative fracture conduits. The organic nature of the shale provided a reducing environment for the subsequent syn-sedimentary deposition of Fe-Mn mineralization in sandstones and calc-silicate as evidenced by the relicts of depositional layering.

Phase 03: Start of deformation with folding of the Otavi carbonates and shales accompanied by rejuvenation of the old fracture system. This gives rise to the well-developed foliation (S2) seen in the layered Fe-Mn bodies.

Phase 04: Continuous deformation from Phase 03 with reactivated old penetrative fractures acting as conduits for ascending hydrothermal fluids, rich in Cu and Pb with minor Zn and Ag, caused hydraulic fracturing.

Phase 05: Continued deformation leads to localized brittle fracturing centered on areas of weakness and highest deformation, rather than in the adjacent rocks. These localized fault and shear zones are defined by fracture cleavage (S3) and contains most of the Cu-Pb (Ag) mineralization (Kotzé, 2019).

2.4.2. Roof Pendants (Ore lenses) Hanging on Rollover Structures model

The model was first documented by Galloway (1988) based on data limited to the upper levels of some underground mining stopes, but none of the drill sections could support the model (Kotzé, 2019). The model comprises two phases:

1) An earlier phase of stratiform emplacement of the Fe-Mn oxide/silicate assemblages on the carbonate platform margin during a final rifting stage.
2) The second phase of stratabound and syntectonic Cu-Pb (Ag) mineralization related to the Damara Orogeny (Figure 2.4.2).

In addition, the model is characterized by karstic roof pendants (ore lenses) hanging on rollover structures along a Regional Structural Monoclinal Trend (RSMT) plunging at $270^{o}/10^{o}$.

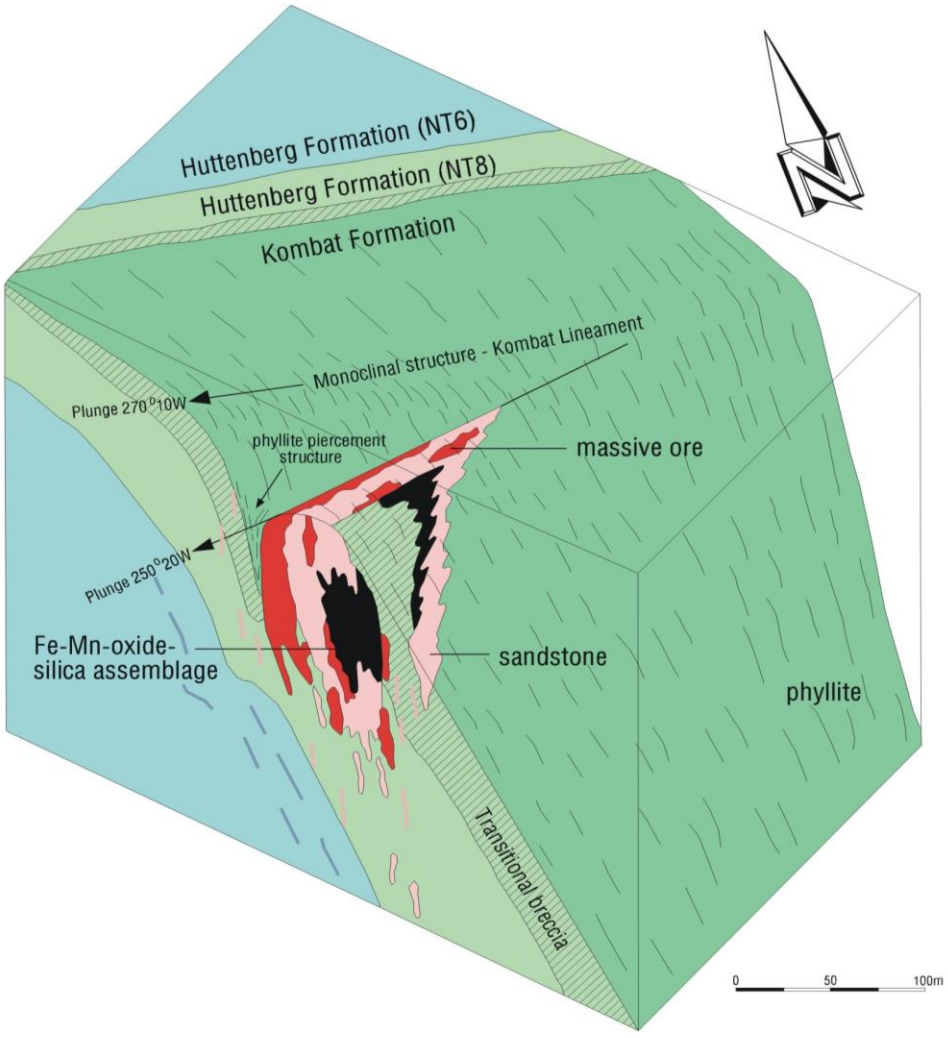

Figure 2.4.2: Regional Structural Monoclinal Trend (RSMT) and "Roof Pendants" (Ore Lenses) Hanging on Rollover Structures model (modified after Galloway, 1988) (Image source: Geological Survey of Namibia).

2.5. Mineralogy of the Kombat deposit - published minerals

A list of minerals found in the Kombat area was compiled from various studies, encompassing 129 minerals of which 16 have been first described from Kombat type locality (Kombat, Grootfontein, n.d.). The list is predominantly composed of oxides and

hydroxide minerals of carbonate/calcite amorphous varieties of minerals such as hydroxylapatite (carbonate-rich hydroxylapatite) and albite (oligoclase). Base metal sulfide ore minerals mostly copper, lead, manganese, iron, as well as zinc and silver appeared in several kinds of literature including Changara (2009); Chukanov (2018); Dunn (1986); Hawthorne (2013); Innes and Chaplin (1986); Bowell et al. (1998).

3. RESEARCH METHODS

This study was based on geochemical and mineralogical studies of ore and host rock samples from the Kombat Mine and the samples collection of the National Earth Science Museum, Windhoek.

3.1. Research Design

The study employed quantitative geochemical analysis of a suite of elements, as well as optical mineralogical studies to identify ore minerals from different ore zones (Fe-Mn and Cu-Pb (Ag)), the associated gangue minerals, mineral textures and their mode of occurrence (distribution). Finally, fluid compositions and pressure-temperature conditions were established through from fluid inclusion studies in order to confirm the depositional conditions of the Kombat-style mineralization.

3.2. Research Instruments

Field investigation and sampling involved the use of a geological hammer, geographic positioning system (GPS) and geological compass. GSN laboratory equipment such as a jaw-crusher, ball-mill and polishing machines (Logitech PM2 and LP50) were used for

sample preparation. Furthermore, a portable X-ray fluorescence (Niton XL3t) and a reflected light microscope (Olympus BX 51) were utilized for sample analysis. X-ray diffraction spectroscopy (XRD) was carried out at the University of Cardiff (UK), and the heating and freezing stage (Linkham TH 600 stage) at Queens University (Canada) were used for mineralogical and fluid inclusions analysis, respectively.

3.3. Procedure

Collectively, fifty rock samples from the Kombat Mine (Appendix 1A) and the National Earth Science Museum (Appendix 1B) were used in this study. The samples from the mine were collected during a three-week field observation period. The samples were split into halves, one half being crushed and milled (<75 μm fraction) to provide homogeneous pulp for XRF whole-rock geochemical analysis to address *Objectives 1.3 (a),* i.e. to establish suitable geochemical signatures which can be used in exploration and, *(b),* i.e to re-evaluate the genetic model of the Kombat polymetallic deposit. A fraction of some of the pulp samples were used for XRD analysis to determine the mineralogical composition of the rocks and subsequently aid in addressing *Objective 1.3 (b).* From the remaining rock samples, polished blocks and thin sections were prepared up to 20 microns for microscopic analysis to determine the nature of the ore, accessory and gangue minerals as well as the mineral paragenesis and microstructures to develop an integrated exploration model for Kombat-type deposits (*Objective 3.1 (c)).* Gangue minerals (calcite, quartz) were sampled for fluid inclusions analysis in order to establish the conditions of ore formation, required for (Objective 3.1 (b)) classification of the

genetic deposit type. The generic deposit class aids to develop a distinct exploration model (*Objective 3.1 (c)*).

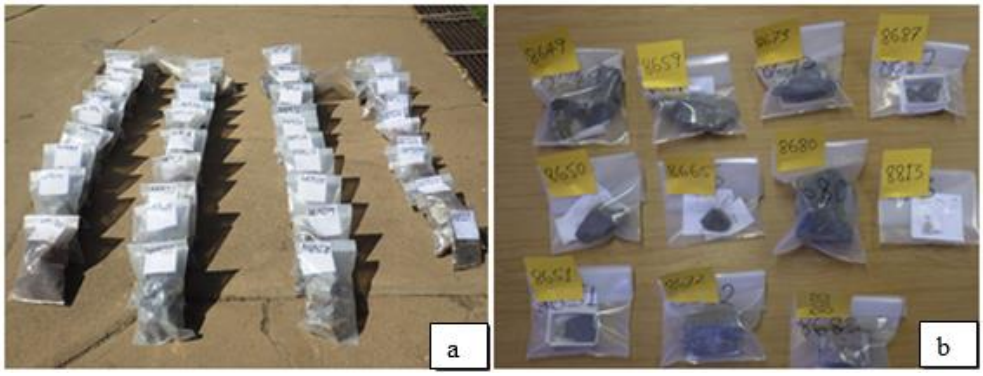

Figure 3.3.1: Shows the bags of rock samples; a) Samples collected from the Kombat Mine during field investigation; b) Samples from the National Earth Science Museum, Windhoek.

3.3.1. XRF sample analysis

A total of forty (40) pulp samples (<75 μm fraction) including four (10% of total samples) in-house standards were subjected to portable XRF whole-rock analysis in order to determine major and trace elements. The process involved filling up a sample holder, covered with a thin plastics film at the top and a sample label at the bottom (Figure 3.3.2). Each pulp sample was placed in the measuring compartment for 120 seconds at mining mode (%) with a portable XRF instrument at the GSN's geochemistry laboratory.

Figure 3.3.2: Sample holders containing the pulp samples ready for analysis (red labeled samples are standards).

3.3.2. XRD sample analysis

A fraction of the material of each of the thirty-two (32) pulp samples was selected for XRD analysis carried out at the University of Cardiff with the assistance of Prof R. Bowell in order to determine mineralogical composition of ore and host rocks.

3.3.3. Optical mineralogical analysis

Twenty-five (25) rock samples were polished up to 20 microns blocks and thin sections using the polishing machines (Logitech PM2 and LP50) at the GSN laboratory. The blocks and thin sections were examined under the reflected/transmitted light microscope in order to determine the nature of ore, accessory and gangue minerals, as well as mineral paragenesis and microstructures.

3.3.4. Fluid inclusions studies

A total of nine (9) gangue mineral samples, mainly quartz and calcite crystals, were selected for fluid inclusion studies. Each sample was placed in the heating and freezing stage chamber (Linkham TH600 stage) which was connected to the microscope for observation of fluid bubbles (liquid). The stage was set at fixed heating rate of 90 ºC per minute, then reduced to 1 ºC per minute close to the point when the bubble (liquid) and the rock (solid) phases start to homogenize into a solution. This temperature was then recorded as the homogenization temperature, representing the minimum temperature of formation. The stage cooled until frozen with N2 gas. Once the solution freezes, the temperature is taken and related to NaCl % solution based on the Shepherd (1981) method (Shepherd, et all., 1985).

4. RESULTS

4.1. Field Observations

The field investigation and sampling was conducted in the open pits particularly the Kombat Central pit, the Iron-Manganese pit near Shaft 03, the 900 East pits (three pits relatively close to each other) and also at the OMEG pits around Gross Otavi. Five (5) rock samples were collected from the Kombat Mine underground level 2, the Asis Far West shaft development dumps, and from surrounding mineralized hills (Figure 4.1.1). The ore samples represented vein-type to breccias and disseminated mineralization, whereas those collected from underground (Appendix 1A) appear to consist of massive sulfide ore minerals.

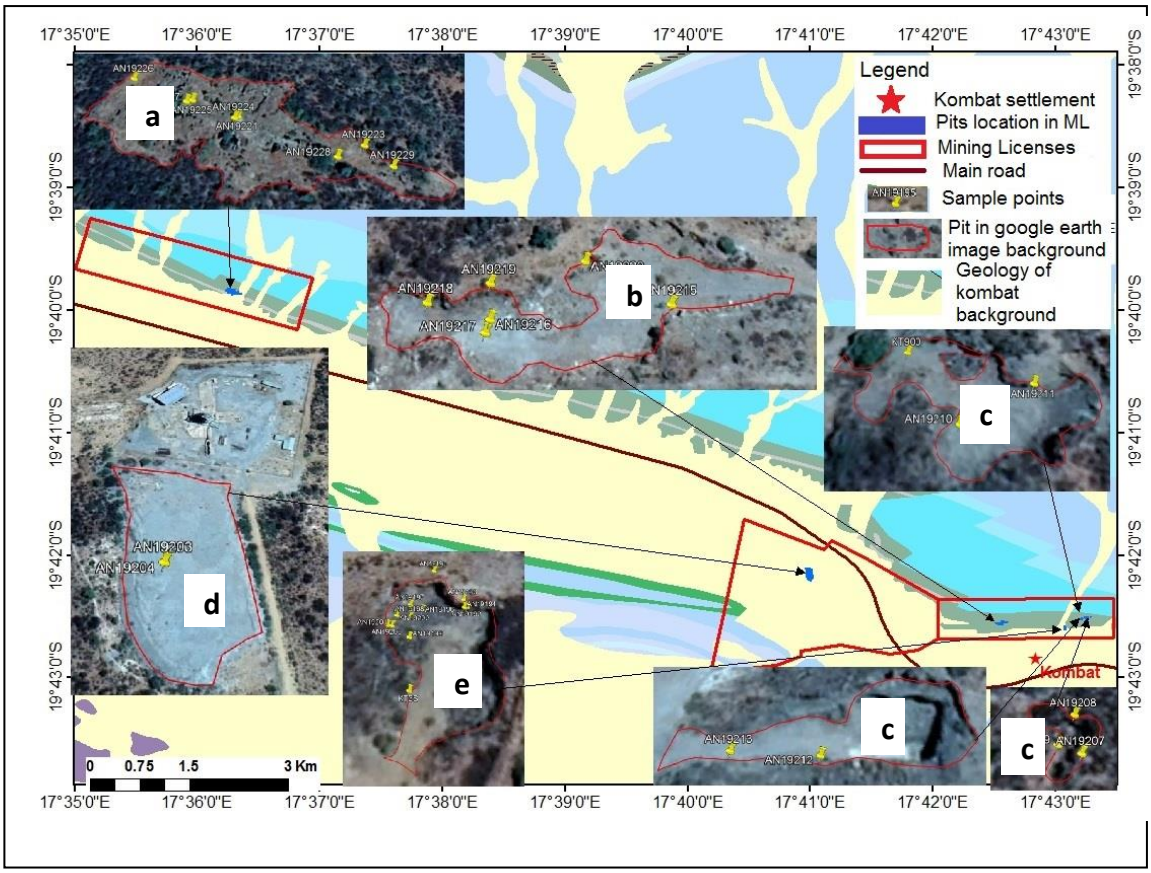

Figure 4.1.1: Sample points (indicated by yellow pins) at the Kombat and Gross Otavi mine pits (pit areas outlined by fade red polygons); a) OMEG pits, b) Kombat Central pit, c) 900-East pits, d) Asis Far West dumps, e) Iron-Manganese pit.

4.1.1. Kombat Central pit

The approximately 100 m long and 50 m wide, but shallow pit of about < 10 m depth (Figure 4.1.1b), contains mostly veins up to 5 cm thick to breccia-textured copper ore minerals. Copper ore is dominated by chalcopyrite, bornite, chalcocite and malachite closely associated with euhedral calcite crystals (Figure 4.1.2 a), minor ferruginous chert and quartz gangue minerals. Also, iron-manganese minerals are hosted in the reddish-

brown hematite/goethite and black manganese oxide dendrites (Figure 4.1.2 b). These minerals are hosted by brecciated, fractured, and bedded to laminated grey dolostone interbedded with laminated dark-grey ferruginous calc-silicate rocks, where bedding (S_0) dips at 45^o to the southwest (S_0: 45^o/198^o) (Figures 4.1.2 c & d). Some 15 cm thick lenses of mainly chalcopyrite, bornite, chalcocite and minor azurite, chrysocolla and malachite ore are found along relative steep fault planes, where the faults dip at moderate to steeply to the southwest (F: 72^o/190^o) (Figure 4.1.2 e & f). Both ore and gangue (quartz, calcite) minerals were sampled for geochemical analysis and fluid inclusions studies, respectively.

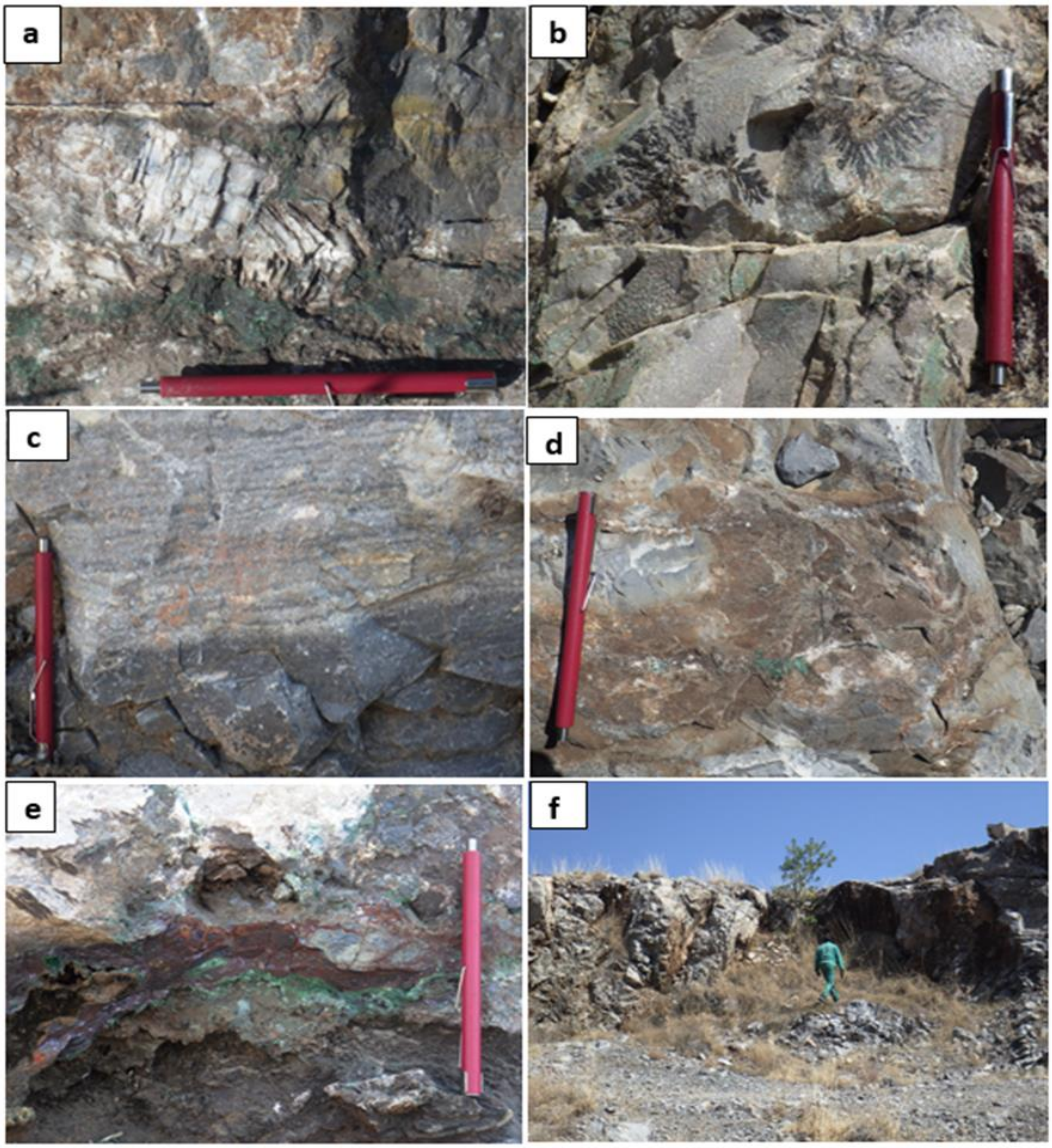

Figure 4.1.2: Central pit observations; a) 15 by 5 cm long euhedral calcite surrounded by malachite and ferruginous chert; b) dendritic manganese oxide stains on the calc-silicate rocks; c) bedded to laminated dark-grey dolostone interbedded with calc-silicate rocks; d) 2 cm wide, malachite veins closely associated with calcite and quartz gangue minerals; e) 15 cm wide chalcopyrite, bornite, chalcocite and azurite lenses stained with

chrysocolla and malachite along the fault plane; f) mineralization controlling fault striking towards the west direction.

4.1.2. Iron-Manganese (Fe-Mn) pit

Next to Shaft 03, Fe-Mn ore is exposed on the walls of a 50 m diameter pit in bands up to 6 m wide alternating with narrow (40 cm wide) breccia zones. The Fe-Mn rich calc-silicate layers contain a paleo-cavity/karst of 1m diameter and 1.5 m high, filled with Cu-ore including malachite, azurite and hematite, gangue minerals such as goethite, limonite, and calcite have been observed (Figure 4.1.3 a, a' and a"). A patch of light-grey sandstone that host traces of pyrite dissemination sites adjacent to the cavity (Figure 4.1.3 b, b'). The calc-silicate layers host bedded Fe-Mn ore that predominantly consists of coarse, dark-grey magnetite which is strongly magnetic and reddish-brown hematite (Figure 4.1.3 c & c'), and alternating with light-brown to creamy dolostone layers containing disseminated to veins of bornite, chalcopyrite sits alongside the breccia zone (Figure 4.1.3 d, d'). The weathered gossan outcrop similar to the aforementioned bedded Fe-Mn calc-silicate hosted ore was observed outside the pit (Figure 4.1.3 e & e'). Most of the copper ore minerals appear localized to a shear fractures crosscutting the light-brown dolostone. The moderate to steeply southwest-dipping shear fractures (F: 80º/178º; 76°/209°; 80°/180°) contain traces of chalcopyrite, bornite, galena and malachite coating. Relicts of presumably sedimentary bedding is preserved by the siliceous dolostone and calc-silicate and contains shear sense such as sigma clast-tails, ladder veins or tension gashes of a reverse fault system (Figure 4.1.4).

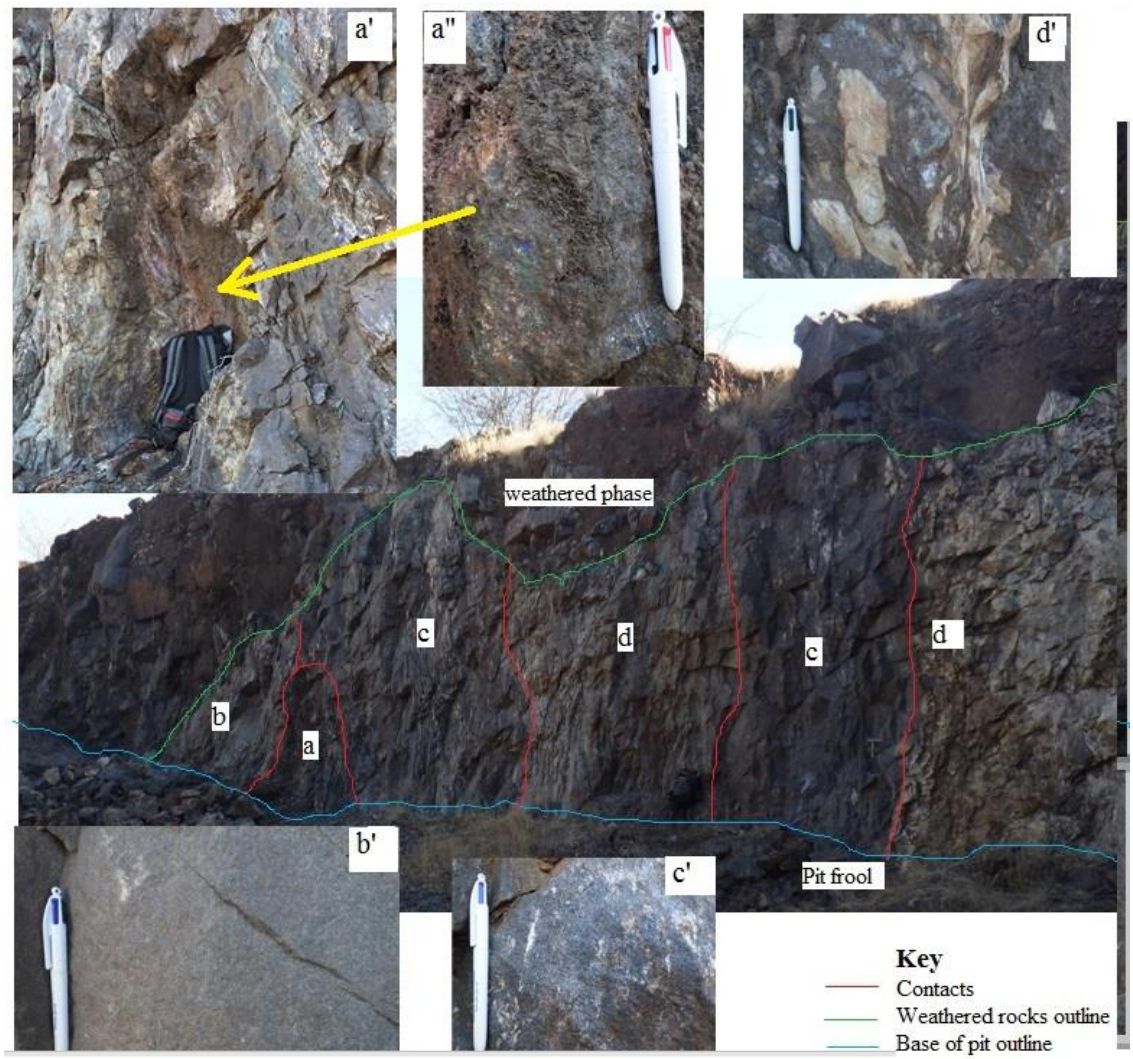

Figure 4.1.3: Fe-Mn pit observations and their zoom in sections; a) Cavity a' with Cu ore minerals a", b) Sandstone b', c) Layered calc-silicate with magnetite c', d) Brecciated calc-silicate d' and dolostone contact zone.

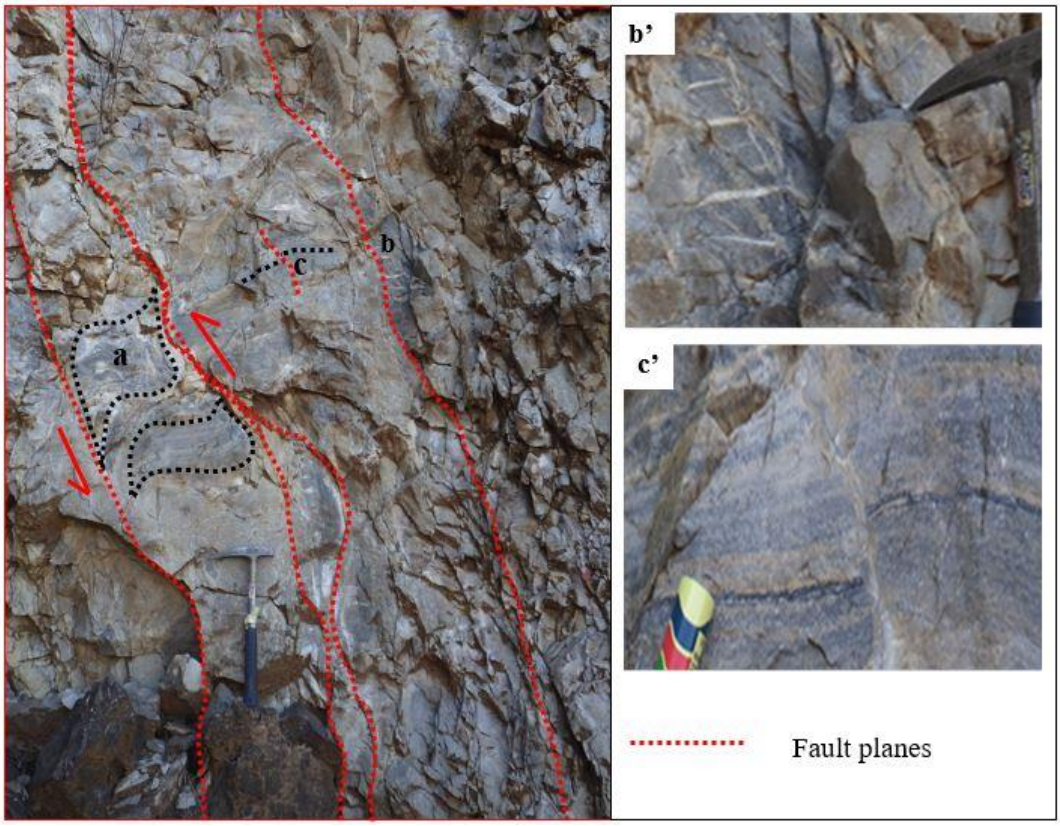

Figure 4.1.4: Sense of shear and evidenced of displacement for a reverse fault system: a) Sigma clast-tails; b) ladder veins / tension gashes with a zoom in b'; c) Fault offset in the calc-silicate layers, zoomed in c' (Looking towards the east direction).

4.1.3. 900-East pits

The three open pits are located within 50 m of each other, ranging in size from 20 to 50 m in diameter (Figure 4.1.1 c). Pit walls consist of well-exposed remnants of laminated, folded calcsilicate layers that contain malachite. A massive-fractured grey dolostone contains both veins and disseminations of chalcopyrite, bornite chalcocite, and galena (Figure 4.1.5 a, b). Occasionally, patches of white calcite crystals are closely associated with quartz and disseminations of ore minerals including galena, pyrite, and

chalcopyrite. Also the ore minerals form rims around the white calcite crystals (Figure 4.1.5 c, d). Fault and cavities structures are exposed on the walls of the pits. The cavities contain matrix-supported ferruginous breccia with recrystallized calcite up to 25 cm wide, dark-grey (smoky) to white crystals that are associated with the malachite (Figure 4.1.5 e). At some places, the cavities appear to be connected by very steep fracture planes (F: 90º/205º), of a fault system (Figure 4.1.5 f), which could be justified by the presence of unmineralized calcite tension gashes (ladder veins) shown in Figure 4.1.5 g.

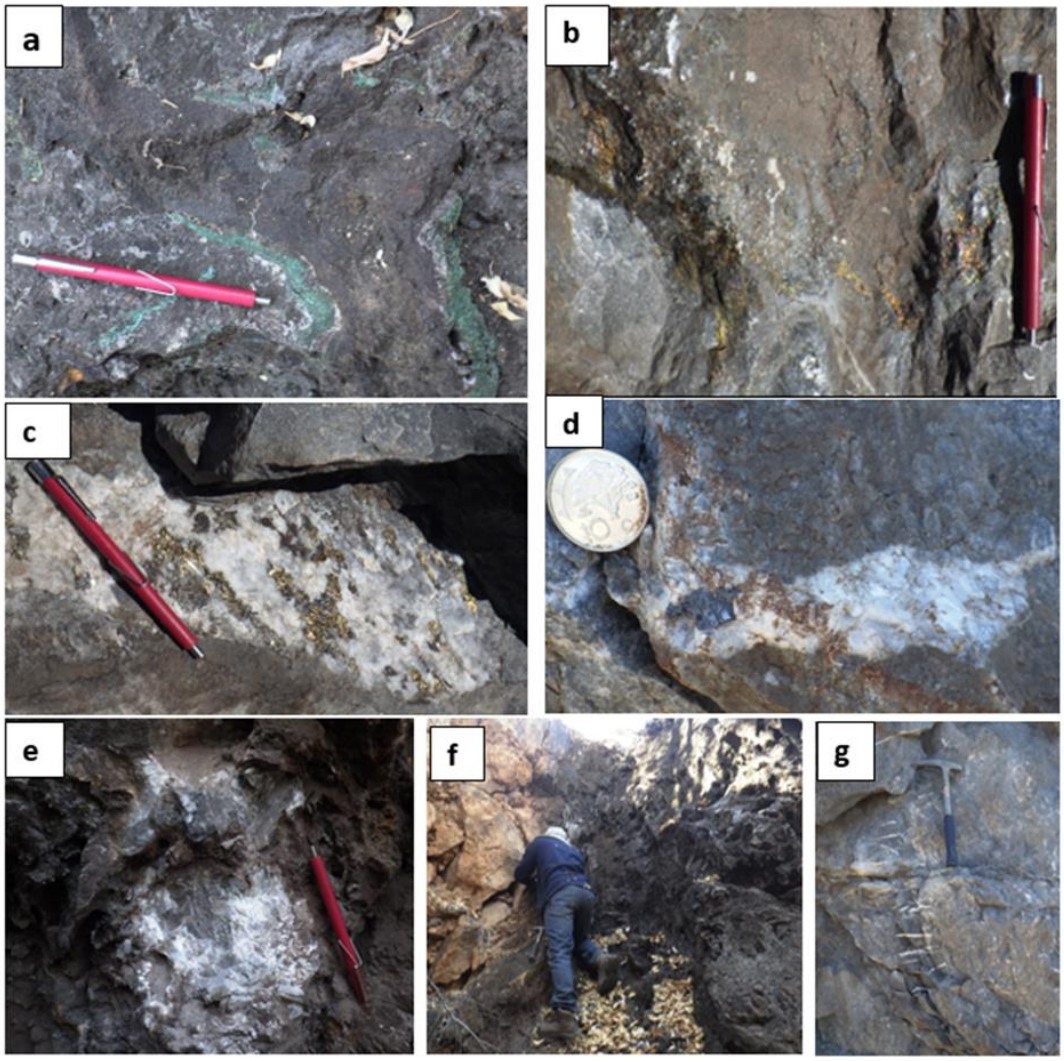

Figure 4.1.5: 900-East pit observations; a) folded malachite veins in calc-silicate; b) grey dolostone with chalcopyrite, bornite, chalcocite and galena veins; c) calcite crystals closely associated with quartz, galena and chalcopyrite fracture fillings; d) calcite with galena crystals; e) smoky calcite crystals in ferruginous breccia; f) fractured fault plane (looking towards the east direction); g) calcite tension gashes.

4.1.4. Asis Far West Shaft development dumps and hill outcrop

The shaft development dumps (Figure 4.1.1d) contain vein- to dissemination-type copper ore consisting mostly of chalcopyrite and bornite with minor chalcocite and surface malachite stains; two random grab samples were collected from this location (Figure 4.1.6 a). Also, a brecciated dolostone hill located at 1.2 km distance south-west from the shaft contains chalcocite and malachite mineralization in karst fractures, and the mineralization is associated with reddish ferruginous chert as well as recrystallized euhedral white calcite crystals (see below: Figure 4.1.6 b).

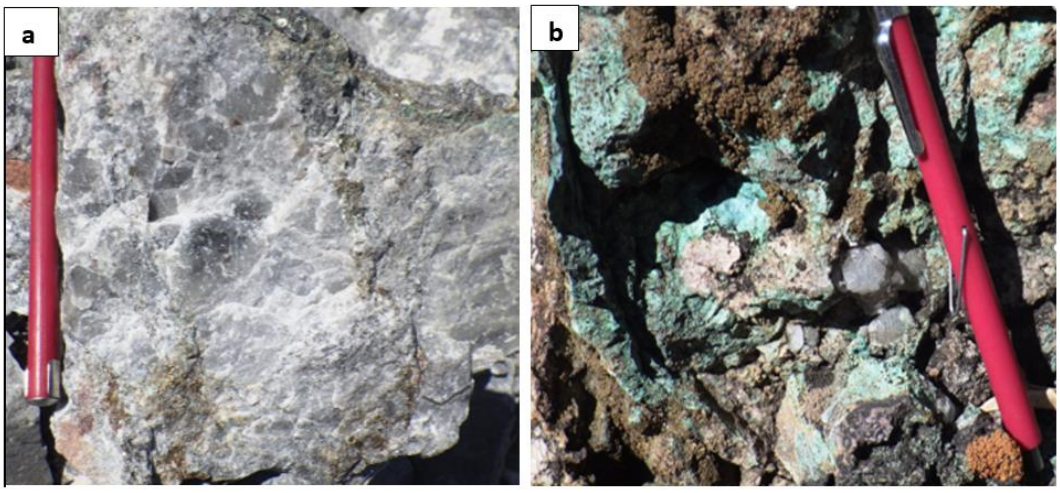

Figure 4.1.6: Asis Far West observations; a) veins of chalcopyrite and bornite from the shaft development dumps; b) chalcopyrite and malachite mineralization in karst fractures and associated with ferruginous chert and euhedral white calcite crystals.

4.1.5. OMEG Gross Otavi pits

Several historically mined narrow pits of about 4 m wide to 30 m long (Figure 4.1.7 a) are in the laminated (S_0: 41°/226°), fractured to brecciated grey dolostone with ferruginous chert. The dolostone contains the paleo-cavities that appear interconnected by steep fault planes (F: 90º/205°; 65°/178°). These cavities are characterized by a reddish-brown ferruginous and matrix-supported breccia deposit containing chalcocite, malachite and hematite ore associated with quartz and calcite gangue minerals (Figure 4.1.7 b). Also, some black manganese detritic structures as well as euhedral to subhedral quartz veins have been observed (Figure 4.1.7 c) and sampled for fluid inclusions analysis. One kilometer further to the west, an adit cut into a hill of laminated grey, ferruginous chert dolostone hosting chalcocite, malachite mineralization along the ramp roof proved unsafe for sampling. But, along the ramp wall is a well-exposed botryoidal shaped unit of brownish calc-silicate and whitish siliceous surfaces (Figure 4.1.7 d), that was sampled.

Figure 4.1.7: OMEG Gross Otavi pits observations; a) historically mined narrow pits (looking towards the west direction); b) matrix-supported breccia deposit of chalcocite, malachite and hematite ore; c) euhedral to subhedral quartz crystals within the quartz veins; d) botryoidal-shaped unit of brownish calc-silicate in the Gross Otavi adit.

The structural measurements such as bedding, lamination planes (S_0) where compared to the mineralized fault and shear fractures (F) on a stereo net analysis. The fault and shear fractures turned out steeper dipping (Figure 4.1.8 a) with an average fracture plane of F: 79°/195°, while bedding and lamination planes S0: 44°/205° are relatively shallow dipping (Figure 4.1.8 b).

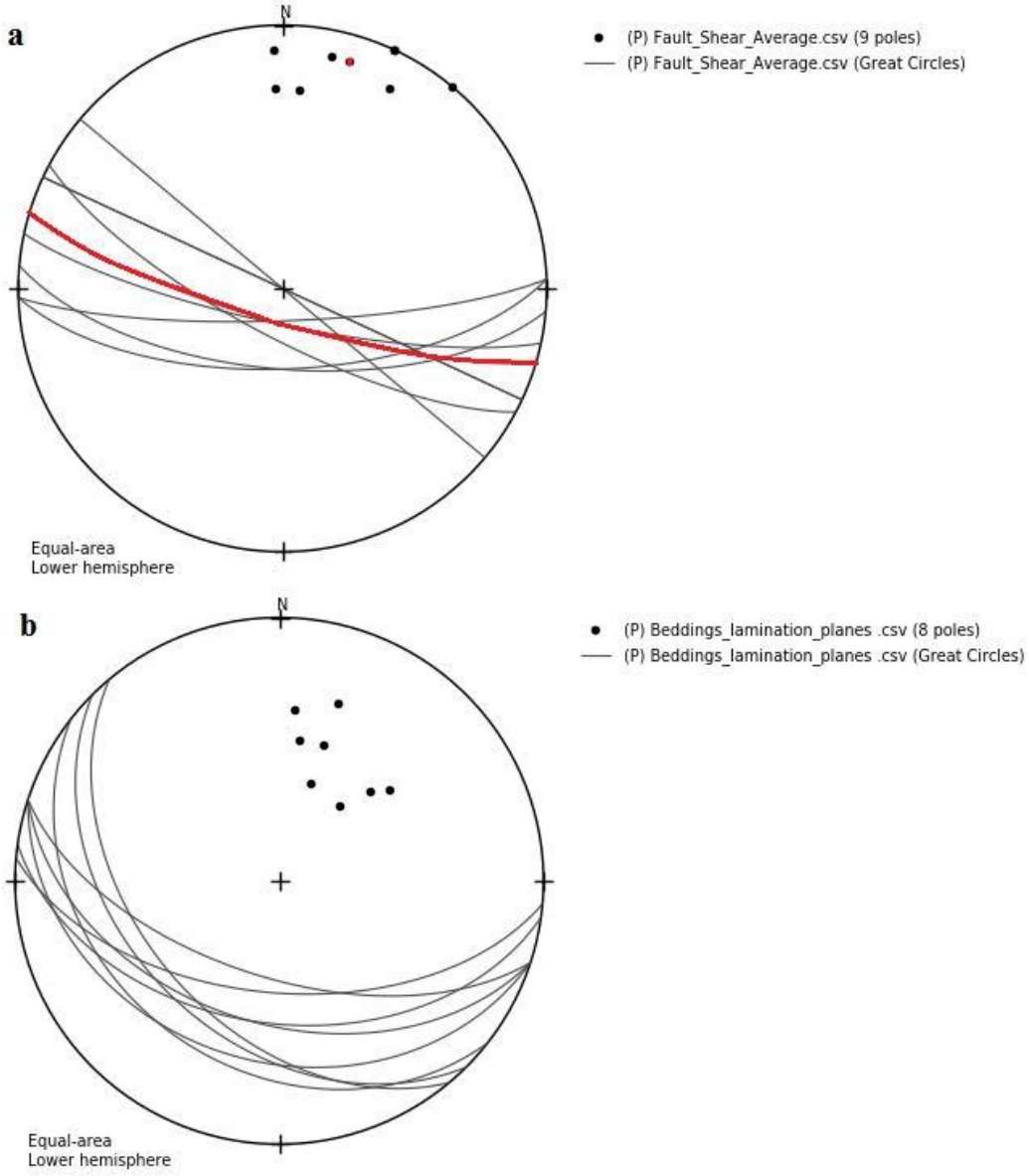

Figure 4.1.8: Structural analysis of field measurements: a) Fault, Shear fractures with an average plane in red (F); b) Sedimentary beddings and laminations (S_o).

4.2. Mineralogy

4.2.1. XRD

Sixty (60) minerals were identified in the Kombat samples based on XRD results obtained from Prof Rob Bowell (Appendix 2B). The minerals list contains major Cu-Pb (Ag-Zn-V) ore mineral chalcopyrite, bornite, covellite and galena, with minor chalcocite, and sphalerite; the major Fe-Mn ore minerals are hausmannite and hematite with minor pyrite, jacobsite, manganite, magnetite, pyrolusite, rhodonite, and pyrobelonite. Associated gangue minerals are dominated by dolomite, quartz, calcite, ankerite, illite, and defrenite with minor albite, biotite, chlorite, kaolinite, muscovite, epidote, anhydrite, gypsum, langite, and allegrite; the rest of the minerals occur in trace quantities.

4.2.2. Optical mineralogy

Twenty-five (25) polished blocks and thin sections were investigated under a transmitted light microscope to establish the textures and paragenetic sequence of the ore and gangue minerals. On the polished surface, there is a bluish metallic luster from bornite and in some places, a yellowish tint from chalcopyrite can be discerned. Examples of the ore minerals from samples collected in the field and National Earth Science Museum are shown in Figures 4.2.1 and 4.2.2.

4.2.2.1 Ore minerals

The polished blocks viewed under 20-micron magnification of reflected light microscope (Figures 4.2.1 and Figure 4.2.2) indicated the brown bornite (Bn) is the dominant ore mineral, followed by yellow to orange chalcopyrite (Cp). Both bornite and chalcopyrite being replaced by light-brown twin lamellae of chalcocite (Cc). The bluish covellite (Cv) exsolution lamellae emerges out of chalcocite and bornite, also some covellite veins cross-cut bornite, chalcopyrite, and chalcocite but, are terminated by faint-yellowish or creamy pyrite (Py). Hence, the copper ore minerals observed could be arranged into the following paragenetic sequence:

Bornite (Bn) →Chalcopyrite (Cp) →Chalcocite (Cc) →Covellite (Cv) →Pyrite (Py).

Iron and manganese ore minerals viewed under reflected light (Figure 4.2.1 f) reveal foliated hausmannite (Hs), coexisting magnetite (Mt) and pyrite (Py); Hematite (Hm) and jacobsite (Jb) appear as exsolution lamellae within the syn-sedimentary chalcopyrite generation, which is associated with bioturbation (Figure 4.2.1c). Hence, the overall paragenetic sequence would be:

Syn-sedimentary (iron-manganese + copper) →Hydrothermal (copper primary ore minerals)→ Secondary copper ore minerals→ Alteration of secondary ore minerals (supergene enrichment).

In other words, paragenetic sequence of Kombat deposit (Table 1) is summarized as follows; Hausmannite (Hs), magnetite (Mt), hematite (Hm), chalcopyrite (Cp), Jacobsite (J), (syn-sedimentary bedded and cross cut by S2) → Bornite (Bn), chalcopyrite (Cp), pyrite (Py), hematite (Hm), and galena (Gl) (galena is observed in hand specimen, see

Figure 4.1.5 d) (hydrothermal associated with fractures) → Chalcocite (Cc), covellite (Cv), Bornite (Bn), exsolution, pyrite (Py) hematite (Hm), (secondary replacement textures along S3) → Chalcocite (Cc), covellite (Cv) veins, pyrite (Py), malachite (Ml), hematite (supergene enrichment) → Malachite (Ml), hematite (Hm), pyrite (Py) (retrograde during weathering, uplifting conditions).

Table 1: Paragenetic sequence of ore minerals at the Kombat Mine

Ore minerals	Syn-sedimentary banded (S0)	Hydrothermal (fractures)	Secondary (S3)	1st Alteration (Enrichment)	2nd Alteration (Oxides)
Hausmannite					
Magnetite					
Jacobsite					
Chalcopyrite					
Galena					
Bornite					
Chalcocite					
Covellite					
Pyrite					
Hematite					
Malachite					

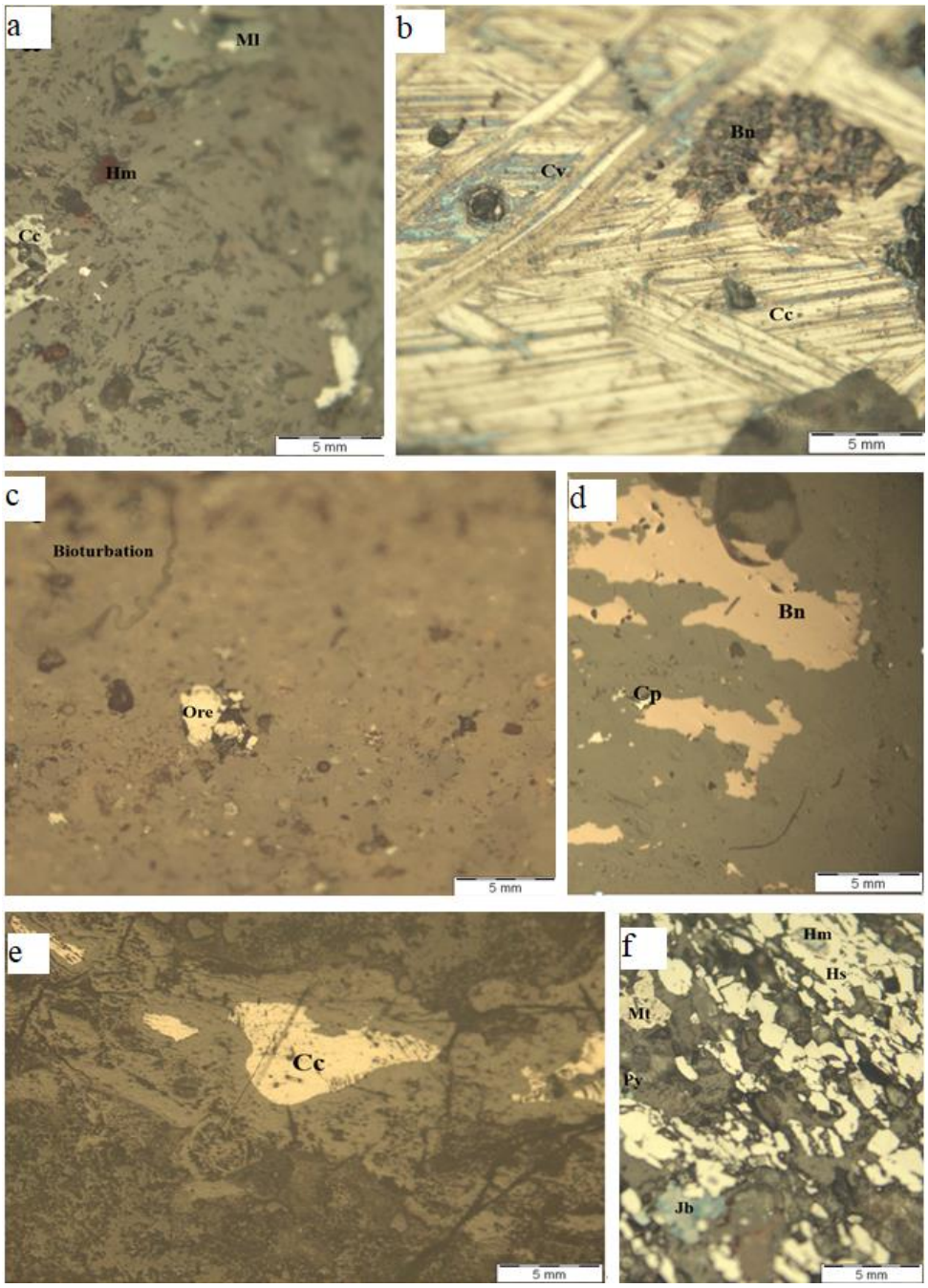

Figure 4.2.1: Field sample ore minerals; a) Sample AN19206: Chalcocite (Cc) surrounded by malachite (Ml) and hematite disseminations (Hm); b) Sample AN19214: Massive chalcocite (Cc) lamellae replacing bornite (Bn) while covellite (Cv) is replacing both bornite and Chalcocite. c) Sample AN19221: Bioturbation (animal

barrow) next to the yellow ore mineral. d) Sample AN19211: Brown bornite (Bn) being replaced by yellow chalcopyrite (Cp). e) Sample AN AN19228: Micro-boudinaged of chalcocite (Cc). f) Sample AN19193: Foliated hausmannite (Hs), magnetite (Mt) pyrite (Py) and hematite (Hm) disseminations with traces of Jacobsite (Jb).

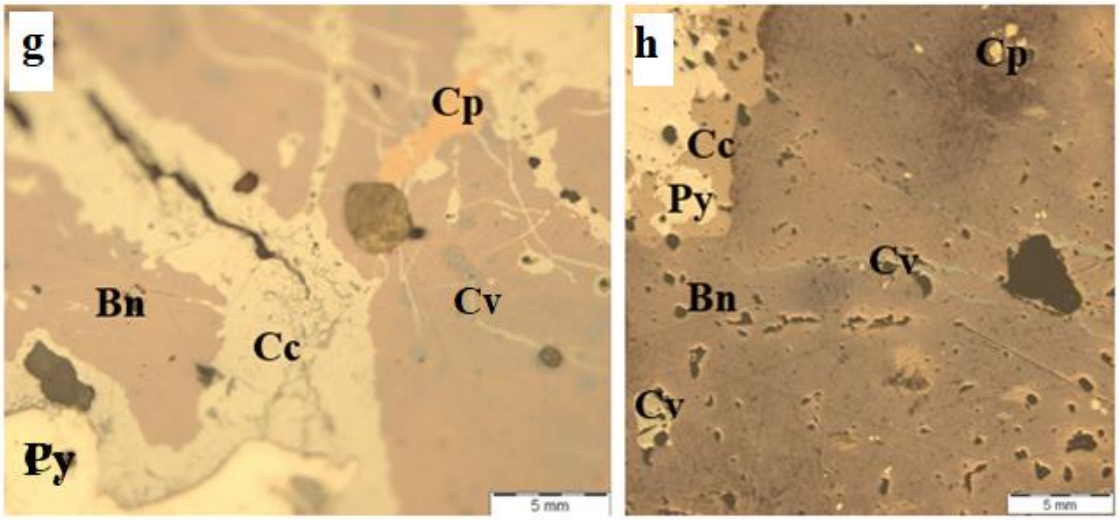

Figure 4.2.2: National Earth Science Museum samples ore minerals; g) Sample 8680: Massive brown bornite (Bn), with exsolved dull-blueish covellite (Cv) and orange chalcopyrite (Cp) replacement of bornite is cross-cut by a vein filled with light-brown chalcocite (Cc) and light-yellow pyrite (Py). h) Sample 8650: Brown bornite (Bn), replaced by chalcopyrite (Cp) and chalcocite (Cc), while covellite veins (Cv) cross-cutting both bornite and chalcocite are terminated by pyrite (Py).

4.2.2.2 Associated Gangue minerals

The petrographic thin sections under polarized light revealed euhedral calcite crystals with lamellae twins, which are completely bounded by distinct crystal faces representing unhindered growth such as crystallization in a hydrothermal fluid, cavity or fault opening, Sample AN19206 (Figure 4.2.3: i). Furthermore, pseudomorphic of amphilole and replaced by ore mineral textures, Sample AN19217 shown in Figure 4.2.3: j, could be related to decompression, particularly to episodes of rapid exhumation during deformation related to Damara collision event, with intergrowths of ore minerals forming at the expense of a previously stable amphiboles. Sample AN19211, Strongly deformed crystal textures such as kinking or bent twin lamellae in calcite/dolomite and partially recrystallized fine-grained polygonal aggregate or cross-cutting subgrain patterns with dendritic inclusion textures of exsolved manganese (Figure 4.2.3 j, k) may represent the brittle-ductile transition textures of deformation. Sample AN19200 and AN19203, granoblastic textures of subhedral and anhedral dolomite, quartz with undulatory extinction, amphiboles with secondary intergrowths of opaque, presumably ore minerals (Figure 4.2.3 l, m) could be due to thermally induced annealing, which created poly-crystalline grain aggregates and dissolution textures(Raith, et. al, 2012). In addition, Sample AN19223 strongly deformed and kinked crystals of dolomite, and Sample AN19223 albite porphyroblasts with sigmoidal inclusion trails defined by tiny calcite and fine-grained muscovite and sericite (Figures 4.2.3 n, o) are strong evidence of rock movements in agreement with the “fracture zone model” (Kotze, 2019).

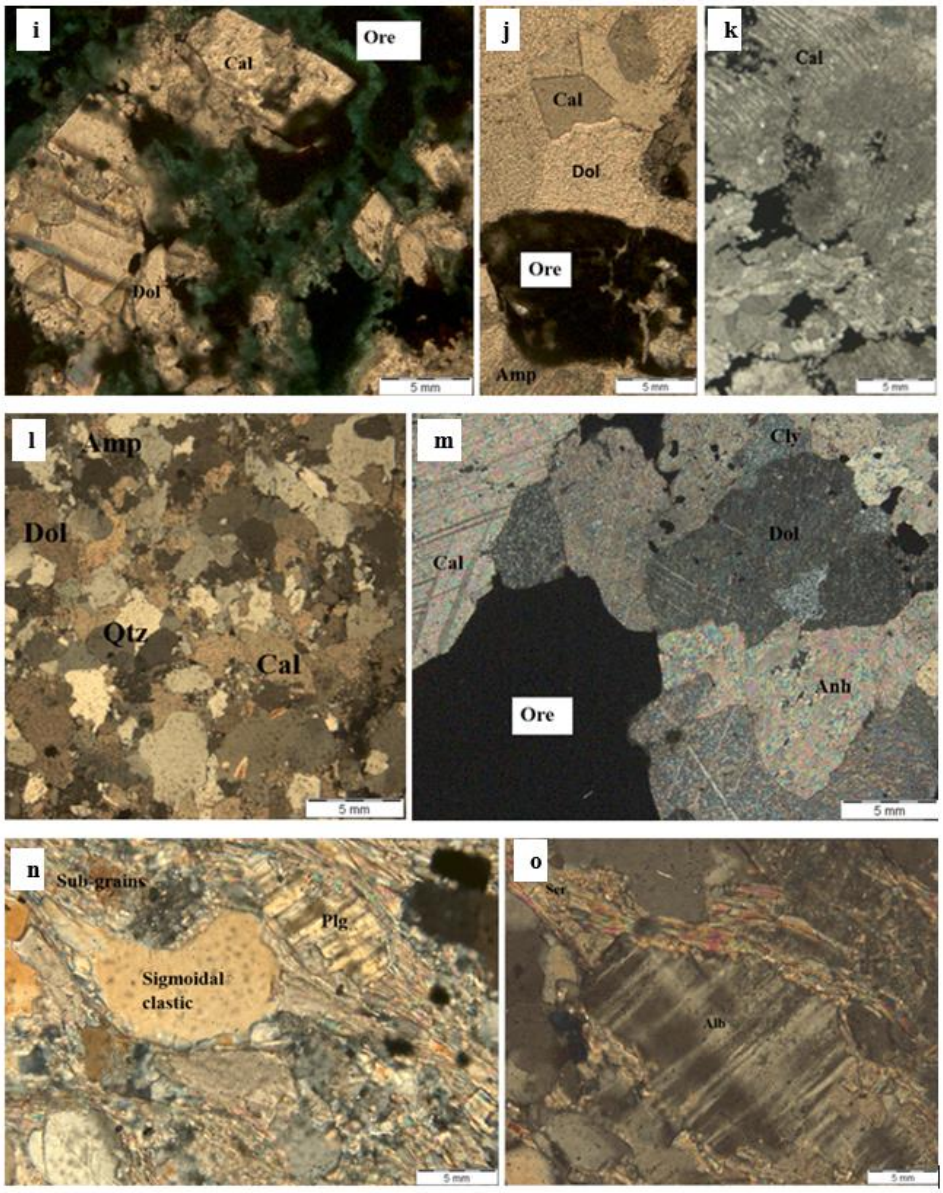

Figure 4.2.3: these are photomicrographs showing gangue minerals in samples; i) Sample AN19206: Euhedral calcite crystals with lamellae twins. J) Sample AN19217: Pseudomorphic replacement of plagioclase and amphiboles by the ore minerals. k) Sample AN19211: Strongly deformed crystals with bent twin lamellae of calcite, subgrain patterns and dendritic textures inclusion; l) Sample AN19200: Granoblastic textures of subhedral and anhedral dolomite, quartz with undulatory extinction, amphiboles with secondary intergrowths of opaque minerals. m) Sample AN19203:

Granoblastic textures of calcite (Cal) with polysynthetic glide twins, dolomite (Dol) with deformation lamellae twins. n) Sample AN19223: Strongly deformed and kinked crystals of dolomite porphyroblasts with sigmoidal inclusion trails defined by tiny calcite. o) Sample AN19223: Sericitization, consumption of the albite (Alb) component produces fine-grained muscovite or sericite.

4.3. Geochemistry

4.3.1. Validation of XRF whole-rock analysis results

The geochemical element analysis results in the Appendix 2A were plotted in Microsoft excel for quality control/quality assurance (QC/QA) using four GSN in-house standards of ST055 (0.5%Cu, 5%Fe); ST25 (2%Cu, 5%Fe); T55 (5% Cu, 5%Fe); and ST205 (20%Cu, 5%Fe). Four blanks B01, B02, B03 and B04 prepared from quartz chips and four duplicates of AN19199, AN19209, AN19219 and 8659 randomly selected from within a group of ten samples arranged according to the increasing sample numbers. The four samples of each QC/QA (blanks/duplicates/standards) group represents 10% of the 40 XRF-analysis results. The QC/QA plots have proven minimal or no contamination which is reflected by the coefficient values (R^2) from 0.99 to 1.0 for copper, iron and manganese shown in Figures 4.3.1 and 4.3.2. The results gave an average wt. %, of Cu: 7.252, Fe: 7.134, Pb: 0.695, Zn: 0.129 and traces of Ag: 0.017.

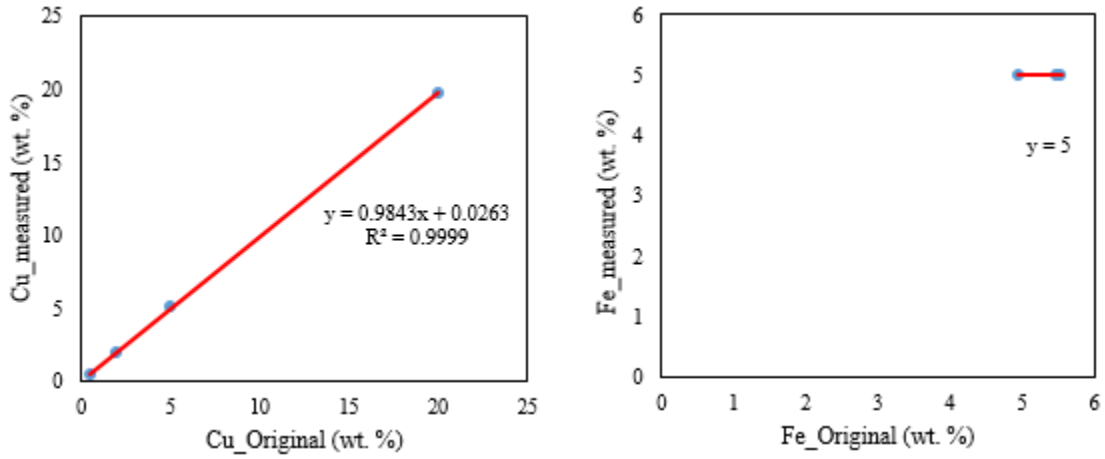

Figure 4.3.1: Plots of the 5 in-house standards original vs measured Cu & Fe -values

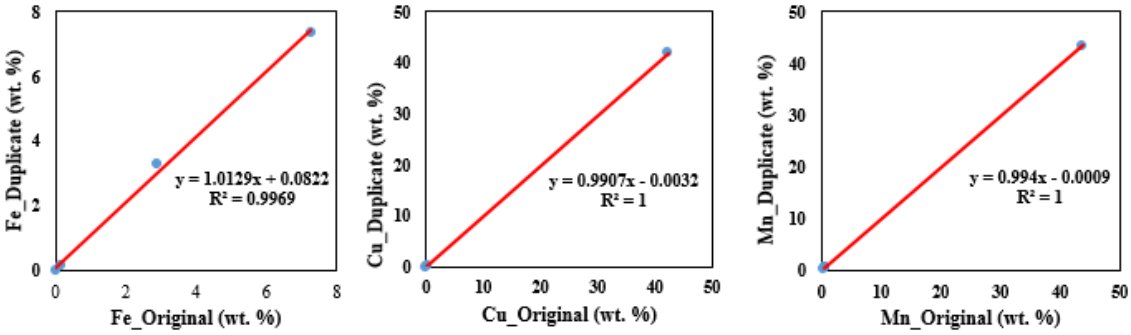

Figure 4.3.2: Original vs duplicate sample measured Fe, Cu and Mn-values.

The Kombat samples plotted on sedimentary rocks discriminant ternary diagram (Figure 4.3.3) fall within a hydrothermal field, with a few samples mostly from the National Earth Science Museum, plotting in the diagenetic field. Another group plotted in the mixed hydrothermal- diagenetic- hydrogenetic field. On sample locality ternary diagram plots (Figure 4.3.4), Central pit, Asis Far West, and 900 East pits reflected the predominant hydrothermal field. Also, dual fields of hydrothermal-diagenetic were observed for the samples from the museum. While some samples from Fe-Mn and OMEG pits indicated mixed fields of hydrothermal-hydrogenetic-diagenetic.

a

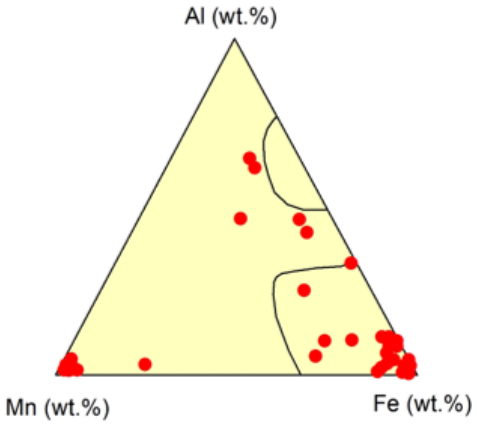

b

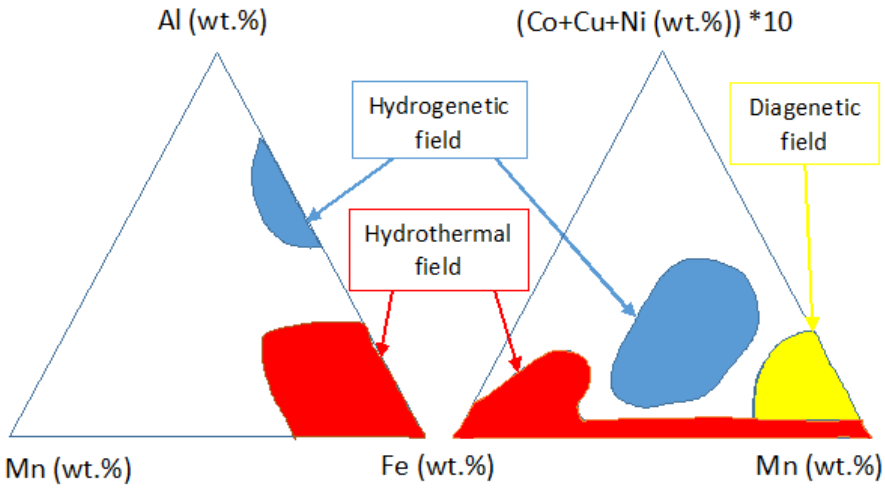

Figure 4.3.3: Comparison of the sedimentary rocks discriminant ternary diagrams; a) Kombat deposit samples; b) Theoretical sedimentary rocks discriminant ternary diagram for Hydrogenetic, hydrothermal and diagenetic fields from modern ferromanganese deposits (after Boström, 1973) adopted from Lechte, et al. (2019)

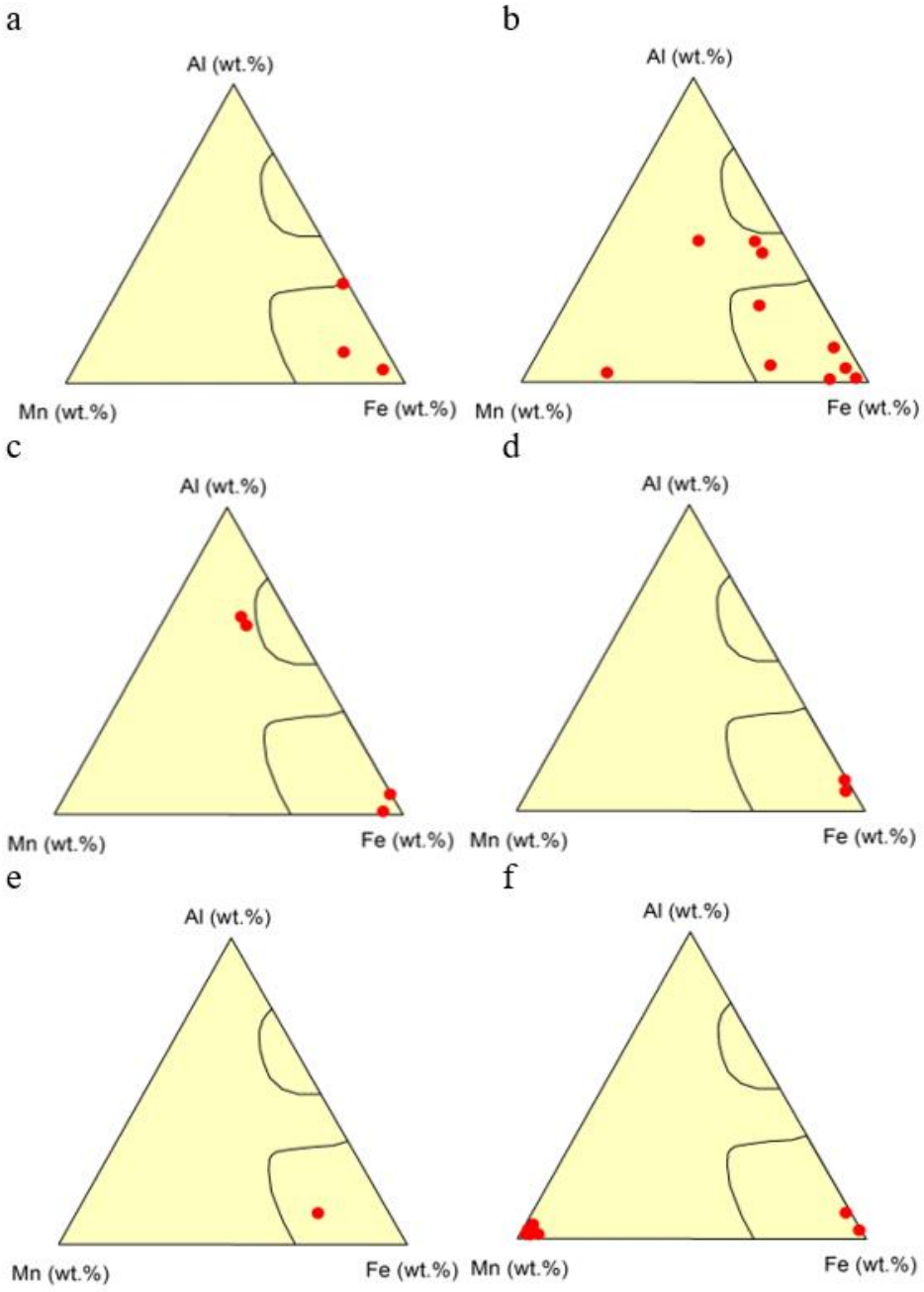

Figure 4.3.4 The Fe-Al-Mn ternary diagram of hydrothermal element provenance of sedimentary rocks (Boström, 1973) plots for Kombat Mine sampled localities: a) Central Pit; b) Fe-Mn Pit; c) OMEG pits; d) Asis Far West; e) 900 East pits; f) National Earth Science Museum.

Plots of Pb-Cu-Zn fields (Figure 4.3. a), are compared to the discriminant ternary diagrams (Figure 4.3.5 b) of VMS/SEDEX (after Franklin *et al*., 1986) as a reference therein Volesky *et al*. (2017) and Bailie *et al*. (2011). Many samples plotted in the Cu-Pb field which is clearly distinct from VMS deposit (Mousivanda *et al*., 2018).

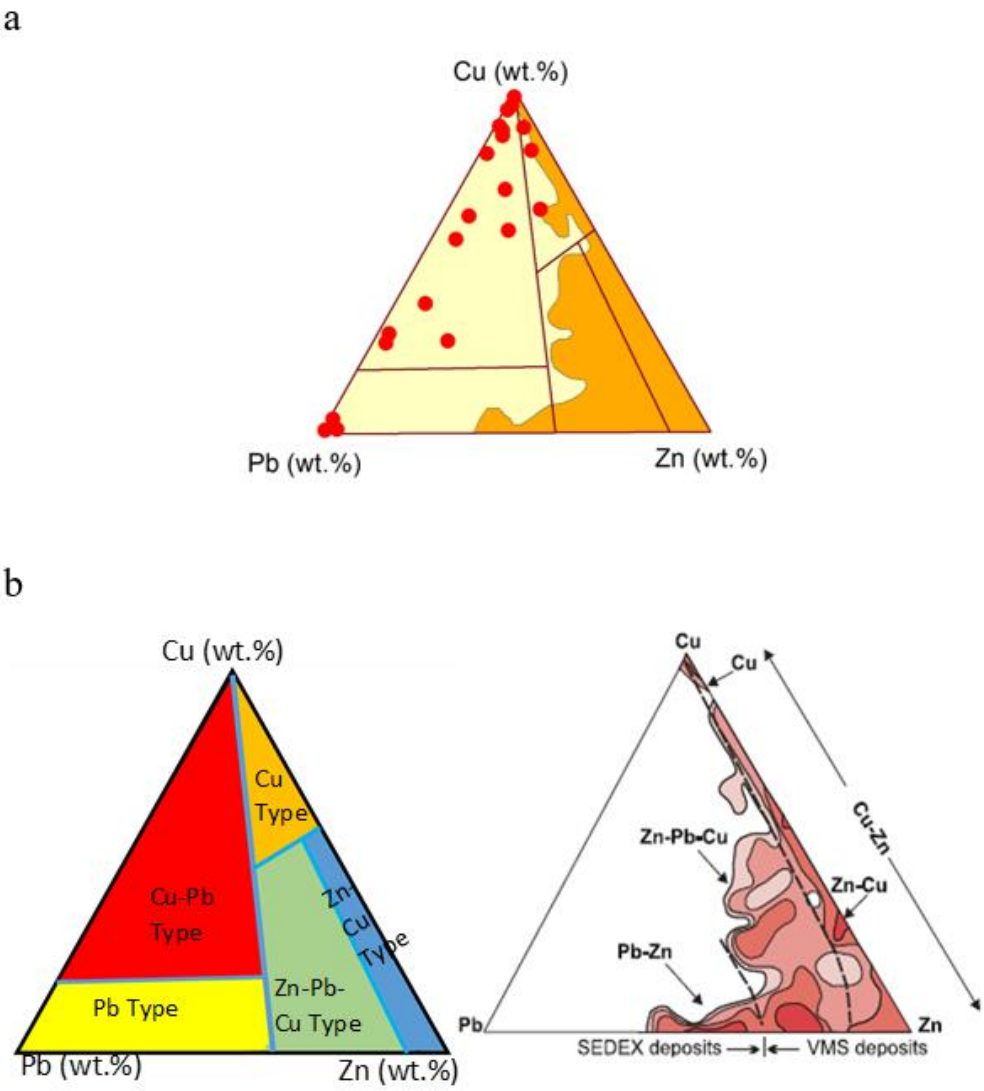

Figure 4.3.5: Comparison of Cu-Pb- Zn Ternary diagrams; a) Samples from the Kombat Mine, b) Pb-Cu-Zn fields after Large (1992) and SEDEX/VMS fields after Franklin et al. (1986, 1992).

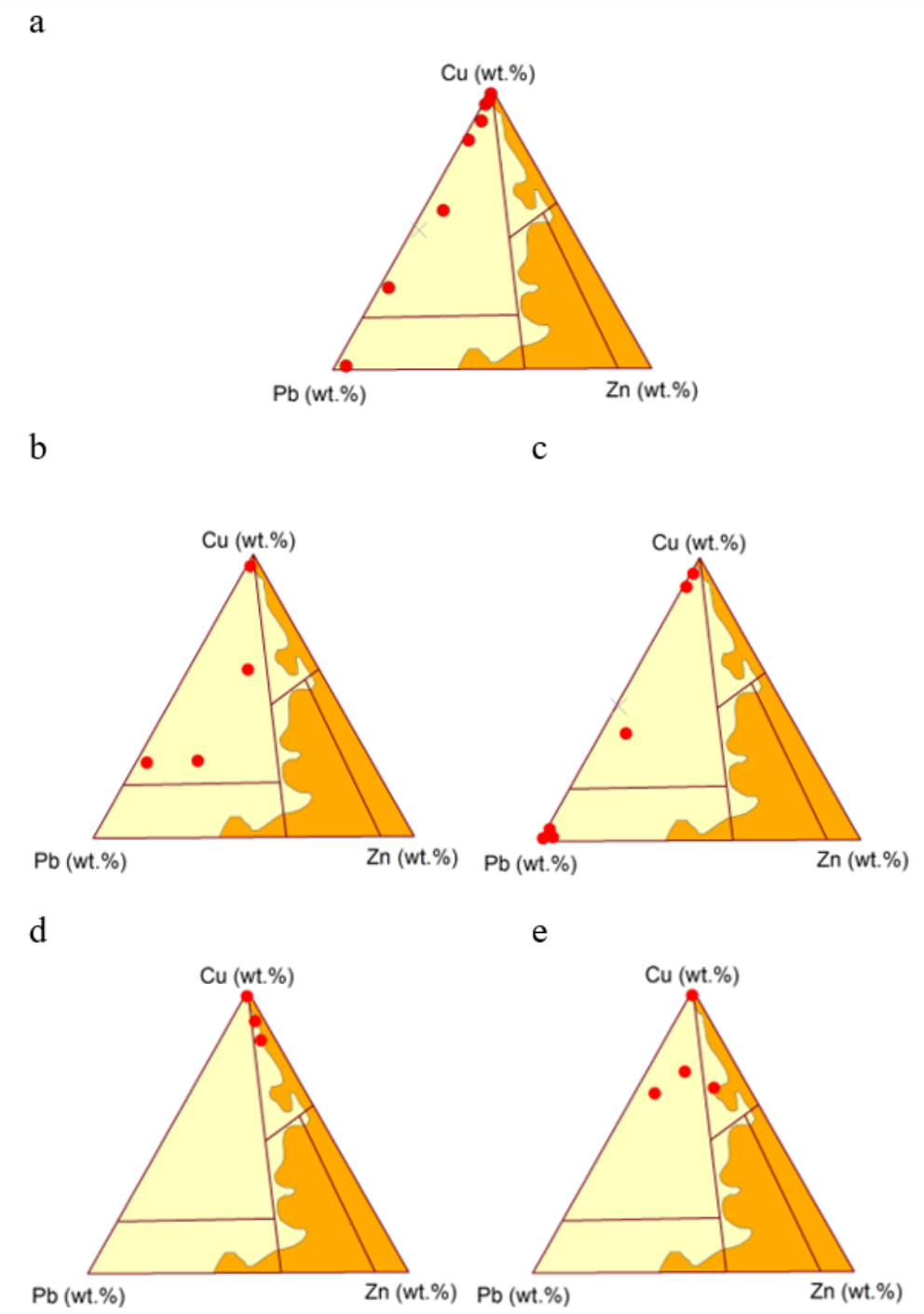

Figure 4.3.6: Cu-Pb-Zn Ternary diagrams of Kombat Mine localities a) Fe-Mn pit; b) OMEG pits; c) Museum; d)Asis Far West; e) 900 East pits, based on Pb-Cu-Zn fields after Large (1992) and SEDEX/VMS fields after Franklin et al. (1986, 1992).

In addition, various elements that were plotted against copper on the binary diagrams displaying Pearson correlation coefficient, a measure of the strength of a linear association between two variables and is denoted by r (Pearson Product-Moment," 2018). Elements displaying a negative Pearson correlation coefficient include Ca, Ba, Mg, P, Sr; Sb; Ti, and Mn (Figure 4.3.7). Contrary, elements such as Ag, S, Zn, Mo, Pb, Fe, As and W showed a positive Pearson correlation coefficient (Figure 4.3.8). Thus, based on the binary diagram Pearson correlation coefficient analysis, some elements were selected for evaluation at the locality scale (Figure 4.3.9). At the different localities, some elements exhibited a significant correlation with copper as indicated by their coefficient of determination values $R^2 \approx 0.70$ or higher.

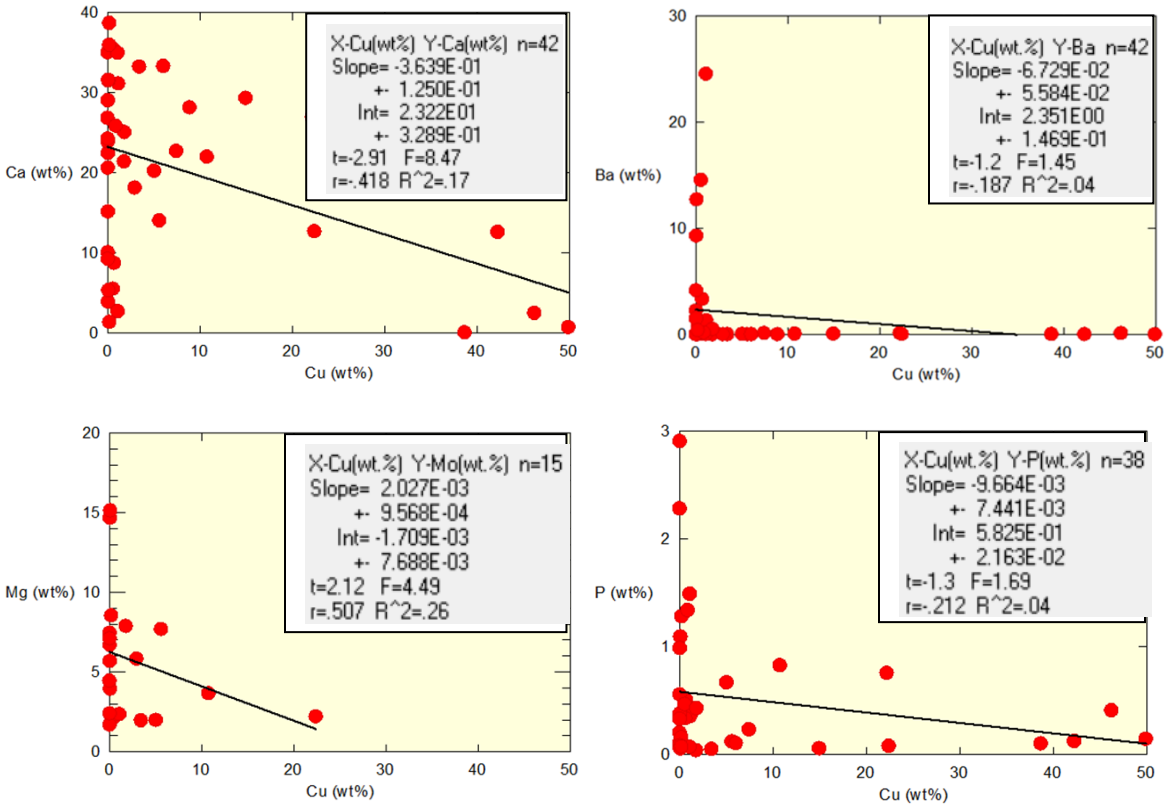

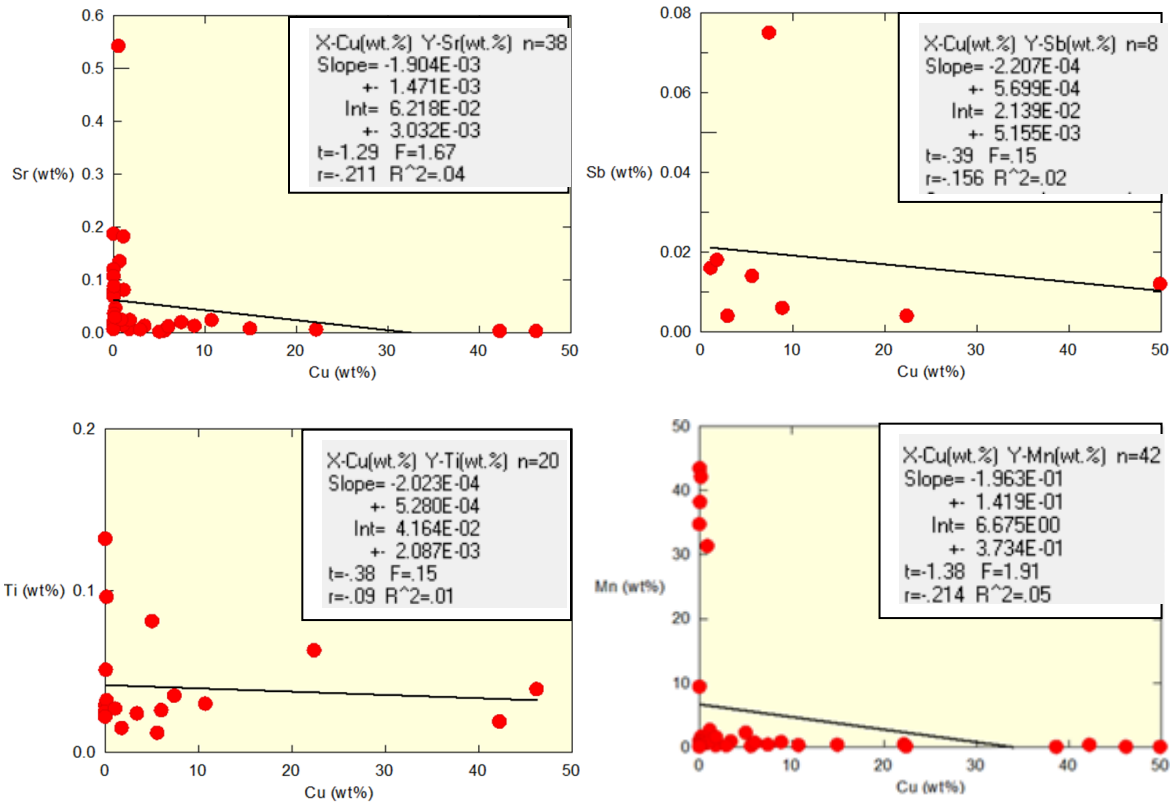

Figure 4.3.6: Elements displaying a negative Pearson correlation coefficient with copper.

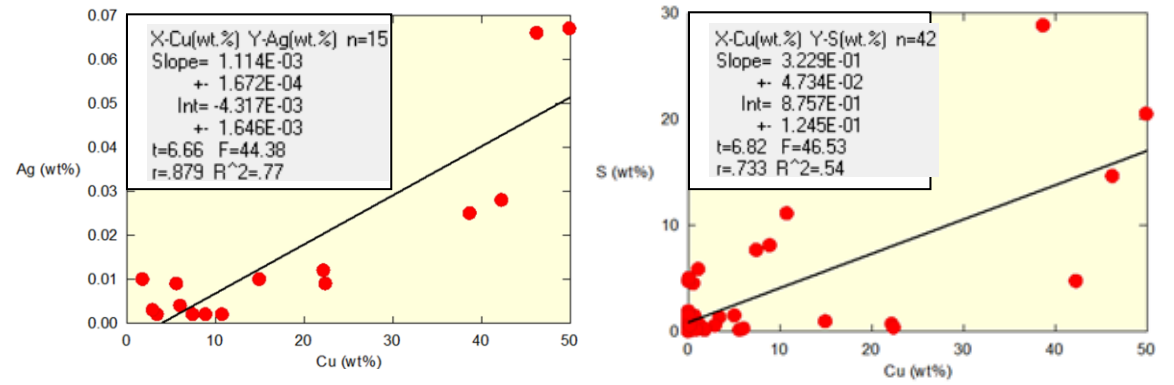

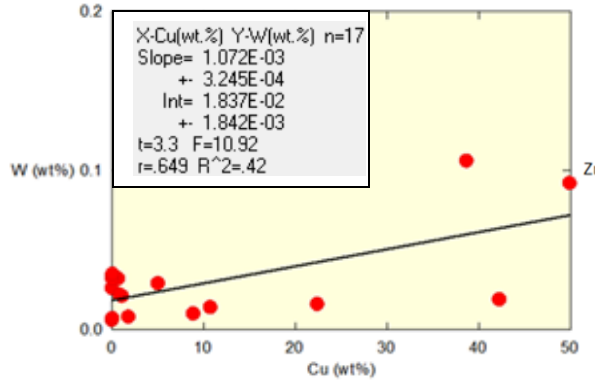
X-Cu(wt.%) Y-W(wt.%) n=17
Slope= 1.072E-03
+- 3.245E-04
Int= 1.837E-02
+- 1.842E-03
t=3.3 F=10.92
r=.649 R^2=.42
W (wt%)
Cu (wt%)

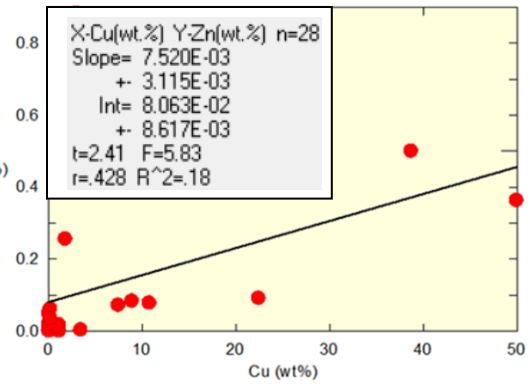
X-Cu(wt.%) Y-Zn(wt.%) n=28
Slope= 7.520E-03
+- 3.115E-03
Int= 8.063E-02
+- 8.617E-03
t=2.41 F=5.83
r=.428 R^2=.18
Zn (wt%)
Cu (wt%)

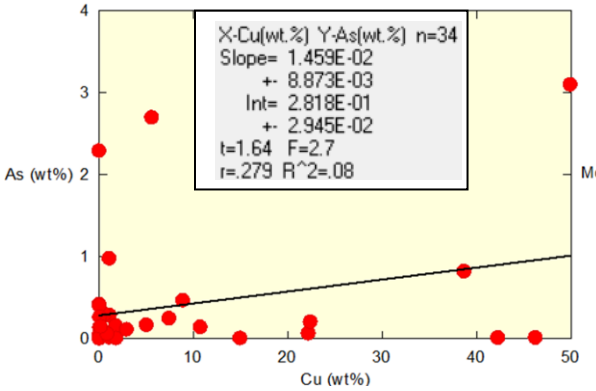
X-Cu(wt.%) Y-As(wt.%) n=34
Slope= 1.459E-02
+- 8.873E-03
Int= 2.818E-01
+- 2.945E-02
t=1.64 F=2.7
r=.279 R^2=.08
As (wt%)
Cu (wt%)

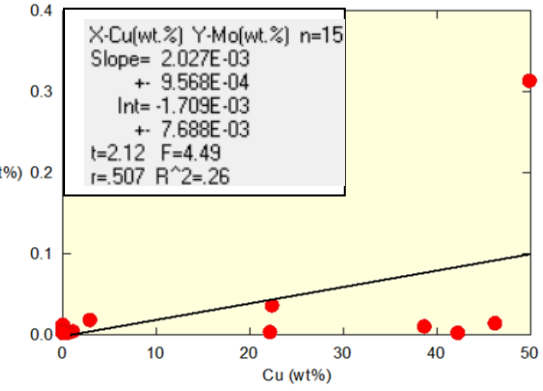
X-Cu(wt.%) Y-Mo(wt.%) n=15
Slope= 2.027E-03
+- 9.568E-04
Int= -1.709E-03
+- 7.688E-03
t=2.12 F=4.49
r=.507 R^2=.26
Mo (wt%)
Cu (wt%)

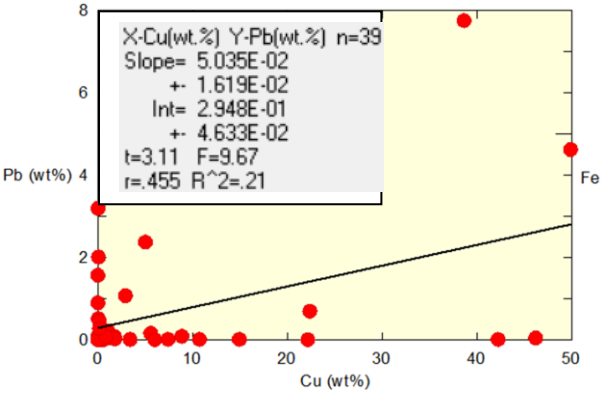
X-Cu(wt.%) Y-Pb(wt.%) n=39
Slope= 5.035E-02
+- 1.619E-02
Int= 2.948E-01
+- 4.633E-02
t=3.11 F=9.67
r=.455 R^2=.21
Pb (wt%)
Cu (wt%)

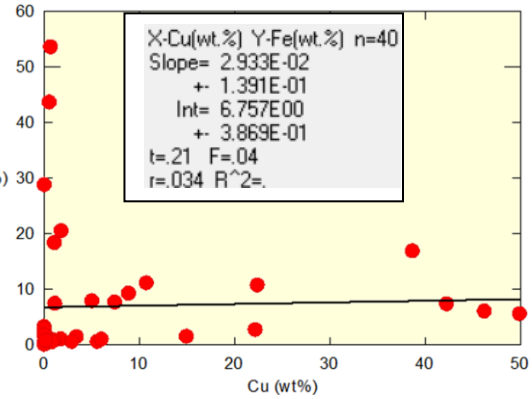
X-Cu(wt.%) Y-Fe(wt.%) n=40
Slope= 2.933E-02
+- 1.391E-01
Int= 6.757E00
+- 3.869E-01
t=.21 F=.04
r=.034 R^2=.
Fe (wt%)
Cu (wt%)

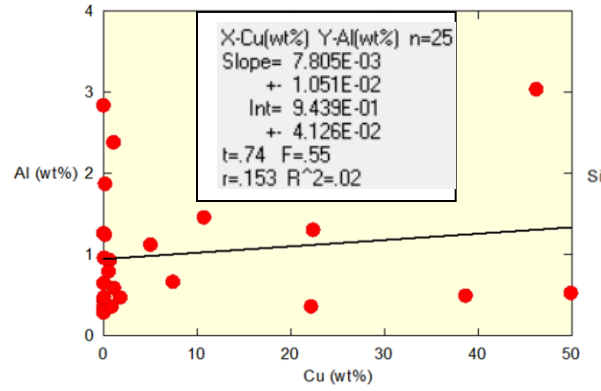
X-Cu(wt%) Y-Al(wt%) n=25
Slope= 7.805E-03
+- 1.051E-02
Int= 9.439E-01
+- 4.126E-02
t=.74 F=.55
r=.153 R^2=.02
Al (wt%)
Cu (wt%)

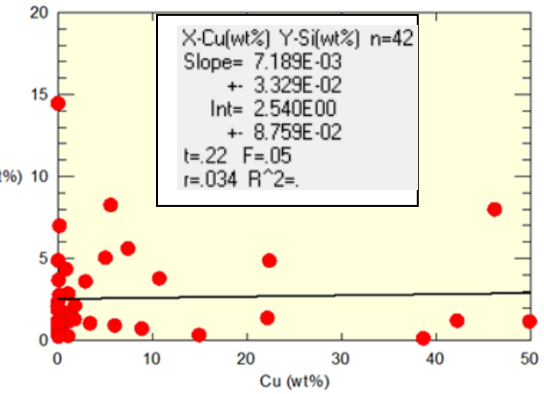
X-Cu(wt%) Y-Si(wt%) n=42
Slope= 7.189E-03
+- 3.329E-02
Int= 2.540E00
+- 8.759E-02
t=.22 F=.05
r=.034 R^2=.
Si (wt%)
Cu (wt%)

Figure 4.3.7: Elements showing a positive Pearson correlation coefficient with copper.

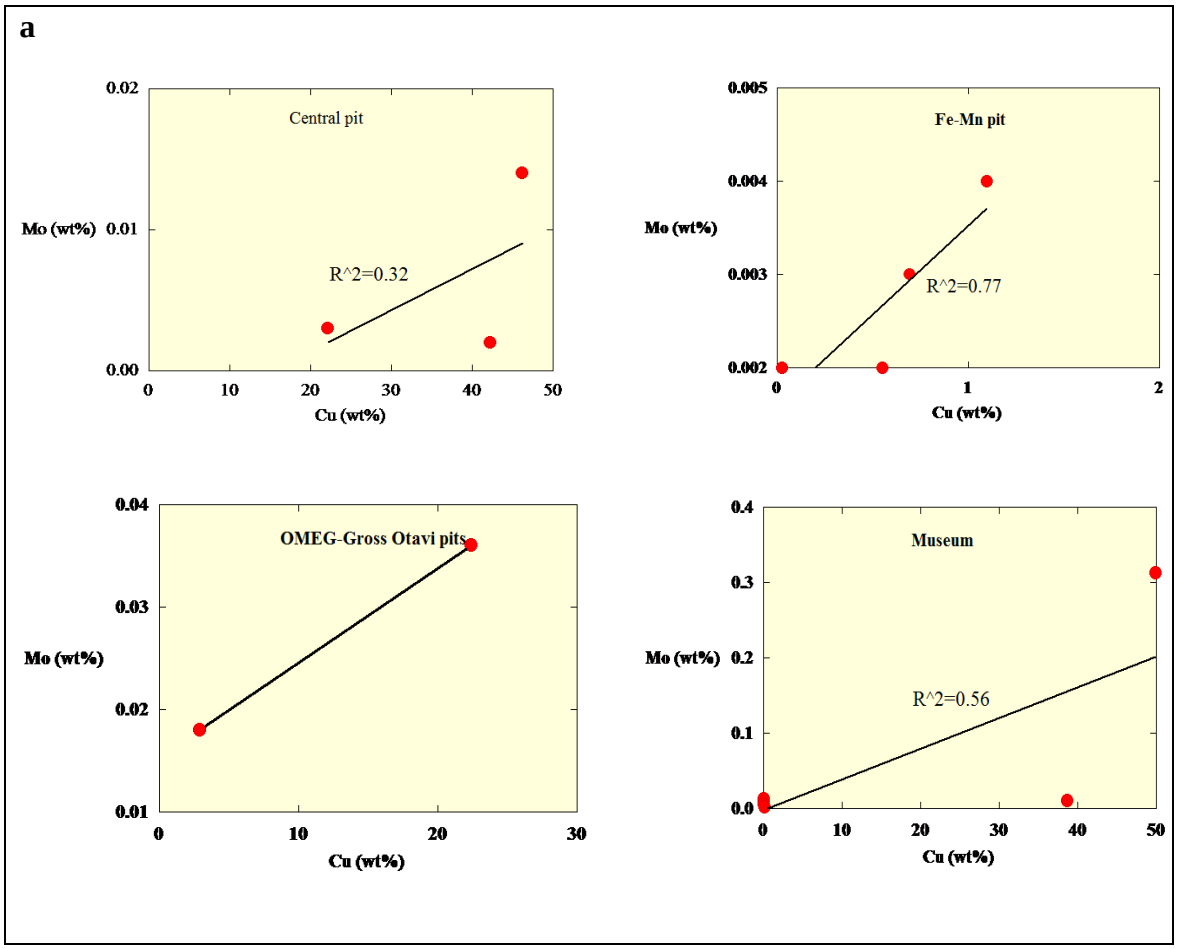

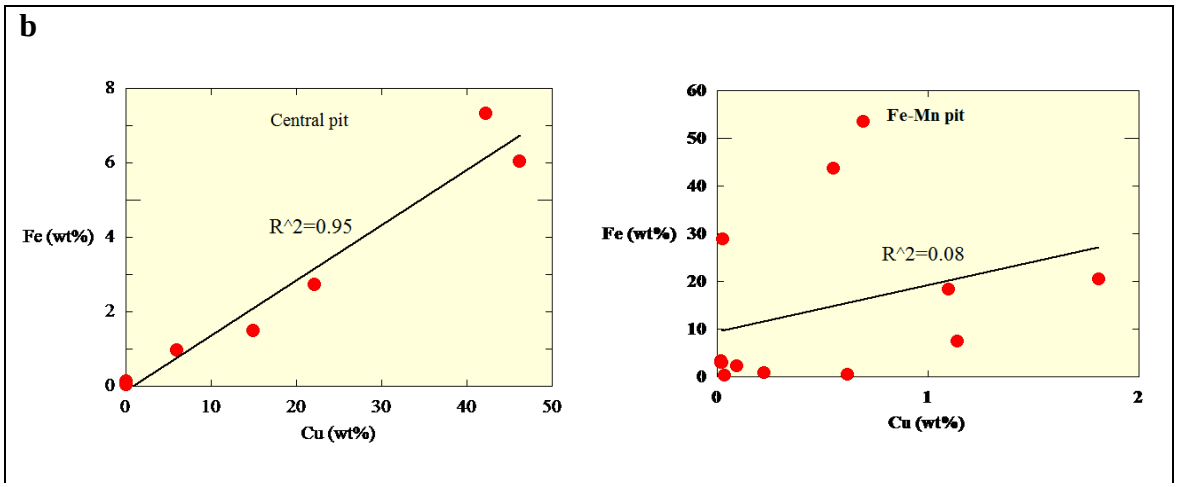

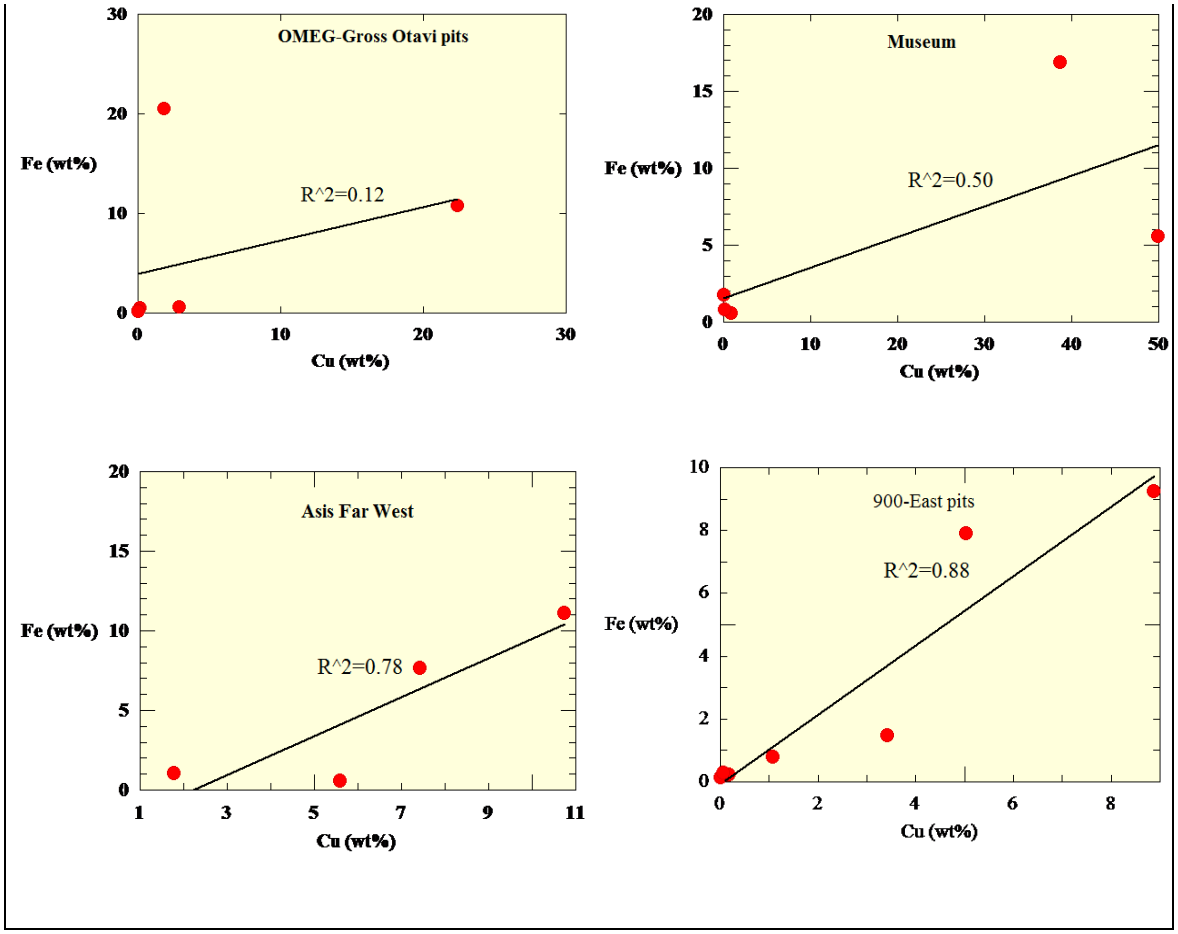
OMEG-Gross Otavi pits
Fe (wt%)
R^2=0.12
Cu (wt%)
Museum
Fe (wt%)
R^2=0.50
Cu (wt%)
Asis Far West
Fe (wt%)
R^2=0.78
Cu (wt%)
900-East pits
Fe (wt%)
R^2=0.88
Cu (wt%)

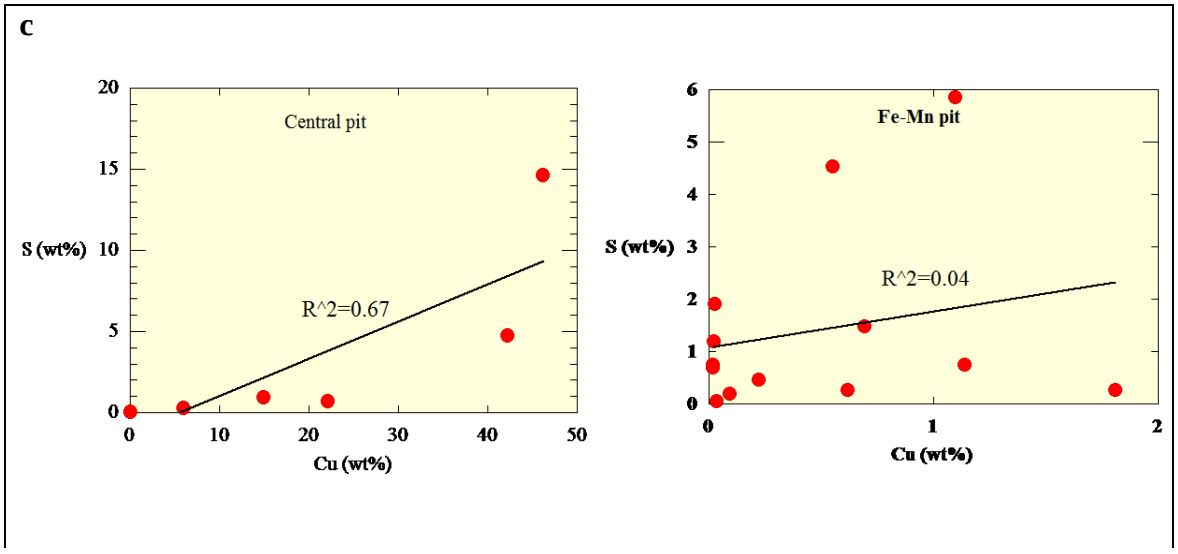
C
Central pit
S (wt%)
R^2=0.67
Cu (wt%)
Fe-Mn pit
S (wt%)
R^2=0.04
Cu (wt%)

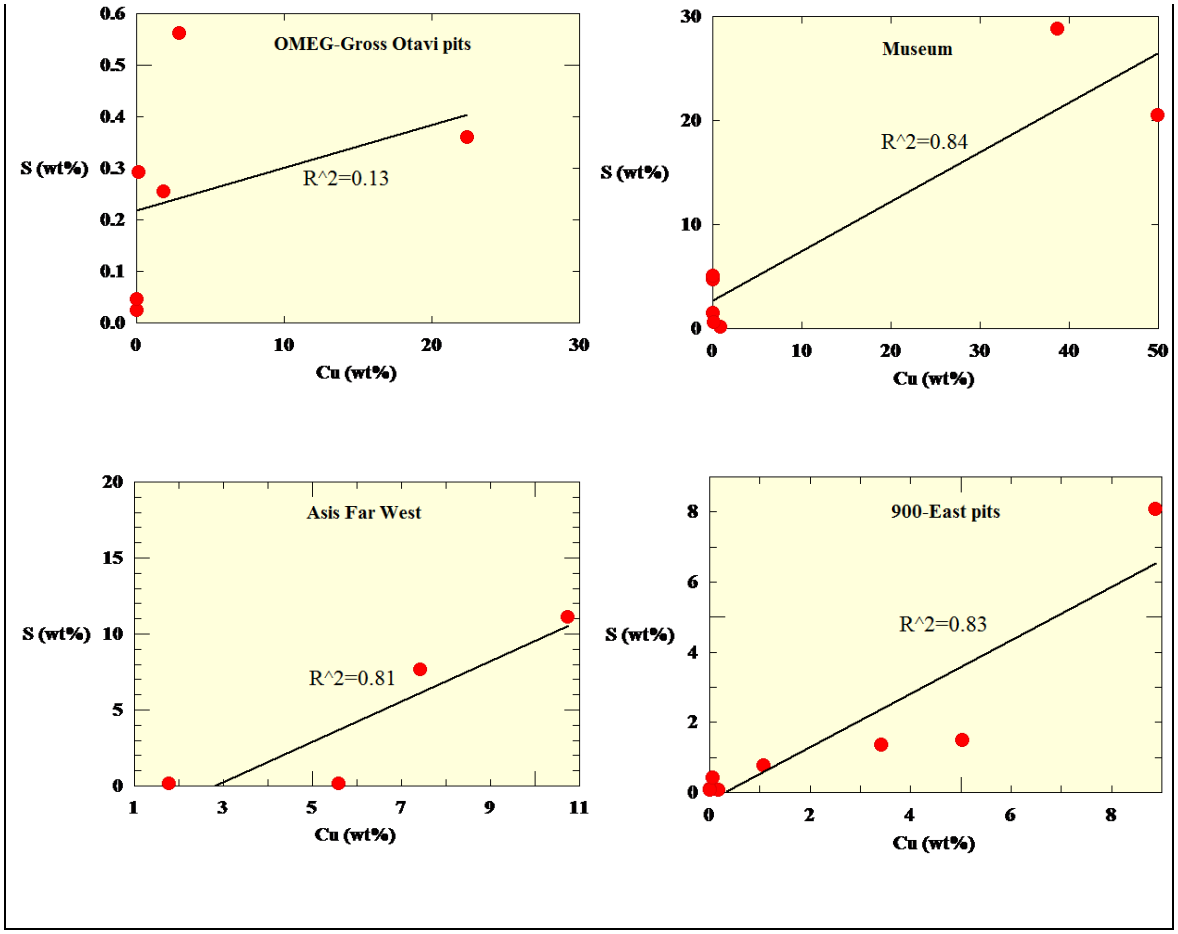
OMEG-Gross Otavi pits
R^2=0.13
S (wt%)
Cu (wt%)
Museum
R^2=0.84
S (wt%)
Cu (wt%)
Asis Far West
R^2=0.81
S (wt%)
Cu (wt%)
900-East pits
R^2=0.83
S (wt%)
Cu (wt%)

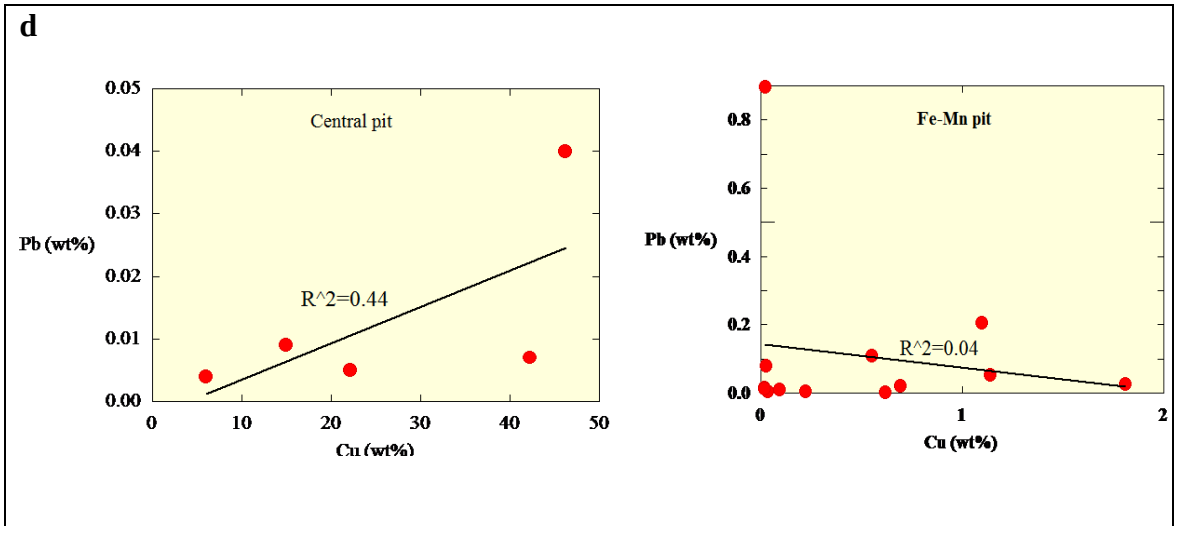
d
Central pit
R^2=0.44
Pb (wt%)
Cu (wt%)
Fe-Mn pit
R^2=0.04
Pb (wt%)
Cu (wt%)

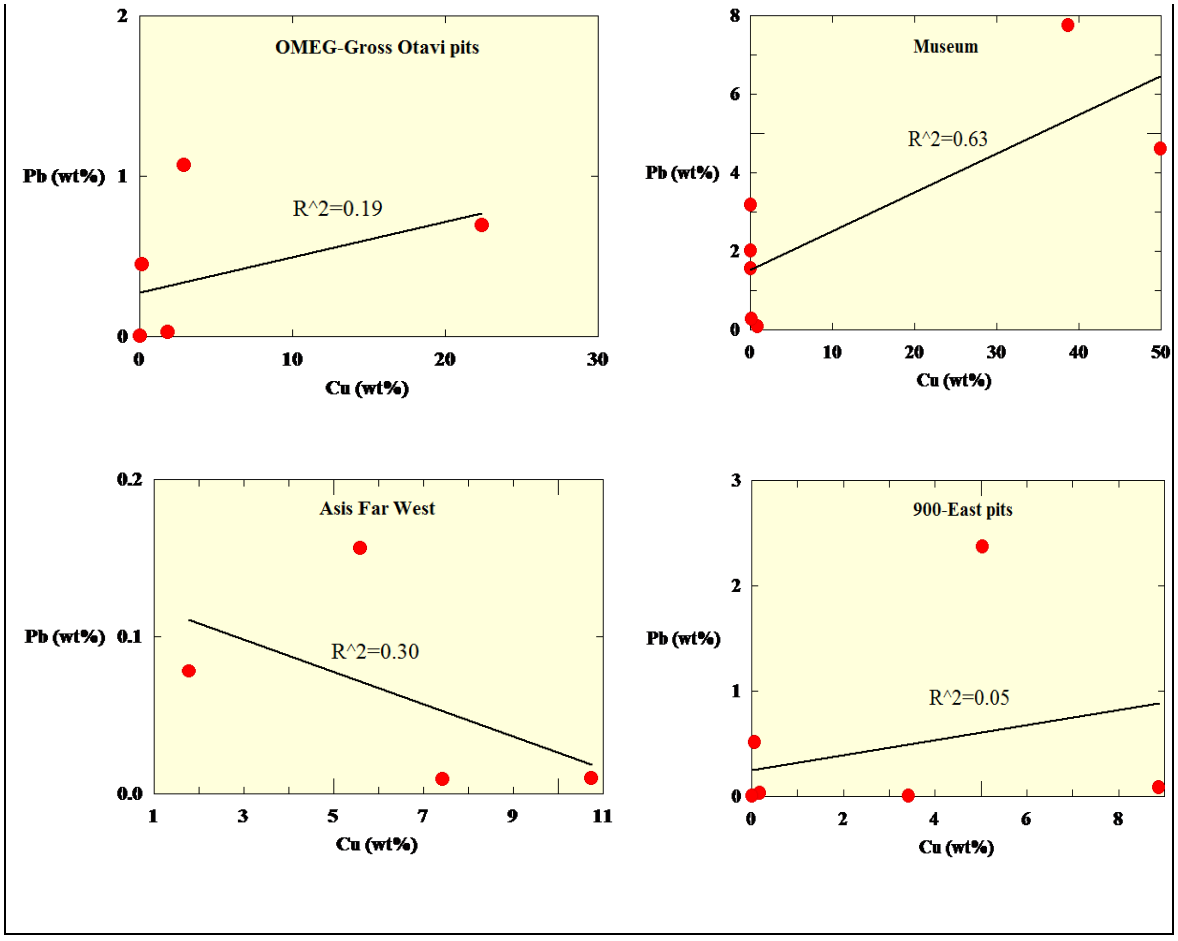
OMEG-Gross Otavi pits
R^2=0.19
Pb (wt%)
Cu (wt%)
Museum
R^2=0.63
Pb (wt%)
Cu (wt%)
Asis Far West
R^2=0.30
Pb (wt%)
Cu (wt%)
900-East pits
R^2=0.05
Pb (wt%)
Cu (wt%)

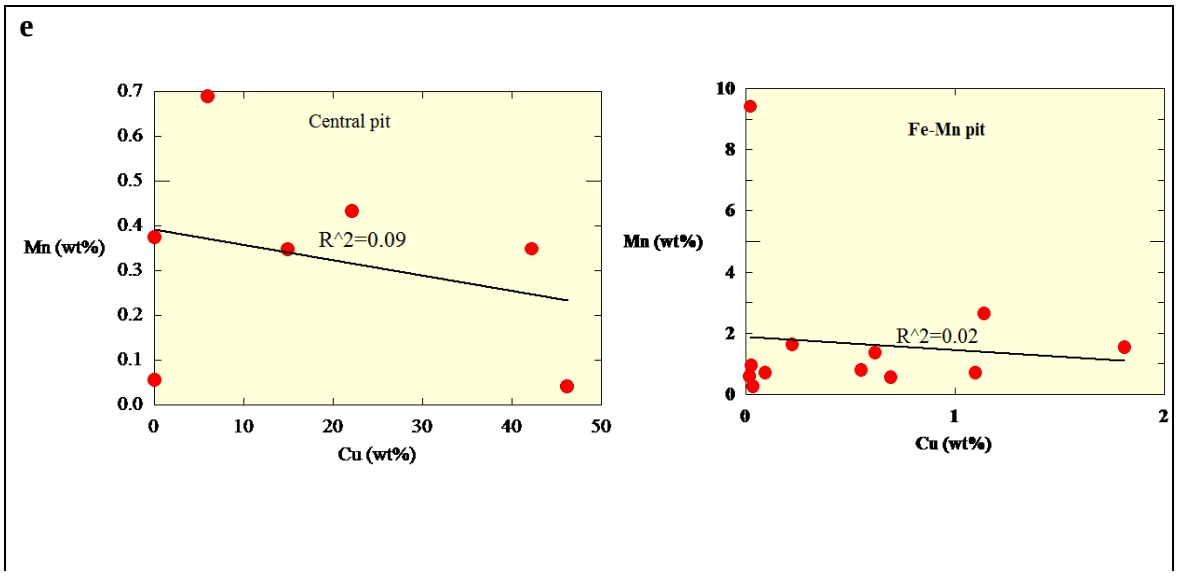
e
Central pit
R^2=0.09
Mn (wt%)
Cu (wt%)
Fe-Mn pit
R^2=0.02
Mn (wt%)
Cu (wt%)

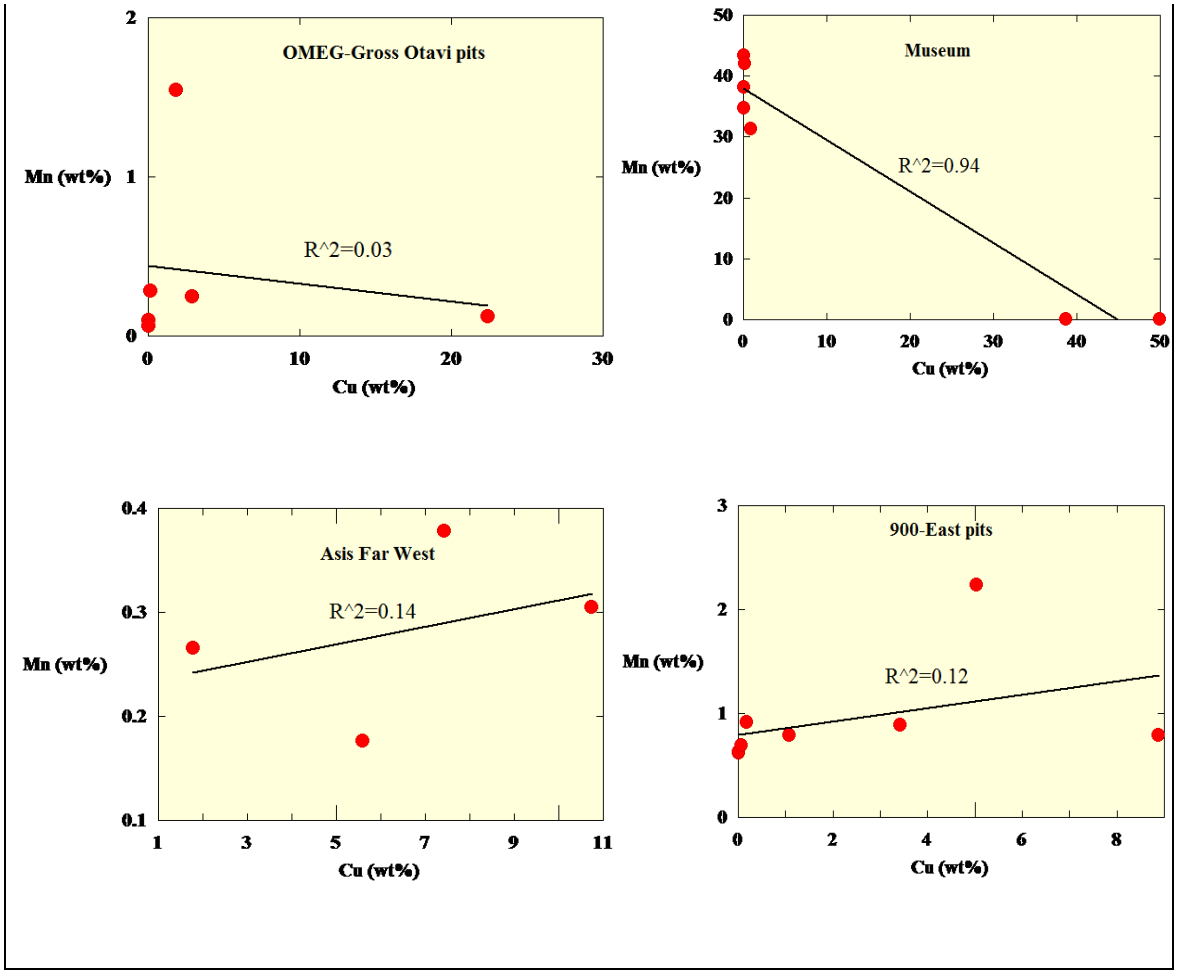
OMEG-Gross Otavi pits
Mn (wt%)
Cu (wt%)
R^2=0.03
Museum
Mn (wt%)
Cu (wt%)
R^2=0.94
Asis Far West
Mn (wt%)
Cu (wt%)
R^2=0.14
900-East pits
Mn (wt%)
Cu (wt%)
R^2=0.12

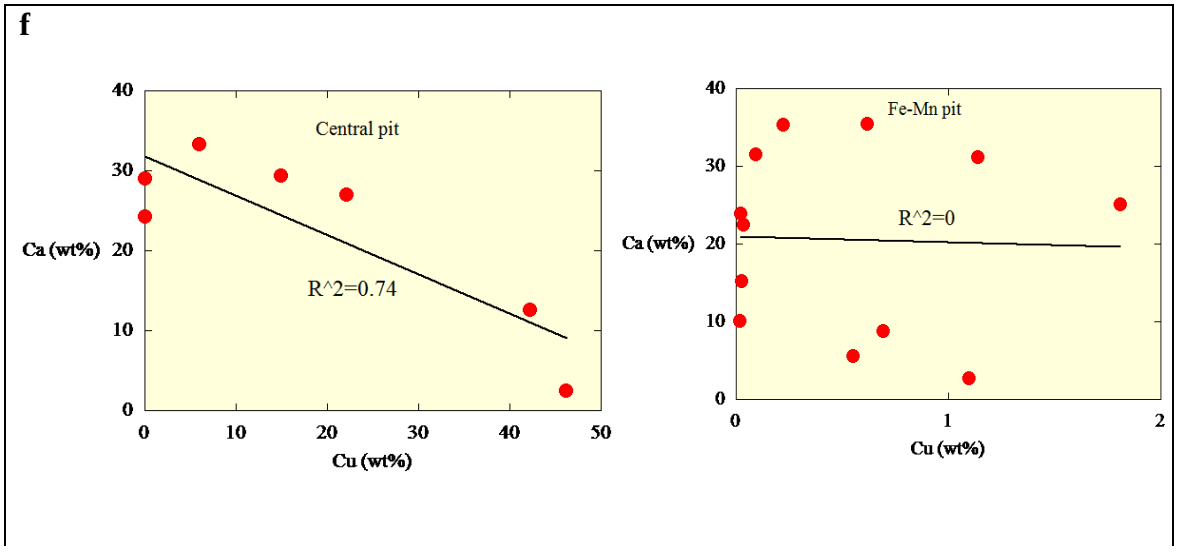
f
Central pit
Ca (wt%)
Cu (wt%)
R^2=0.74
Fe-Mn pit
Ca (wt%)
Cu (wt%)
R^2=0

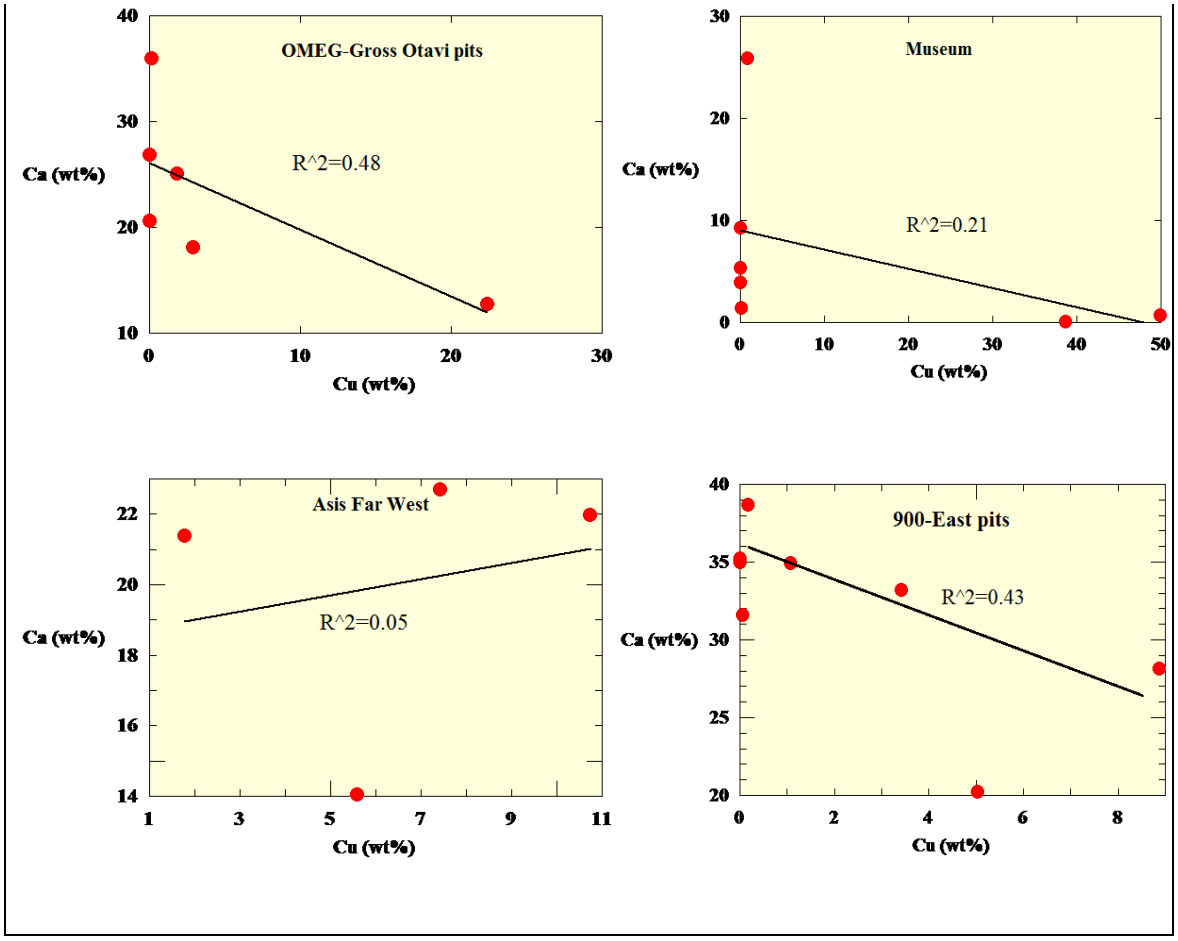
OMEG-Gross Otavi pits
R^2=0.48
Ca (wt%)
Cu (wt%)
Museum
R^2=0.21
Ca (wt%)
Cu (wt%)
Asis Far West
R^2=0.05
Ca (wt%)
Cu (wt%)
900-East pits
R^2=0.43
Ca (wt%)
Cu (wt%)

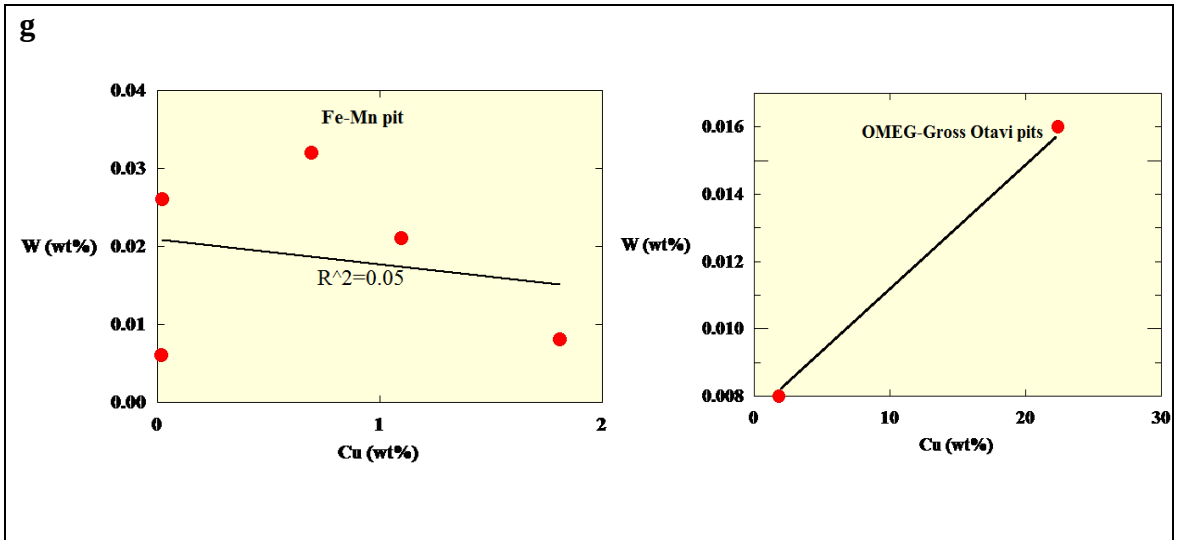
g
Fe-Mn pit
R^2=0.05
W (wt%)
Cu (wt%)
OMEG-Gross Otavi pits
W (wt%)
Cu (wt%)

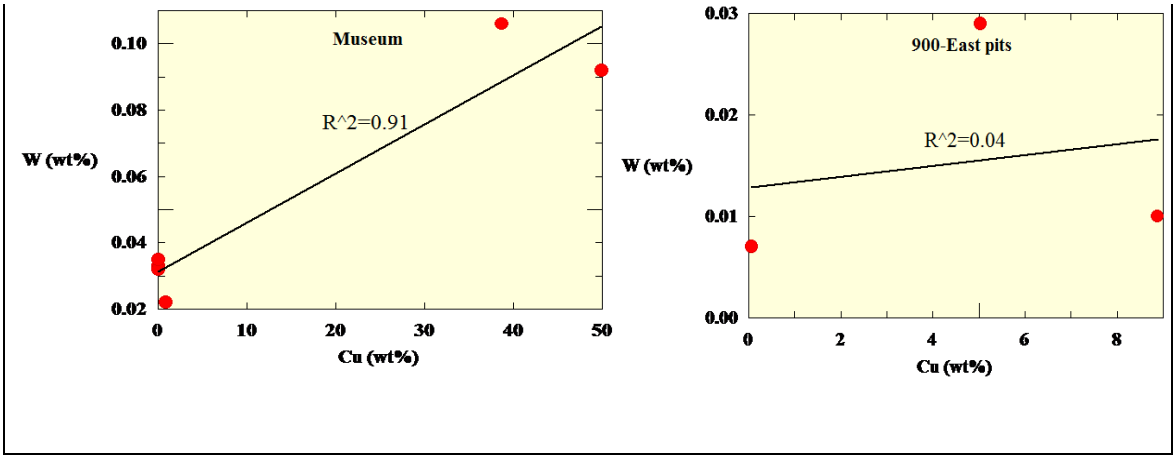

Figure 4.3.8: Binary diagrams plotting copper against various elements showing some significant correlation with copper at locality scale: a) Molybdenum (Mo); b) Iron (Fe); c) Sulfur (S); d) Lead (Pb); e) Manganese (Mn); f) Calcium (Ca); g) Tungsten (W).

4.3.2. Fluid inclusions

Between five to eleven inclusions per sample comprising of calcite, quartz, sphalerite, wulfenite and cerussite were primary or second-generation (see Appendix 2C). The binary diagrams (after Bussell *et al*., 1990) in Figure 4.3.10 a, b show that the mean homogenization temperature of primary inclusions ranges from 64 °C to 302 °C, while that of secondary inclusions is slightly lower (58 °C to 167 °C). Contrary, mean freezing temperatures range from -29.9 °C to -1.8 °C which gave the salinity records from 2.1 to 26.4 wt %. NaCl equivalent. Mean homogenization temperature corrections were applied based on diagrams for correcting fluid inclusion homogenization temperatures for compositions ranging from 0 to 25 percent NaCl up to 400°C and 200 MPa (Potter, 1977). A pressure of 2 kilobars or 200 MPa for the Otavi Mountainland deposits (Deane, 1995) was used. Corrected temperatures of total homogenization range from 160 °C to 200 °C (Figure 4.3.11).

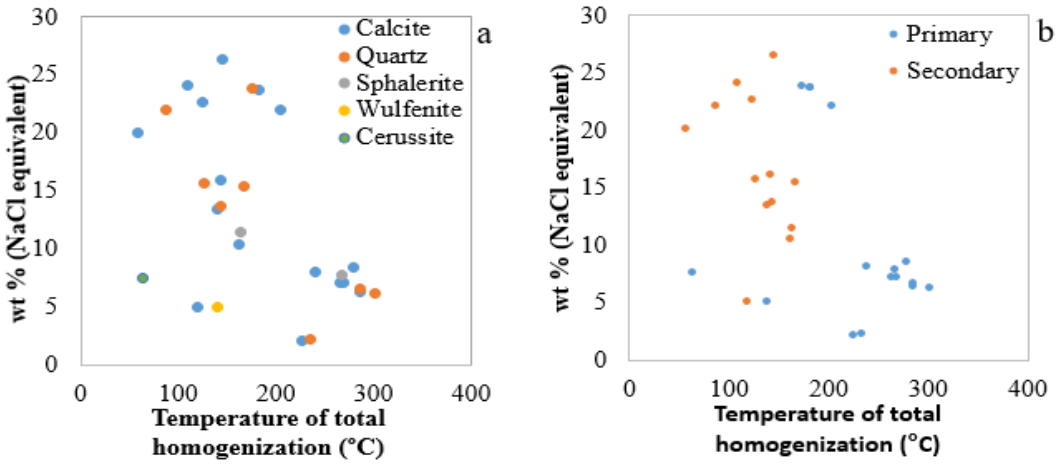

Figure 4.3.9: Salinity-homogenization temperature diagrams for fluid inclusions a) from various minerals; b) generation of deposition (after Busell et al., 1990).

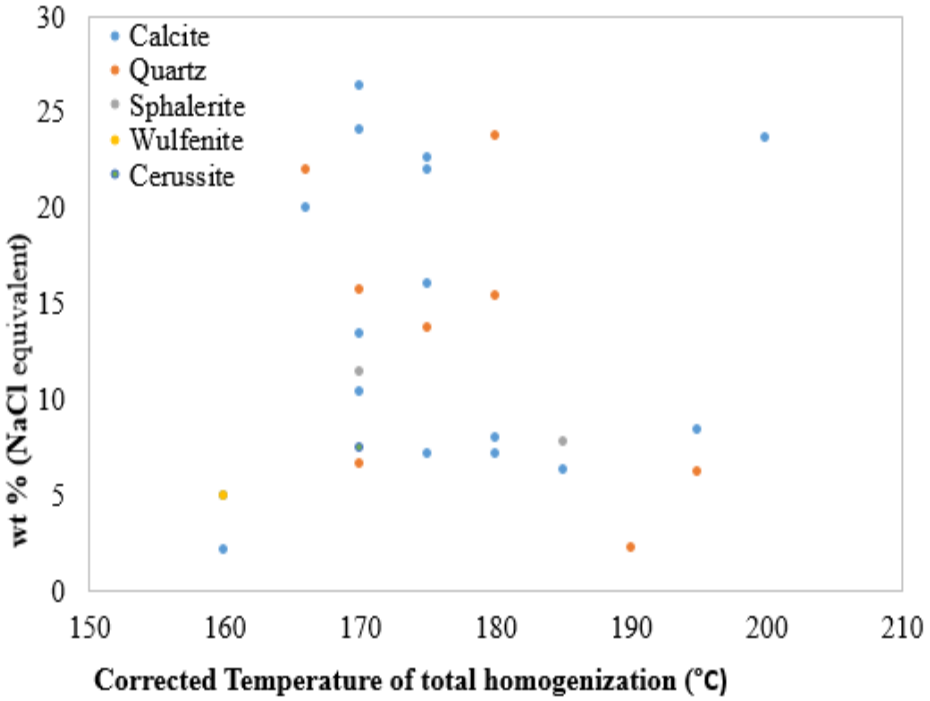

Figure 4.3.10: Salinity-corrected homogenization temperature based on diagrams for correcting fluid inclusion homogenization temperatures (Potter, 1977) for fluid inclusions from various minerals (after Bussell et al., 1990).

5. DISCUSSION:

In order to develop an appropriate exploration model for Kombat-style mineralization, it is necessary to classify the generic deposit type by means of geochemical interpretation, optical mineralogical studies and field observations.

5.1. Re-evaluation of Kombat-style polymetallic deposit

5.1.1. Field Observations

The hydrothermal cavity, fracture fill, and breccia-style systems such as those at Gross Otavi and the Kombat Mine pits (Figures 4.1.2 to 4.1.7) are tectonically controlled, epigenetic characteristics of the MVT-type deposits (Paradis et al., 2007). Where the ores are deposited is also determined by lithology transitions, whereby the Cu-Pb ores are bounded to the upper Hüttenberg dolostone and the calc-silicate rocks (Figure 4.1:3), as a result of changes in both the vertical and lateral permeability of the rocks in a carbonate platform sequences (Leach et al., 2010). The mineralization exhibit limited or irregular primary dispersion patterns are similar to an analog MVT deposit study by McQueen (2015). Host rock alteration is limited and generally restricted to dolomitization characterized by smoky and white euhedral calcite which are often surrounded by grey rims of chalcopyrite, and galena halos (Figures 4.1.2 a; 4.1.5 c, e, g; 4.1.6 b) and silicification reflected by quartz veins (Figure 4.1.5 c; 4.1.7 c) around steeply-dipping, east-west striking (F: 79°/195°) controlling structures namely cavities, faults and shear fractures. Furthermore, relatively porous calc-silicate hosting the bedded Fe-Mn ore might have provided the metal precipitation space (aquifer) during the

different hydrothermal fluid episodes (Figure 4.1.4). Phyllite represents a less permeable unit which created a trap for the metalliferous hydrothermal fluid, while its enrichment in organic matter may have provided the necessary conditions for metal precipitation.

5.1.2. Optical Mineralogy

Through transmitted and reflected light microscopic study of polished and thin sections (Figures 4.2.1and 4.2.2), Cu-Pb (Ag) and Fe-Mn ore minerals were identified. The foliated, bedded samples of iron-manganese ore contain pre-dominantly hausmannite (Hs), magnetite (Mt), pyrite (Py), and chalcopyrite (Cp). The presence of bioturbation and relicts of beddings preserved in the calc-silicate (host rocks) indicates a syn-sedimentary deposit (Baniak et al., 2015; Deane, 2006) associated with secondary hematite (Hm), and jacobsite (Jb) mineralization.

The Copper-lead ores consist of bornite (Bn) and chalcopyrite (Cp) are both being replaced by twin lamellae textures of chalcocite (Cc) and exsolution of covellite (Cv) after bornite and chalcocite, while covellite veins have been terminated by pyrite (Py). These copper ore minerals are associated with hydrothermal dissolution and dolostone replacement features common in and about MVT deposits (Leach et al., 2010). The hydrothermal fluid generation requires three components: 1. Brine source: possibly, the evaporation of Khomas seawater and halide dissolution generated the basinal sediment brine (section 4.3.2). 2. Sulfur source: through a metamorphic breakdown of sulfate minerals and organic materials, 3. Metal source: metals may have been leached from the underlying sedimentary package through which the brines migrated (Leach and Sangster, 1997). During brine migration, the replacement textures (Figure 4.2.3)

observed could indicate leaching of copper, zinc, and tin from clays, micas, and amphiboles, whereas lead is likely from sandstones, (Skinner, 1997).

5.1.3. Fluid inclusion

The fluid inclusions indicated an average homogenization temperature of 183°C confirming a hydrothermal system and the salinity of 12.85 NaCl wt. % equivalent is indicating a brine fluid was responsible for the Kombat deposit. The brine-hydrothermal fluid system falls within the range of an MVT-type deposit conditions (Leach et al., 2010; Leach and Sangster, 1993; Paradis et al., 2007). Hence, the corrected mean temperature values on diagrams for correcting fluid inclusion homogenization temperatures (Potter, 1977) suggest that Kombat deposit originated under temperatures ranging from 160°C to 200°C, and salinity of 2.1 to 26.7 wt.% NaCl (Figure 4.3.11). This satisfies the typical physico-chemistry conditions of MVT deposits originate from saline basinal metalliferous fluids at temperatures in the range of 75 to 200°C at crustal level (≤1km) (Leach and Sangster, 1993; Giordano and Barnes, 1981).

5.1.4. Geochemistry

On the discriminant diagram for sedimentary rocks (Boström, 1973; Figure 4.3.3) all samples from Kombat Mine pits falls in the hydrothermal field, suggesting a hydrothermal process is predominantly responsible for Kombat mineralization. A few samples fall in the diagenetic field and mixed fields. Therefore, the evaluation of individual sample locality indicated strong hydrothermal mineralization on the Kombat Central pit, the Asis Far West dumps and the 900 East pits (Figure 4.3.4 a, d, e). Dual

generic fields comprised of hydrothermal and diagenetic components were revealed by the samples from the National Earth Science Museum (Figure 4.3.4 f), indicating that both processes took place. A diagenetic process could be associated with bedded Fe-Mn ore samples and may represent deposition in a marine environment (Qiu et al., 2018; Bailie et al., 2011). Some samples from the Fe-Mn pit and OMEG pits plotted in the hydrothermal-diagenetic-hydrogenetic and hydrogenetic-diagenetic mixed fields respectively (Figure 4.3.4 b, c), which indicates that the hydrogenetic-diagenetic processes would be responsible for Mn, Cu and Ni concentrations provided that the sedimentary column was under oxic conditions. The change to a suboxic conditions would promote high Mn and Fe concertation (Calvert and Piper, 1984; Schultz, 2006), and therefore contributed to the stratiform Fe-Mn (Cu) mineralization. This indicates that the stratiform Fe-Mn were syn-sedimentary marine deposits, were contaminated at a later stage by Cu-Pb rich hydrothermal fluids and is in agreement with the fracture zone model (Kotze, 2019).

The VMS/SEDEX (MVT) discriminant ternary diagrams (Franklin et al., 1986; 1992; Large, 1992) pinpointed a Cu-Pb type of MVT deposit (Figure 4.3.5). However, the evaluation of sample localities indicated that the Asis Far West dumps (Figure 4.3.6 d) falls in the Cu-type VMS field which is possibly due to weathering during a long exposure of the shaft development dumps.

In summary, the primary hydrothermal sulfides deposition formed by metamorphic dehydration, which supplied the sulfur and brines from tectonic pumping related to the Damara Orogeny, and the upward migration of the hydrothermal brines, that leached

metals from the underlying package of sediments. Hence, the paragenetic sequence observed could have originated in the following metallogenic events:

1. Syn-sedimentary deposition of Fe-Mn mineralisation evident by the well-preserved beddings (S0) and bioturbation (Figure 4.1.4 c) seen in the layered Fe-Mn calc-silicate bodies (Figure 4.1.3 c) and crosscut by foliation (S2) (Figure 4.1.4).

2. Penetrative fractures acting as passageways for ascending hydrothermal fluids rich in Cu and Pb; subsequent hydraulic fractures (veins) are filled with primary copper minerals (Figure 4.1.4 b).

3. Further deformation leads to localized brittle fracturing/faulting and remobilization of primary mineralization as well as the formation of secondary minerals along fracture cleavage/faults (S3) (Figure 4.1.2 e).

4. The first phase of alteration of secondary ore minerals (S3) leads to supergene enrichment of breccia ore minerals in zones of lower stress such as cavities and fractures (Figure 4.1.6).

5. Finally, the ore minerals are exposed to retrograde conditions during weathering, uplifting, and erosion causing the second phase of alteration and formation of oxide ores. The paragenetic sequence is summarized in Table 1, while Figure 5.1.1 summarizes the subsequent genetic model.

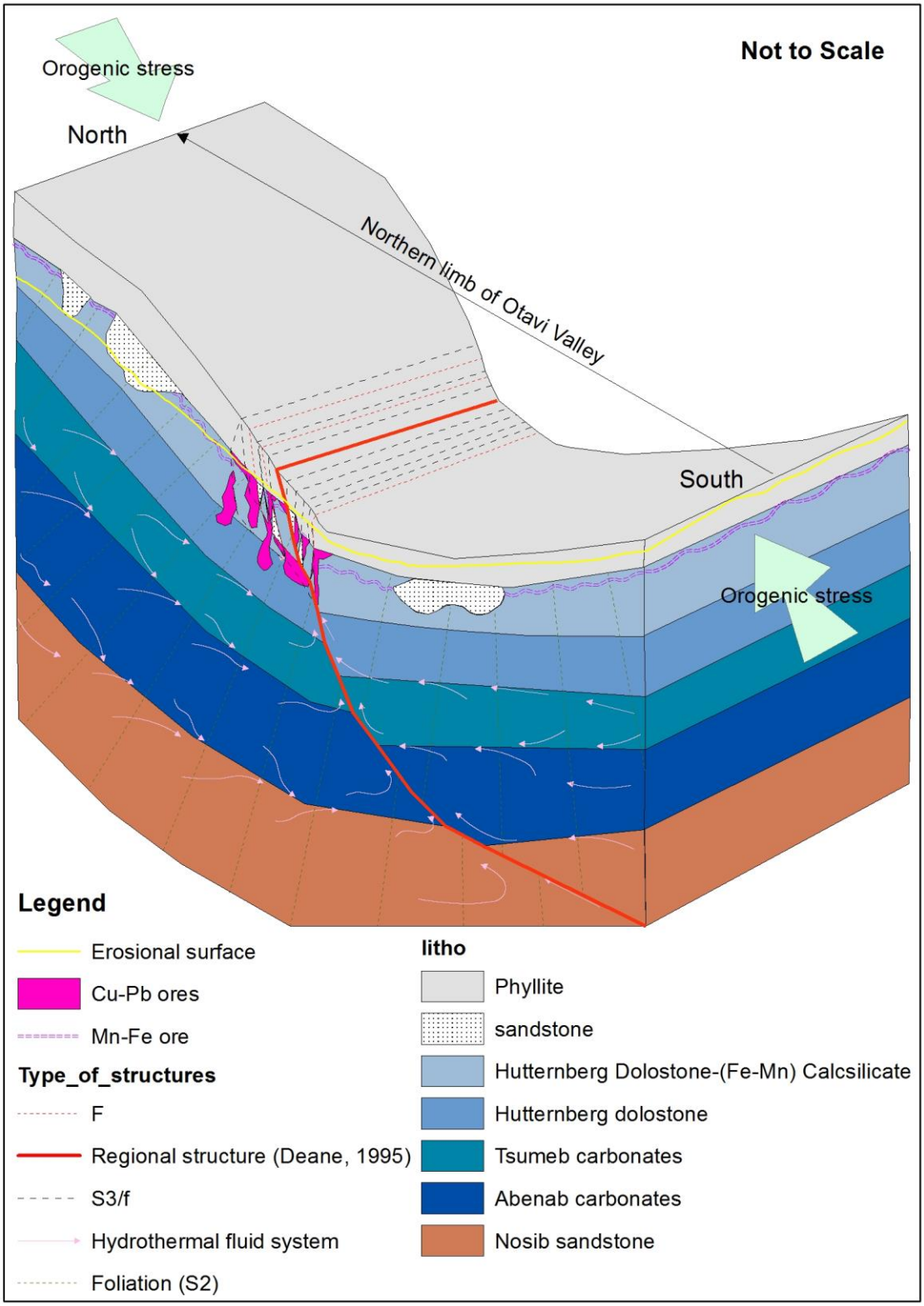

Figure 5.1.1 The Kombat Mine ore genetic model

The Kombat Mine ore genetic model (Figure 5.1.1) conforms to the Regional Structural Monoclinal Trend (RSMT) mapped by Deane (1995) as supported by both the Fracture Zone model and Roof Pendants (Ore lenses) Hanging on Rollover Structures model. Similarly, the syn-sedimentary Fe-Mn ore appears in the same order however, lack of Fe-Mn ore in the underground mining and drilling data (Kotze 2019) deviated the model from roof pendants (ore lenses) hanging on rollover structures. This model reflected a close relationship with the Fracture Zone model via shared penetrative fractures acting as conduits for ascending Cu-Pb rich hydrothermal fluids (F). Localized brittle fractures, faults, cavities and shear zones defined by fracture cleavage (S3/f) in which the Cu-Pb ore of the MVT –type mineralization was deposited.

5.2. Mineralogical and geochemical indicators for Kombat-style polymetallic deposit

Binary diagrams for various elements (wt. %) against copper (wt. %) established eight (8) elements showing some significant linear association with copper (Pearson correlation coefficient = r) and correlations (coefficient of determination= R^2). Negative linear associations displayed by Ca (medium: r =0.4), Mg (large: r = 0.5), may indicate the elements being replaced by base metals. While positive linear associations exist for Ag, S, W, Mo (strong: r= 0.5 to 1.0), Pb, Zn (medium: r = 0.3 to 0.5) giving the anomalous values which can be used for geochemical (element) exploration indicators (Table 2). At the locality scale (Figure 4.3.9), some significant correlations (R^2=0.70 or higher) exists for S from Asis Far West, 900-East and Museum; for Fe on samples from Central, 900-East, Asis Far West; for W on samples from Museum; for Mo on

samples from Fe-Mn pit. Whilst, for Ca on samples from Central pit and Mn for samples from the Museum exhibited an inverse relationship with the copper. Asis Far West samples exhibited opposite linear associations for Pb (-ve) and Ca (+ve), hence, further investigations may be required. Associated alterations such as dolomitization mirrored by an increase in the Mg/Ca ratio (Emsbo, 2009) and silicification by high silica (Si) content in hydrothermally altered carbonate rocks.

The XRD results confirmed possible mineralogical indicators associated with Kombat-type deposit and which are corresponding to elements (XRF results) that can be used for geochemical exploration (Table 2 & 3). The confirmed exploration indicators for Kombat MVT-type deposit are predominantly chalcopyrite, bornite, and covellite (Cu, Fe, S); galena; Minor concentrations of chalcocite (Cu, S); sphalerite (Zn, S); pyrobelonite (Pb, Mn, V); And traces of malachite (Cu); langite and brochantite (Cu, S) tennantite (Cu, Fe, Zn, As, S); smithsonite (Zn); cerussite, asisite, damaraite and phosgenite (Pb); kombatite (Pb, V); duftite (Pb, Cu, As); hedyphane and mimetite (Pb, As); hamatophanite (Pb, Fe); wulfenite (Pb, Mo); rhodochrosite, crednerite (Cu, Mn) minerals. The associated gangue minerals are dolomite (Mg), calcite (Ca) have been confirmed by both geochemistry XRF, XRD and field observations. White to grey euhedral calcite crystals up to 15 X 5 cm appears in fractures, cavity fillings with some quartz (Si) veins. Minor anhydrite, gypsum (Ca), and traces of baryte ($BaSO_4$) could justify the use of Ba in geochemical exploration indicators.

The hausmannite (Mn) and hematite (Fe, S), minor concentrations of pyrite (Fe, S); jacobsite (Mn, Fe); pyrobelonite (Pb, Mn, V); manganite, pyrolusite, rhodonite (Mn),

and magnetite (Fe). And traces of rhodochrosite, kutnahorite (Mn), and crednerite (Cu, Mn) minerals would indicate the presence of Fe-Mn synsedimentary-type deposit associated with the MVT-type deposit of the Kombat Mine.

Table 2: Geochemical (elements) exploration indicators for existing mineralization based on portable XRF analysis

Anomaly (XRF)	Cu (wt.%)	S (wt.%)	Pb (wt.%)	As (wt.%)	Zn (wt.%)	V (wt.%)	W (wt.%)	Mo (wt.%)	Ag (wt.%)
Sampled ore	7.252	3.229	0.695	0.414	0.129	0.035	0.030	0.029	0.017
Mined ore	2.000	0.891	0.192	0.114	0.036	0.010	0.008	0.008	0.005
Cut off grade	0.500	0.223	0.048	0.029	0.009	0.002	0.002	0.002	0.001

Table 3: Mineralogical exploration indicators for existing mineralization based on XRD analysis

Mineral	Formula	Ca	Ba	Mn	Cu	S	Pb	Fe	Zn	Mo	As	V
Chalcopyrite	CuFeS3											
Bornite	Cu5FeS4											
Covellite	CuS											
Galena	PbS											
Hausmannite	Mn3O5											
Hematite	Fe2O4											
Chalcocite	Cu2S											
Langite	Cu4[(OH)61 SO4].H20.											
Sphalerite	ZnS											
Pyrite	FeS3											
Magnetite	Fe3O5											
Jacobsite	MnFe2O5											
Manganite	MnO(OH)											
Pyrolusite	MnO3											
Rhodonite	MnSiO4											
Pyrobelonite	PbMn2+VO4(OH)											
Malachite	Cu2(CO3)(OH)3											
Tennantite	Cu6[Cu4(Fe,Zn)2]As4S14											
Brochantite	Cu4SO4(OH)7											
Crednerite	CuMnO3											
Duftite	PbCu(AsO4)(OH)											
Cerussite	PbCO4											
Kombatite	Pb14(VO4)O9Cl5											
Asisite	Pb7SiO9Cl3											
Hedyphane	Ca2Pb3(AsO4)3Cl											
Hamatophanite	Pb4Fe3O8(OH,Cl)											
Damaraite	Pb3O2(OH)Cl											
Mimetite	Pb5(AsO4)3Cl											
Wulfenite	Pb(MoO4)											
Phosgenite	Pb2CO3Cl3											
Rhodochrosite	MnCO4											
Kutnahorite	CaMn(CO3)3											
Smithsonite	ZnCO4											
Gypsum	CaSO4·2H2O											
Anhydrite	CaSO5											
Baryte	BaSO4											

Key	
Trace	
Minor	
Major	

5.3. Exploration model for Kombat-style mineralization

The Kombat Mineralization exploration model would commerce with investigating the upper Hüttenberg dolostone, and calc-silicates lithological changes of the carbonate platform sequences (Leach et al., 2010). In the carbonate platform sequence, look for hydrothermal alterations such as dolomitization and silicification which are limited to tectonic structural control, characteristics of the MVT-type deposits (Paradis et al., 2007). The tectonic structural control features include east-west striking cavities, faults and shear fractures at an average steep dip of 79°/195° (figure 4.1:8). Follow up field investigation would identify the mineralogical indicators for existing ore minerals, and associated gangue minerals (Table 3). On an outcrop scale, the dissolution and dolostone replacement textures associated with Cu-Pb ores can be observed (Figure 4.1.6 b; 4.1.7 a, b), common in and about MVT deposits (Leach et al., 2010). Geochemical soil and rock sampling for portable XRF analysis carried out at 1:10 000 scale or 50-100 m gridding would generate drill targets using the pathfinder elements (Table 2). The XRD and optical sample analysis can be used to confirm the potential ore minerals that contribute to the anomalous values of portable XRF results, thus, increase the exploration target confidence.

6. CONCLUSION

The carbonate hosted Kombat-style mineralization is structurally controlled and consists of small discrete vertical ore zones constrained to faults, shear fractures, and karst resembling the typical characteristics of a Mississippi Valley-type (MVT) deposit. This MVT-type deposit was formed by brine-hydrothermal fluid system, with an average temperature and salinity conditions of 183°C and 12.85 wt. % NaCl equivalent respectively. A less permeable phyllite at the base of Kombat formation formed a trap for the brine-hydrothermal fluid, and facilitated the deposition of Cu-Pb dominated ore within the upper Hüttenberg dolostone. Chemical control of organic-rich phyllite/shale provided reducing conditions which facilitated ore precipitation out of the hydrothermal fluids. The Cu-Pb ore is associated with Syn-sedimentary bedded Fe-Mn ore hosted in the calc-silicate rocks and slivers of sandstone. This Fe-Mn mineralization were deposited by diagenetic as well as mixed diagenetic-hydrogenetic processes within the sedimentary basin.

Suitable geochemical exploration indicators or pathfinder for anomalous values (wt. %) of Cu: 0.5 to 7.252; S: 0.223 to 3.229; Pb: 0.048 to 0.695; As: 0.029 to 0.414; Zn: 0.009 to 0.129; W, V, Mo and Ag: 0.001 to 0.035 each were based on the portable XRF sample analysis. The mineralogical exploration indicators based on field observations, optical mineralogy and XRD prospecting, include major ore minerals such as chalcopyrite, bornite, covellite, galena, and minor chalcocite, sphalerite, pyrite, jacobsite, pyrobelonite for the MVT type deposit. Whereas, hausmannite, hematite with minor concentrations of manganite, pyrolusite, rhodonite, magnetite for the syn-sedimentary stratiform deposit. Malachite, langite; brochantite, tennantite, smithsonite,

cerussite, asisite, damaraite, phosgenite, kombatite, duftite, hedyphane, mimetite, hamatophanite, wulfenite, rhodochrosite, kutnahorite, crednerite might be in traces or absent. The associated gangue minerals are predominantly dolomite (Mg), calcite (Ca) and quartz (Si), traces of anhydrite, gypsum and baryte. Overall, mineralogical, geochemical exploration indicators based on XRD and XRF results are summarized in Table 2 &3.

The exploration model for Kombat MVT-type deposit can be based on field mapping focusing on the south-southwest steep dipping (F: 79°/195°) faults and shear fractures. On the outcrop scale, one should look for recrystallization textures including euhedral calcite, quartz, tension gashes (veins), often associated with Cu-Pb ore minerals. In addition, follow up geochemical soil/rock survey at 1:10 000 scale or at 50-100m grid distance (Hao *et al*., 2018) using a portable XRF complemented by XRD could help to delineate small discrete ore zones based on established mineralogical and geochemical exploration indicators. Finally, magnetic data can be used to delineate associated Syn-sedimentary stratiform Fe-Mn deposit which are associated with the MVT-type deposit at the Kombat Mine.

7. RECOMMENDATIONS

Based on this study, it is confirmed that the Cu-Pb Kombat Mine mineralization is an MVT-type deposit similar to Tsumeb MVT deposit. Therefore, the author recommends that OML is potentially prospective for the Cu-Pb MVT-type deposits. Re-evaluation of some of the over 600 uneconomic occurrences of mineralization in OML (Turner *et al*., 2012), using the geochemistry, mineralogy and fluid inclusions is required to establish and confirm their genetic deposit-type. Once the genetic deposit-type is confirmed, the right exploration approach can be applied. This study recommends for the application of geochemical exploration methods to identify potential Cu-Pb MVT targets in areas without outcrops (calcrete, overburden) using the established mineralogical and geochemical exploration indicators of minerals around the OML and elsewhere. Finally, the Asis Far West locality deposit classification and geochemical results are not conclusive, hence, this study suggests further geochemical investigations using increased number of in-situ samples as well as fluid inclusions to determine whether the Asis Far West is part of the Kombat Cu-Pb MVT-type deposit.

REFERENCES

Bailie, R., Gutzmer, J., 2011. Age and primary architecture of the Copperton Zn-Cu VMS deposit, Northern Cape Province, South Africa. Ore Geology Reviews, 39, 164–179.

Baniak G. M., Gingras M.K., Burns B.A., Pemberton S.G., 2015. Petrophysical Characterization of Bioturbated Sandstone Reservoir Facies In the Upper Jurassic Ula Formation, Norwegian North Sea, Europe. Journal of Sedimentary Research, 85(1), 62-81.

Bowell, R. J., Ermolina, O., Plas, W. V., Us, J. V., Steiner, M., 2013. Minerals of the Kaokoveld District Kunene Region, Namibia. The Mineralogical Record, 44, 21.

Bussell, M. A., Alpers, C. N., Petersen, U., Shepherd, T. J., Bermudez, C., Baxter, A. N., 1990. The Ag-Mn-Pb-Zn Vein, Replacement, and Skarn Deposits of Uchucchacua, Peru: Studies of Structure, Mineralogy, Metal Zoning, Sr Isotopes, and Fluid Inclusions. Economic Geology, 85, 1348-1383.

Cairncross, B., 1997. The Otavi Mountain Land Cu-Pb-Zn-V deposits, Namibia. Mineralogical Record, 28, 109-130.

Changara, L., 2009. The lithological and structural controls on mineralization at Kombat Mines, Otavi Mountainland, northern Namibia. University of Namibia. Widhoek: Unpublished.

Chukanov, N. N., 2018. Janchevite, Pb7V5+(O8.5□0.5)Cl2, a new mineral from Kombat mine, Namibia. Canadian Mineralogist, 56, 159-165.

Deane, J., 1993. The Controls on “Contact-type” Cu-Pb (Ag) Mineralization within the Tsumeb Subgroup of the Otavi Valley syncline. Cape Town: Unpublished.

Deane, J., 1995. The structural evolution of the Kombat deposits, Otavi Mountainland, Namibia. Communications for geological. Survey of Namibia, 10, 99-107.

Dunn, P. P.C., 1986. Johninnesite, a new sodium manganese arsenosilicate from the Kombat Mine, Namibia. Mineralogical Magazine, 50(358), 667-670.

Emsbo, P., 2009. Geologic Criteria for the Assessment of Sedimentary Exhalative (Sedex) Zn-Pb-Ag Deposits Exhalative (Sedex) Zn-Pb-Ag Deposits. Department of the Interior. Reston, Virginia: U.S. Geological Survey.

European Discovery, Development, and Early Exploitation., 2015. Retrieved from http://www.tsumeb.com/en/history/european-discovery/ (accessed 20.09.19).

Galloway, C., 1988. The Geology of Kombat Mine and Environs. TCL Internal Report. (Unpublished).

Giordano, T., 1981. Lead transport in Mississippi Valley-Type oresolutions. Economic Geology, 76, 2200-2211.

Goscombe, B., Gray D., Armstrong, R., Foster, A. D., Vogl, J., 2005. Event geochronology of the Pan-African Kaoko Belt, Namibia. Precambrian Research , 140 , 103.e1–103.e41.

Hao, D., Jun, W., 2018. Applied Geophysics: Electrical and Electromagnetic Methods. Lucture Series . Windhoek: Unpublished.

Hawthorne, F. A., 2013. Carlfrancisite: Mn32+(Mn2+,Mg,Fe3+,Al)42(As3+O3)2(As5+O4)4[(Si,As5+)O4]6[(As5+,Si)O4]2(OH)42, a new arseno-silicate mineral from the Kombat mine, Otavi Valley, Namibia. American Mineralogist, 10(98), 1693-1696.

Hoal, K.O., Hoal, B.G., Griffin, W.L., Armstrong, R.A., 2000. Characterization of the age and nature of the lithosphere in the Tsumkwe region, Namibia. Communs geol. Surv. Namibia, 12, 23-30

Hoffman, P. F., Halverson, G. P., Schrag, D. P., 1998. A Neoproterozoic Snowball Earth. Journal of Science, 281, 1342-1346.

Innes, J., Chaplin, R., 1986. Ore bodies of the Kombat mine, South West Africa/Namibia. In: Mineral Deposits of Southern Africa . (C. M. Anhaeusser, Ed.) Geological Society of South Africa, 1789-1805.

Kamona, A., Günzel, A., 2007. Stratigraphy and base metal mineralization in the Otavi Mountain Land, Northern Namibia—a review and regional interpretation. Gondwana Research, 3, 396–413.

Kombat, Grootfontein., n.d. Kombat, Grootfontein, Otjozondjupa Region, Namibia. Retraived from https://www.mindat.org/loc-235838.html/ (accessed 20.09.19).

Kotzé, W. H., 2019. Kombat Mining Complex and Otavi Valley mineral deposits and occurrences. Unpublished report, Trigon Metals Inc.

Laukamp, C., 2006. Structural and fluid system evolution in the Otavi Mountainland (Namibia) and its significance for the genesis of sulphide and nonsulphide mineralization. PhD thesis, Universita¨t Heidelberg.

Leach, D.L., Sangster, D., 1993. Mississippi Valley-Type lead-zinc deposits. (R. Kirkham, W. Sinclair, R. Thorpe, & J. Duke, Eds.) 40, 289-314.

Leach, D.L., Taylor, R.D., Fey, D.L., Diehl, S.F., and Saltus, R.W., 2010. A deposit model for Mississippi Valley-Type lead-zinc ores, chap. A of Mineral deposit models for resource assessment: U.S. Geological Survey Scientific Investigations Report 2010–5070–A, 52.

Lechte, M. A., Wallace, M. W., Hoffmann, K., 2019. Glacio-marine iron formation deposition in a c. 700 Ma glaciated margin: insights from the Chuos Formation, Namibia. School of Earth Sciences, University of Melbourne, Parkville.

McQueen, K. G., 2015. Ore deposit types and their primary expressions. Retrieved from https://www.researchgate.net/publication/267839370/ (accessed 10.08.19).

Melcher, F., Lodziak, J., Vetter, U., 2004. Sulfide mineralization in the Otavi Mountain Land, Namibia.

Minz, F., 2008. The Kombat ore deposit, Otavi Mountainland (Northern Namibia). Advanced Seminars, Institute for Geology, Technical University Berg Academy, Freiberg.

Miller, R. M., 2008. The Geology of Namibia. Ministry of Mines and Energy, Geological Survey, Windhoek, Namibia, 1.

Moreno, C., González, F., Sáez, R., 2019. Basin Evolution and Massive Sulfide Deposition at Rammelsberg (Germany): Updating the Subsidence Analysis. Minerals. University of Huelva, Spain. Minerals, 9, 1, (45).

Mousivanda, F., Rastadb, E., Peterc, J. M., Maghfourib, S., 2018. Metallogeny of volcanogenic massive sulfide deposits of Iran1. Ore Geology Reviews, 95, 974–1007.

Pearson Product-Moment Correlation., 2018. Retraived from https://statistics.laerd.com/statistical-guides/pearson-correlation-coefficient-statistical-guide.php/ (accessed 20.09.19).

Potter, R. W., 1977. Pressure corrections for fluid-inclusions homogenization temperatures based on the volumetric properties of the systen NaCI-H20. Journal of. Research U.S. Geological Survey, 5, 603-607.

Puritch, E., Routledge, R., Sutcliffe, R., Burga, D., Hayden, A., 2014. NI-43-101 & 43-101F1 Technical Report and Resource Estimate on the Kombat copper project, Grootfontein district, Otjozondjupa region, Namibia latitude 19o 42’35’’S longitude 17o 42’09’’E UTM Zone 33K 783301 m E 7818395Ms for Kombat Copper Inc. P&E Mining Consultants Inc, Toronto.

Paradis, S., Hannigan, P., and Dewing, K., 2007, Mississippi Valley-type lead-zinc deposits, in Goodfellow, W.D., ed., Mineral Deposits of Canada: A Synthesis of Major Deposit-Types, District Metallogeny, the Evolution of Geological Provinces, and Exploration Methods: Geological Association of Canada, Mineral Deposits Division, Special Publication No. 5, 185-203.

Qiu, W. J., Zhou, M., Liu, Z., 2018. Late Paleozoic SEDEX deposits in South China formed in a carbonate platform at the northern margin of Gondwana. Journal of Asian Earth Sciences, 156, 41-58.

Raith, M., Raase, P., Reinhardt, J., 2012. Guide to Thin Section Microscopy. (2, Ed.) Roidestraße; Steendiek; Durban: Open Access Publication e-book.

Randive, K. R., Hari, K. R., Dora, M. L., Malpe, D. B., Bhondwe, A. A., 2014. Study of Fluid Inclusions: Methods, Techniques and Applications. Gonduwana. Geology. Magazine, 19-28.

Shepherd, T. J., Rankin, A. H., Alderton, D. H., 1985. A practical guide to fluid inclusion studies. New York: Glasgow : Blackie.

Skinner, B., 1997. Hydrothermal mineral deposits: what we do and don't know. (3rd ed.). (H. Barnes, Ed.) New York: John Wiley and Sons, N.

Trompette, R. 1997. Neoproterozoic (c. 600 Ma) aggregation of western Gondwana: a tentative scenario. Precambrian Research, 82, 101–112.

Turner, R., Siida, O. I., Rumsey, M. S., Krivovichev, S. V., Stanley, C. J., Spratt, J., 2012. Hereroite and vladkrivovichevite: two novel lead oxychlorides from the Kombat mine, Namibia. Mineralogical Magazine, 76(4), 883–890.

Van Heerden, D., Engelmann, U., and Odendaal, N.J., 2018. NI 43-101 Technical Report on the Kombat Copper Project, Namibia – Mineral Resource Report. Trigon Metals Inc, Toronto, Canada.

Volesky, J., Leybourne, M., Stern, R., Peter, J. M., D.Layton-Matthews, Rice, S., Johnson, P., 2017. Metavolcanic host rocks, mineralization,and gossans of the Shaib al Tair and Rabathan volcanogenic massive sulphide deposits of the Wadi Bidah Mineral District, Saudi Arabia. International Geology Review, 59(16), 1975–2002

APPENDICES

Appendix 1 A: Field observations way points and sample list

SAMPLE ID	LATITUDE (DD)	LONGITUDE (DD)	ROCK RELATIONSHIPS AND OUTCROP LITHOLOGIES	STRUCTURES	AZIMUTH	DIP	Geochemistry	Thin section	Fluid inclusion	PHOTOS	LOCALITY
AN19192	-19 42' 34.95960"	17 43' 04.62360"	Cu-Pb disseminated ore, mainly Cp-Bn-Cc/Gl hosted by the whitish-creamy to light-brown dolostone with Ml stains. Some thin magnetite-hematite bands up to 30 cm thick alternatinting with argillicious chloritic laminations have been observed.	Foliations	145	80	XRF/XRD	X	X	35-38	Pit near shaft 3
AN19193	-19 42' 34.86960"	17 43' 04.59480"	Fe-Mn badded ore, comprises of coarse dominant dark-grey magnetite to reddish- brown hematite band up to 1m width.	Foliations	145	80	XRF/XRD	X		39-44	Pit near shaft 3
AN19194	-19 42' 34.97040"	17 43' 04.60560"	Cu-Pb and Fe-Mn brecciated ore, the breccia contact zone along thebadded Fe-Mn margins comprises of dolostone clastics and Mt-Hm-Cp-Cc-Gl along the clastics boundaries. Ml coating have been observed on both groundmass and clastic phases.	Breccia			XRF/XRD	X		45-54	Pit near shaft 3
AN19195	-19 42' 34.48080"	17 43' 04.24560"	Cu-Pb vein/ fracture infilling ore, Strongly sheared and brecciated lingt-brown dolostome containing Bn-Cp-Gl and Ml coating along the fractures. Relicts of presumebly sedimentary beddings have been observed on silicious dolostone and chert clastics.	Shear planes	178	80	XRF/XRD			55-66	Pit near shaft 3
				Shear planes	209	76					
AN19196	-19 42' 35.00280"	17 43' 04.13760"	Host Rock, Light-brown to whitish-creamy dolostone with few stains of malachite on the pit wall parallel to the fracture plans and also parallel to the ore zones.	fracture planes	180	80	XRF/XRD	X		67-70	Pit near shaft 3
AN19197	-19 42' 35.08920"	17 43' 04.01160"	Host Rock, Light-brown to whitish-creamy dolostone with argillicious (chloritic) and calc-silicate thin layers containing Mt-Hm, Py-Cp dissemination. The unit make a relatively sharp contact with the adjucent Fe-Mn bedded ore.	Foliations			XRF/XRD			78-83	Pit near shaft 3
AN19198	-19 42' 34.94160"	17 43' 04.00080"	Fe-Mn Bedded ore, comprises of coarse dominant dark-grey magnetite to reddish- brown hematite band up to 6m width. Some breccia zones up to 40cm wide have been observed within and along the ore margins.				XRF/XRD			84-95	Pit near shaft 3
AN19199	-19 42' 35.33400"	17 43' 04.02240"	Sandstone band, sandwhiched between the Fe-Mn argillicious cal-silicate layers and the phyllitic band . The sandstone contains Py dissemination.				XRF/XRD	X		123-128	Pit near shaft 3
AN19200	-19 42' 35.19000"	17 43' 03.77400"	Cu-Pb Ore Cavity filling, The carvity 1m diameter and 1,5 m height cavity along the contact zone between Fe-Mn ore and Sandstone bands contain Ml-Mn mineralisations within the clay minerals and calcite intergrowth.				XRF/XRD			107-113	Pit near shaft 3

AN19201	-19 42' 35.19720"	17 43' 03.82440"	cal-silicate-chlorite layers between the Fe-Mn ore bands				XRF/XRD	X		102-106	Pit near shaft 3
AN19202	-19 42' 35.07480"	17 43' 03.86400"	Fe-Mn Bedded ore, comprises of coarse dominant dark-grey magnetite to reddish- brown hematite band.				XRF			96-101	Pit near shaft 3
AN19203	-19 42' 09.51840"	17 40' 58.86840"	Cu-Pb (Ag) ore, comprises of Bn-Cp-Cc-Gl massive minerals and dominantly along dolostone fractures. Few disseminations are observed and malachite stainings associated with sulfide oxidation.				XRF/XRD	X		140-155	Wast dump of Oasis W shaft
AN19204	-19 42' 09.52200"	17 40' 58.86120"	Cu-Pb (Ag) ore, comprises of Bn-Cp-Cc-Gl massive minerals and dominantly along dolostone fractures. Few disseminations are observed and malachite stainings associated with sulfide oxidation.				XRF			140-155	Wast dump of Oasis W shaft
AN19205	-19 42' 50.65200"	17 40' 43.44600"	Brecciated dolostone hills with Cc-Ml mineralsations along fracturs. Some reddish hematite stains associated with chert and recrystaliased calcite minerals.	Fractures	282	80	XRF			157-166	hill near Oasis W shaft
				foliation	19	71					
AN19206	-19 42' 48.27960"	17 40' 39.86760"	Brecciated dolostone hills with Cc-Ml mineralsations along fracturs. Some reddish hematite stains associated with chert and recrystaliased calcite minerals.				XRF/XRD	X		167-175	hill near Oasis W shaft
AN19207	-19 42' 30.28680"	17 43' 17.02200"	Cu-Fe Ore, Brecciated dolostone calastics with Ml-Hm/Gt mineralsations in the matrix. Some reddish hematite stains associated with chert and recrystaliased calcite minerals.		220	90	XRF			177-189	Pit 900 far East
AN19208	-19 42' 29.96280"	17 43' 16.96080"	Recrystaliased calcite minerals associated the malachite in the feruginous breccia matrix or fault gouge. The whitish to grey euhedral calcite crystals are up to 25cm wide with some dark-grey tint could be due to galena (Pb), may indicate the presence of paleo-curvity to provide the required free growth space.	Fault plane	205	90	XRF/XRD	X	X	190-227	Pit 900 far East
				Fractures	303	81					
AN19209	-19 42' 30.21480"	17 43' 16.83120"	Host rock, Light brown to whitish-creamy dolostone clastics up to 1m width with no visible mineralisation. It is surrouded by malachite-hematite matric along the clastic boundaries.				XRF/XRD	X		228-231	Pit 900 far East
AN19210	-19 42' 30.66480"	17 43' 14.76120"	Cu-Pb Ore, Massive and fractured grey dolostone containing Cp-Bn-Cc/Gl-Py minerals along fractures, forming a network vien to patches of massive ore. The ore minerals appeaed to have formed reams around associated euhedral calcite crystals.				XRF/XRD			253-261	Pit 900 East
AN19211	-19 42' 30.31560"	17 43' 15.43800"	Cu-Pb Ore, Massive and fractured grey dolostone containing Cp-Bn-Cc/Gl-Py ore minerals along fractures, forming a network vien to patches of massive ore.				XRF/XRD	X		262-267	Pit 900 East
AN19212	-19 42' 31.33080"	17 43' 11.84880"	Cu-Pb Ore, Massive and fractured grey dolostone containing Cp-Bn and euhedral Gl ore minerals forming a network vien to patches of massive ore. Associated with quartz and calcite guanges.				XRF/XRD	X			Adit 900

AN19213	-19 42' 31.28400"	17 43' 11.11440"	Host Rock, Massive, grey dolostone with recrystallised calcite and quartz infill along sigmoidal vein structures. Some euhedral galena, chalcopyrite crystals are intimentry associated with calcite and quatz guange minerals.				XRF/XRD				Adit 900
AN19214			Level 2 along the main ramp,Cu-Pb Ore, Massive Cp-Bn-Cc-Az and Gl menerals with Ml stains on the rock surface.				XRF/XRD	X			No:1 Shaft Asis Wast
AN19215	-19 42' 33.02640"	17 42' 34.44840"	Cu-Pb Ore, Bedded to laminated, dark-grey dolostone with Cc viens up to 5cm wide intimentry associated with euhedral calcite crystals and quartz veins and also along lamination. Ml coatings	lamination	198	60	XRF			219-296	Pit Central
				lamination	199	33					
AN19216	-19 42' 33.26040"	17 42' 31.84920"	Cu/Mn-Fe Ore, Bedded, dark-grey dolostone with Cc-Hm veins and also along beddings associated with black detritic textures of Mn mineralisations and Ml coatings. Association of quartz and calcite guange minerals have been abserved.	Beddings	188	45	XRF			299-309	Pit Central
AN19217	-19 42' 33.44400"	17 42' 31.79160"	Host rock, Bedded dark-grey calc-silicate comprises of fine to medium-grained quartz/calcit-biotite-chert minerals alternating with grey laminated dolostone. Calcite and quartz veins along the bedding planes.	Beddings	185	55	XRF/XRD	X		310-316	Pit Central
AN19218	-19 42' 33.02280"	17 42' 30.94200"	Cu/Mn-Fe Ore, Brecciated, ferruginous dolostone calstics and Ml-Hm-Dt-Cp-Cc-Brn in matrix of the dextral fault guange textures and associated with quartz and calcite guange minerals.	Fault plane	192	79	XRF			317-325	Pit Central
AN19219	-19 42' 32.73480"	17 42' 31.82400"	Cu-Fe Ore, Brecciated, ferruginous dolostone and calc-silicate calstics with Cp-Cc-Bn-Hm in the matrix of the dextral fault guange textures and associated with chert and calcite guange minerals.	Fault plane	185	65	XRF/XRD			326-342	Pit Central
AN19220	-19 42' 32.39640"	17 42' 33.21000"	Host rocks, Laminated dark-grey calc-silicate bedds alternating with grey dolostone, quartz and calcite minerals without visible ore minerals.	lamination	218	30	XRF/XRD	X		344-352	Pit Central
AN19221			Botroidal shaped nodule layer with brownish calc-silicate nuclei and white silicious (quartz) outer layers.				XRF/XRD	X		520-525	Gross Otavi Adit
AN19222	-19 39' 51.94080"	17 35' 53.97360"	Host rocks, Laminated grey dolostone with ferruginouse chert and no visible ore minerals. This hosts Cc-Ml mineralisations observed along the roof of an adit, not sampled due to unsafe lose hunging rocks.	lamination	230	45	XRF/XRD			526-531	Gross Otavi Adit
AN19223	-19 39' 51.24240"	17 36' 20.02320"	Euhedral to subhedral quartz crystals mainly from the breccia clastics of the fault guonge deposition. It is associated with historically mined chalcocite and malachite clastics in the ferruginous matrix supported across dolostone curvities.						X		Gross Otavi Germans Workings
AN19224	-19 39' 50.65200"	17 36' 17.18280"	Euhedral to subhedral quartz crystals mainly from the breccia clastics of the fault guonge deposition. It is associated with historically mined chalcocite and malachite clastics in the ferruginous matrix supported across dolostone curvities.						X		Gross Otavi Germans Workings

AN19225	-19 39' 50.22720"	17 36' 16.19280"	Cu-Fe Ore, reddish brown ferruginous and matrix supported breccia of the fault guonge deposition. It comprises of Cc-Ml and Hm ore minerals associated quartz, calcite and dolostone clastics of guonge minerals concentrated in dolostone curvities.	Fault plane & lamination	205	90	XRF/XRD	X		541-547	Gross Otavi Germans Workings
				lamination	226	41					
AN19226	-19 39' 49.65480"	17 36' 14.76720"	Euhedral to subhedral quartz crystals mainly from the breccia clastics of the fault guonge deposition. It is associated with historically mined chalcocite and malachite clastics in the ferruginous matrix supported.						X		Gross Otavi Germans Workings
AN19227	-19 39' 50.26320"	17 36' 16.05960"	Host rocks, Laminated and brecciated grey dolostone with ferruginouse chert and few visible malachite minerals. This hosts 4 m wide up to 30 striking curvities previousely filled with Cc-Ml clastics in the ferruginous matrix supported breccia.				XRF			552-553	Gross Otavi Germans Workings
AN19228	-19 39' 51.52320"	17 36' 19.41120"	Cu-Pb (Ag) ore, Brecciated or fractured light-grey dolostone comprises of Cc-Gl vein network minerals and dominantly along dolostone fractures. Mn-detrical textures are observed and malachite stainings associated with micro-curvities.				XRF/XRD	X			Gross Otavi Germans Workings
AN19229	-19 39' 51.70680"	17 36' 20.58840"	Euhedral to subhedral quartz crystals from the quartz vein along the laminated grey dolostone. It is associated with calcite infilling fractutres parallel to the fault planes with malachite stains and malachite clastics in the ferruginous matrix supported across dolostone curvities.	Fault plane & lamination	178	65			X	554-575	Gross Otavi Germans Workings
				lamination	199	46					
AN19230	-19 42' 30.15360"	17 43' 14.61000"	Euhedral Calcite crystals surrounded by Gal-Cpy-Mal mineralsations ream. These crystals grow along mineralised veins/ fractures in the grey dolostone.						X	587-589	Pit 900 East
AN19231	-19 42' 31.48200"	17 43' 11.33040"	Euhedral calcite crystals surrounded by Gl-Cp-Ml mineralsations ream. These crystals grow along mineralised veins/ fractures in the grey dolostone associated with unmineralised calcite lander viens(tension guases).						X	590-594	Adit 900
AN19232	-19 42' 35.29800"	17 43' 03.16920"	Fe-Mn Bedded ore, comprises of coarse dominant dark-grey magnetite to reddish- brown hematite band in a surface weathered gossans.							598-599	Pit near shaft 3
AN19233	-19 42' 35.08200"	17 43' 03.59040"	Strongly sheared and brecciated lingt-brown dolostome containing Bn-Cp-Gl and Ml coating along the fractures. Relicts of presumebly sedimentary beddings have been observed on silicious dolostone and chert clastics.					X		600-602	Pit near shaft 3

Appendices 1 B: list of Kombat Mine samples provided by the National Earth Science Museum of the Geological Survey of Namibia.

SAMPLE ID	LOCALITY	ROCK RELATIONSHIPS AND OUTCROP LITHOLOGIES	Fluid inclusion	Thin section	Geochemistry: XRF	Geochemistry: XRD
8650	Level 8, stope 302	Massive sulphide (Cu-Ore): coarse-grained Bornite-chalcopyrite.		X	X	X
8651	West level 16, main drive.	Massive sulphide (Cu-Ore): coarse-grained bornite-chalcopyrite-pyrite in sharp contain with cream-white dolostone. Greenish malachite ream filling up the 2-3mm contact zone.	X			
8659	Level 5, stpe 11.5.	Foliated, Schistose, Biotite-chlorite-Calcsilicate-garnet schist with Magnetite-specular hematite (Fe-Mn ore) and covellite.		X	X	X
8665	Level 5, southern stope.	Brecciated Calcsilicate-biotite schist with brown dolostone and garnet clastics, associated with traces of bornite-chalcopyrite.		X	X	X
8673	Level 10, west stope 11.5	Foliated, Schistose, Biotite-chlorite-Calcsilicate-garnet schist with traces of magnetite-hematite and covellite.		X	X	X
8680	Open-pit D6.	Massive to disseminated sulphide (Cu-ore) bornite-chalcopyrite-pyrite ± sphalerite ± galena with oxidised, irregular carbonate surface with malachite stains. Associated gangue minerals include calcsilicate-biotite-chlorite.		X	X	X
8687	Level 12	Foliated Calcsilicate- biotite-chlorite schist.		X	X	X
8683	West-Asisc-level 11, stope 15 east, south-side	Foliated, breccia with felspathic sandstone and biotite schist clastics in the calcsilicate-chlorte ground mass.		X	X	X
8672	Level 5, stope 0.1	Calcsilicate or grain stone with medium crystalline of quartz-calcite-biotite-chlorite and pink Mn-silicates (rhodonite) vein.		X	X	X
8649	Main mine, level 15 stope 80	Foliated, Schistose, Biotite-chlorite-Calcsilicate-garnet schist with traces of pyrite, chalcopyrite, and galena.		X	X	X
8813	Nortern- pillar, level 3, stope 15 east.	Clear quartz crystals		X	X	X

Appendix 2A: portable XRF whole rock analysis results for Kombat Mine samples.

SAMPLE	Mo (wt%)	Zr (wt%)	Sr (wt%)	Rb (wt%)	Pb (wt%)	As (wt%)	Zn (wt%)	W (wt%)	Cu (wt%)	Ni (wt%)	Co (wt%)	Fe (wt%)	Mn (wt%)	Cr (wt%)	V (wt%)	Ti (wt%)	Ca (wt%)	K (wt%)	S (wt%)	Ba (wt%)	Sb (wt%)	Cd (wt%)	Ag (wt%)	Bal (wt%)	Nb (wt%)	Al (wt%)	P (wt%)	Si (wt%)	Cl (wt%)	Mg (wt%)
AN19192	0	0	0.047	0	0.004	0.131	0.003	0	0.223	0.008	0	0.774	1.615	0	0	0	35.25	0.035	0.449	0.976	0	0	0	57.42	0	0	1.281	0.778	0	0
AN19193	0.003	0	0.135	0	0.021	0.032	0	0.032	0.694	0.022	0	53.57	0.551	0.025	0	0	8.73	0.072	1.474	3.343	0	0	0	27.18	0	0.928	0.508	1.658	0.011	0
AN19194	0	0	0.081	0	0.052	0.284	0.002	0	1.141	0.007	0.042	7.435	2.64	0	0	0	31.11	0.173	0.737	1.348	0	0	0	50.28	0	0.583	0.353	1.157	0	0
AN19195	0	0	0.02	0	0.002	0.296	0.007	0	0.618	0	0	0.439	1.357	0	0	0	35.39	0.078	0.257	0.04	0	0	0	56.7	0	0	0.335	1.025	0	2.202
AN19196	0	0	0.009	0	0.003	0.018	0	0	0.035	0	0	0.261	0.24	0	0	0.029	22.44	0.227	0.043	0.024	0	0	0	67.37	0	0.435	0.379	1.814	0	5.678
ST55	0	0	0	0	0	0	0	0.009	5.096	0	0	5.543	0	0	0	0	0.066	0	0.027	0.016	0	0	0	60.38	0	0.153	0	27.7	0	0
AN19197	0	0	0.036	0.002	0.009	0.133	0.003	0	0.093	0	0	2.196	0.704	0	0	0.051	31.47	0.566	0.196	0.129	0	0	0	57.67	0	0.956	1.093	3.677	0	0
AN19198	0.002	0	0.187	0	0.08	0.034	0.004	0	0.029	0.026	0.043	28.78	0.937	0.026	0	0	15.15	0.449	1.902	4.161	0	0	0	40.08	0.002	1.26	0.986	4.863	0	0
AN19199	0	0.008	0.079	0.006	0.015	0.003	0	0.006	0.019	0.006	0	3.28	0.574	0.011	0	0.132	10.06	1.88	0.742	1.493	0	0	0	62.84	0	2.834	0.555	14.45	0	0
AN19199b	0	0	0.078	0.006	0.012	0.004	0.002	0	0.019	0.009	0	2.874	0.572	0.009	0	0.129	9.538	1.937	0.695	1.558	0	0	0	63.82	0	2.949	0.529	14.26	0	0
AN19200	0.004	0	0.182	0.002	0.205	0.977	0.019	0.021	1.097	0.049	0	18.36	0.706	0	0	0	2.695	0.526	5.854	24.54	0.016	0	0	36.98	0.002	2.379	1.489	2.841	0	0
AN19201	0	0	0.12	0	0.895	2.289	0.016	0.026	0.022	0.017	0.022	2.95	9.407	0	0	0	23.84	0.05	1.191	2.245	0	0	0	53.01	0	0.343	0.202	2.331	0.021	0
B01	0	0	0	0	0	0	0	0	0	0	0	0.333	0	0	0	0	0.105	0	0	0.006	0	0	0	67.78	0	0	0	30.77	0	0
AN19202	0.002	0	0.542	0	0.108	0.077	0	0	0.552	0.053	0	43.63	0.782	0.035	0	0	5.51	0.073	4.521	14.56	0	0	0	24.35	0	0.787	0.466	0.995	0	0
AN19203	0	0	0.024	0	0.01	0.139	0.079	0.014	10.75	0	0	11.12	0.305	0	0.024	0.03	21.98	0.313	11.11	0.078	0	0	0.002	33.3	0	1.454	0.826	3.765	0.019	3.658
AN19204	0	0	0.02	0	0.009	0.246	0.073	0	7.432	0	0	7.663	0.378	0	0	0.035	22.68	0.227	7.667	0.14	0.075	0	0.002	45.84	0	0.661	0.231	5.597	0	0
AN19205	0	0	0.004	0	0.156	2.695	0.417	0	5.602	0	0	0.564	0.176	0	0	0.012	14.03	0	0.145	0.023	0.014	0.004	0.009	59.07	0	0	0.119	8.248	0	7.692
AN19206	0	0	0.007	0	0.078	0.158	0.257	0	1.771	0	0	1.024	0.266	0	0	0.015	21.38	0	0.131	0.015	0.018	0.005	0.01	64.67	0	0	0.038	1.281	0	7.876
ST25	0	0	0	0	0	0.006	0	0.007	1.966	0	0	5.495	0	0	0	0	0.356	0	0.046	0.016	0	0	0	62.18	0	0	0	28.82	0	0
AN19207	0	0	0.002	0.002	2.367	0.166	0.434	0.029	5.034	0	0	7.91	2.237	0	0.018	0.081	20.22	0.296	1.493	0.053	0	0.009	0	49.78	0	1.119	0.668	5.03	0.054	1.982
AN19208	0	0	0.024	0	0.028	0.012	0.063	0	0.18	0	0	0.222	0.913	0	0	0.032	38.65	0	0.067	0.028	0	0.002	0	57.7	0	0	0.128	0.895	0.025	0
AN19209	0	0	0.013	0	0.003	0.002	0.002	0	0.013	0	0	0.134	0.617	0.008	0	0.025	35	0	0.082	0.022	0	0	0	60.68	0	0	0.104	0.576	0	1.687
AN19209b	0	0	0.013	0	0.003	0.002	0	0	0.015	0	0	0.143	0.629	0.006	0	0.042	35.24	0	0.074	0.023	0	0	0	60.13	0	0	0.07	0.613	0	1.969
AN19210	0	0	0.014	0	0	0.014	0.002	0	1.071	0	0	0.79	0.787	0.007	0	0.027	34.94	0	0.758	0.022	0	0	0	57.88	0	0	0.07	0.258	0	2.356
AN19211	0	0	0.013	0	0.007	0	0.004	0	3.42	0	0	1.459	0.887	0	0	0.024	33.21	0	1.353	0.026	0	0	0.002	55.54	0	0	0.05	1.032	0.009	1.958
B02	0	0	0	0	0	0	0	0	0	0	0	0.324	0	0	0	0	0.068	0	0	0.007	0	0	0	66.39	0	0	0	31.92	0	0
AN19212	0	0	0.013	0	0.082	0.465	0.084	0.01	8.882	0	0	9.254	0.79	0	0	0	28.13	0	8.09	0.028	0.006	0.002	0.002	42.4	0	0	0	0.714	0.019	0
AN19213	0	0	0.011	0	0.511	0	0	0.007	0.058	0	0	0.273	0.689	0.006	0	0	31.56	0	0.42	0.021	0	0	0	60.55	0	0	0	0.936	0	3.936
AN19214	0.014	0	0.003	0	0.04	0.011	0	0	46.23	0	0	6.031	0.04	0	0	0.039	2.487	0.451	14.63	0.126	0	0	0.066	17.38	0	3.032	0.408	7.982	0.02	0
AN19215	0	0	0.008	0	0.009	0.004	0	0	14.95	0	0	1.483	0.347	0	0	0	29.3	0	0.941	0.073	0	0	0.01	51.5	0	0	0.057	0.317	0	0
AN19216	0.003	0	0.006	0	0.005	0.064	0	0	22.18	0	0	2.733	0.433	0	0	0	26.94	0.143	0.692	0.133	0	0	0.012	43.18	0	0.359	0.756	1.359	0	0
AN19217	0	0	0.019	0	0	0	0	0	0.019	0	0	0.132	0.375	0.011	0	0.022	29.02	0.047	0.059	0.069	0	0	0	58.45	0	0	2.906	1.18	0	6.695
AN19218	0	0	0.012	0	0.004	0	0	0	6.032	0	0	0.969	0.688	0	0	0.026	33.29	0	0.287	0.027	0	0	0.004	56.62	0	0	0.104	0.902	0.011	0
AN19219	0.002	0	0.003	0	0.007	0.009	0	0.019	42.26	0	0	7.331	0.348	0	0	0.019	12.59	0.039	4.736	0.034	0	0	0.028	29.97	0	0	0.123	1.194	0.024	0
AN19219b	0	0	0.003	0	0.008	0.005	0	0.014	41.86	0	0	7.267	0.35	0	0	0	12.57	0.05	4.724	0.039	0	0	0.029	30.22	0	0.362	0.157	1.306	0.018	0
AN19220	0	0	0.013	0	0	0	0	0	0.012	0	0	0.047	0.056	0.005	0	0.022	24.23	0.037	0.053	0.021	0	0	0	64.17	0	0	2.281	0.45	0	7.457
ST055	0	0	0	0	0.009	0	0	0	0.431	0	0	4.944	0	0	0	0	0.042	0	0.032	0.014	0	0	0	61.58	0	0	0	31.94	0	0
AN19221	0	0	0	0	0.451	0	0.023	0	0.183	0	0	0.496	0.281	0.01	0.06	0.096	35.93	0.191	0.292	0.113	0	0	0	56.67	0	1.241	0.157	2.765	0.023	0
B03	0	0	0	0	<LOD	0	0	0	0.004	0	0	0.205	0	0	0	0	0.052	0	0	0.006	0	0	0	66.38	0	0	0	32.35	0	0
AN19222	0	0	0.007	0	0.006	0	0.002	0	0.003	0	0	0.264	0.096	0	0	0	26.81	0	0.024	0.029	0	0	0	65.19	0	0	0	2.074	0	4.446
AN19225	0.036	0	0	0	0.693	0.203	0.092	0.016	22.4	0	0	10.73	0.121	0	0.024	0.063	12.68	0.112	0.36	0.048	0.004	0	0.009	42.93	0	1.3	0.078	4.86	0.015	2.205
AN19227	0	0	0.007	0	0.005	0	0	0	0.023	0	0	0.098	0.062	0	0	0.022	20.59	0.105	0.046	0.028	0	0	0	68.52	0	0.284	0.075	2.027	0	7.105
AN19228	0.018	0	0.006	0	1.067	0.11	0.884	0	2.928	0	0.011	0.562	0.245	0	0	0	18.11	0.046	0.561	0.025	0.004	0.076	0.003	64.87	0	0	0	3.589	0	5.827
AN19232	0	0	0.024	0	0.025	0.003	0	0.008	1.81	0.007	0.035	20.51	1.543	0.024	0	0	25.04	0	0.255	0.527	0	0	0	46.19	0	0.468	0.429	2.109	0	0
ST205	0	0	0	0	<LOD	0	0	0.017	19.68	0	0	5.523	0	0	0	0	0.055	0	0.039	0.021	0	0	0	54.49	0	0	0.392	18.78	0	0
8649	0.009	0	0.107	0	1.563	0.418	0.051	0.033	0.017	0.012	0	1.756	34.72	0	0	0	9.231	0	1.509	1.501	0	0	0	43.42	0.002	0.457	0.328	0.996	0.392	2.399
8650	0.01	0	0	0	7.745	0.819	0.501	0.106	38.67	0	0	16.88	0.025	0	0	0	0.066	0	28.81	0.041	0	0.012	0.025	4.378	0	0.49	0.101	0.112	0.175	0
8659	0.012	0	0.068	0.002	3.188	0.402	0.023	0.032	0.049	0.027	0.056	0	43.41	0	0	0	3.902	0	4.704	9.296	0	0	0	18	0.002	0.643	0.082	0.29	0.11	14.66
8659b	0.012	0	0.067	0.002	3.247	0.408	0.025	0.04	0.04	0.022	0.055	0	43.68	0	0	0	4.059	0	4.594	9.506	0	0	0	19.21	0.002	0.534	0.146	0.343	0.108	12.9
8672	0	0	0.025	0	0.078	0.06	0.014	0.022	0.862	0.007	0.023	0.542	31.29	0.037	0.05	0	25.84	0	0.166	0.189	0	0	0	33.55	0.003	0.356	1.339	4.337	0.141	0
8673	0.005	0	0.088	0	2.007	0.262	0.022	0.035	0.081	0.029	0.05	0	38.18	0	0	0	5.328	0	5.016	12.71	0	0	0	19.27	0.002	0.472	0.054	0.221	0.031	15.13
B04	0	0	0	0	0	0	0	0	0	0	0	0.27	0	0	0	0	0.035	0	0	0.014	0	0	0	68.99	0	0	0	29.68	0	0
8680	0.313	0	0	0	4.615	3.096	0.364	0.092	49.92	0	0.016	5.565	0.029	0	0	0	0.715	0	20.49	0.028	0.012	0.019	0.067	9.319	0	0.524	0.143	1.141	0.127	<LOD
8683	0.002	0	0.029	0	0.271	0.146	0.036	0	0.191	0.007	0.015	0.779	42.09	0	0	0	1.371	0	0.547	0.409	0	0	0	35.6	0.002	1.868	0.073	6.98	0.027	8.543
Average	**0.008**	**1E-04**	**0.04**	**4E-04**	**0.571**	**0.263**	**0.065**	**0.011**	**6.79**	**0.006**	**0.007**	**5.776**	**4.948**	**0.004**	**0.003**	**0.018**	**17.2**	**0.15**	**2.65**	**1.666**	**0.003**	**0.002**	**0.005**	**48.74**	**3E-04**	**0.541**	**0.383**	**6.616**	**0.026**	**2.422**

Appendices 2B: XRD mineralogical analysis results for Kombat Mine samples.

Sample Numb	Pyrite	Chalcopyrite	Galena	Sphalerite	Bornite	Chalcocite	Covellite	Tennantite	Calcite	Aragonite	Ankerite	Cerussite	Dolomite	Rhodochrosite	Grootfonteinit	Kutnahorite	Malachite	Smithsonite	Crednerite	Hematite	Hausmannite	Jacobsite	Manganite	Magnetite	Pyrolusite	Descloizite	Kombatite	Asisite	Alleghenyite	pyrobelonite	Holdawayite	Albite	Biotite	Britvinite	Chlorite	Chrysocolla	Clinozoisite	Epidote	Illite	Kaolinite	Muscovite	Quartz	Richterite	Rhodonite	Defrenite	Duftite	Hedyphane	Mimetite	Sahlinite	Wulfenite	Anhydrite	Gypsum	Baryte	Brochantite	Langite	Damaraite	Hematophanit	Mendipite	Phosgenite
AN19192	*	**	*	*	*	*			**		*		**	*			*			**			*												**					*		*	**																
AN19193									**				**			***			*	***	***	**																													*											
AN19194	*	*	*		*	**	*		*	*	*	*	**	*		*	*	*	*		**	**			*	*						**	*		*					*		***	**	*																
AN19195	*	*				*			***	**	**	*	***				*	*	*	*																				*						*				*		*	*		*		*	*				
AN19196									***				***				*																	*				*	**	*	**	*	*																
AN19197		*				*			**	*	*		***	*		**				*	*	*										*			**		*	*	**	**	**	**	*										*	*		*					
AN19198									**				***			**				**	***	**	**	**									*				*	*						*	**																	
AN19199									**				***			**				**	***	**	**	**									*				*	*						*	**																	
AN19200	*	**	***			**	*																												*			***	**	*	***																	
AN19201									***	*	***		*			*				***	***	**	**	**									*	*											**	**				**												
AN19203	*	**	***	*	**	**	*	*					*				*																						*	*	***									*			*	**						
AN19206						**			***				***				**			*													*								*	**										**								
AN19208			*						***								*			**															*				**		**																	
AN19209									**				***							**													*						**		*	**																	
AN19210	**	**	**	**	*	*			**				***				*																						*		***			*		*							*						
AN19211	**	**	**	**	*	*			**				***				*																						*		***			*		*							*						
AN19212	**	**	**	**	*	*			**				***				*																						*		***			*		*							*	*					
AN19213		*	*						***				***				*	*					*													*			*		***												*					
AN19214	**	**	**	**	*	*			**				***				*																						*		***			*		*							*	*					
AN19217									***																																***																	
AN19219	**	**	**	**	*	*			**				***				*																						*		***			*		*							*	*					
AN19220									***																																***													*					
AN19221									***				**																			*	*		*	*					***													*					
AN19222									***				***																								*	*		***																	
AN19225	**	**	**	**	*	*			**				***				*															*							*	***			*		*								*					
AN19228		*	*			**	*		**				***			*	*			*												*						*	*	***																	
8649									**		*			**						**	***		*																	*		***			*		*											*				
8650	**	***	*	*	**	*																															*	**	*	**	**																				
8659	*								**					**	*	**			*		***	**	*		**		*	*	*		*					*	**	**	*		*			**		*		*									*				
8672											**			**		**				**	***	*			*				**	**																													
8673																					***	**			**								**	*	*			*		*	*				*	**														
8680	**	**	**		***		***																																																					

KEY		
*	trace	<1%
**	minor	1-10%
***	major	>10%

Appendix 2C: Heating and freezing (Linkham TH600) stage fluid inclusion analysis results for Kombat Mine samples.

Sample	Host	Type	Number inclusions analysed	Mean Freezing temp, °C	Standard Deviation	Eqiu NaCl wt %	Mean Homogenization Temp, °C	Standard Deviation	Corrected Temp, °C (Potter., 1977) at 2kbr (Deane, 1995)
AN19208	Calcite	secondary	5	-3.5	1.3	5	120	64	160
	Calcite	primary	6	-6.5	2.1	8	240	23.1	180
AN19223	Quartz	secondary	5	-12.3	4.8	13.7	144	17.3	175
		primary	5	-4.6	1.9	6.2	302	27.2	195
	Calcite	secondary	5	-12	3.3	13.4	140	12.3	170
		primary	5	-4.8	2.6	6.3	286	27.2	185
AN19224	Quartz	secondary	5	-14.6	6.1	15.7	127	14.3	170
		primary	5	-1.9	1.6	2.2	235	18.5	190
	Calcite	secondary	5	-15.6	5.4	16	143	15.5	175
		primary	5	-1.8	1.2	2.1	226	31.7	160
AN19226	Quartz	secondary	5	-15.3	3.8	15.4	167	38.6	180
		primary	5	-5.3	2.6	6.6	286	24.3	170
	Calcite	secondary	5	-9.9	2.1	10.4	163	8.8	170
		primary	5	-5.8	4.2	7.1	270	3.9	180
	Sphalerite	secondary	3	-10.2	3.3	11.4	164	10.9	170
		primary	5	-6.3	1.7	7.8	267	19.8	185
	Wulfenite	primary	5	-3.5	2.1	5	140	23	160
AN19229	Quartz	secondary	5	-20	4.5	22	88	12	166
		primary	5	-21.9	5.5	23.8	175	17.6	180
	Calcite	secondary	5	-18.9	7.7	20	58	29.9	166
		primary	5	-20	9.6	22	205	24.3	175
AN19230	Calcite	secondary	5	-22	10.4	24.1	110	17.4	170
		primary	5	-7.2	1.1	8.4	280	21.4	195
AN19231	Calcite	secondary	5	-20.9	4.6	22.6	125	11.4	175
		primary	5	-5.8	2.3	7.1	265	12.2	175
8813	Cerussite	primary	7	-5.8	1.8	7.5	64	16.5	170
8659	Calcite	secondary	5	-26.6	7.9	26.4	146	19.2	170
		primary	5	-21.7	6.6	23.7	182	21.3	200
Averange			**5**	**-11.6**		**12.85**	**183**		**176**

Appendix 3: Kombat Mine access permit for field investigation/research purpose.

TRIGON METALS

KOMBAT MINE

PERMISSION FOR PRIVATE VEHICLES

1. Approval is hereby granted to ABNER NGHOONGOLOLA in his/~~her~~ capacity as CHIEF GEO SYNTIST / ~~contractor~~ to enter the mine premises with his/~~her~~ private vehicle for the period 16/7/2019 to UNTIL FURTHER / ~~permanent~~. NOTICE
   Model TOYOTA Reg. no. GRN 8023 Colour SILVER

2. The prescribed identification sticker available from Rubicon Security Services must be displayed on a conspicuous place on the private vehicle. Not applicable until mine operations commence.

3. Kombat Mine reserves the right to search and inspect vehicles and any containers which are taken into or out of Kombat Mine's premises.

4. The approval may be withdrawn at any time.

JF LUSSE

OPERATIONS MANAGER

LIABILITY RELEASE

I, ABNER NGHOONGOLOLA HEREBY ACCEPT THE ABOVEMENTIONED CONDITIONS AND IN CONSIDERATION OF Kombat Mine permitting my private vehicle onto the mine premises. I hereby agree that the vehicle is driven and stored at my own risk. I hereby release and discharge the Company of and from all actions, causes of action, claims and demands of every nature and kind which I may now or can any time hereafter have against the Company for or an account of any loss or damage.

SIGNATURE

16/07/19
DATE